Bar force profiles in LC refining

Matthias Aigner
BSc, Montanuniversität Leoben, 2015
MSc, Montanuniversität Leoben, 2016

A Dissertation Submitted in Partial Fulfillment
of the Requirements for the Degree of

DOCTOR OF PHILOSOPHY

in the Department of Mechanical Engineering

Bar force profiles in LC refining

Matthias Aigner
BSc, Montanuniversität Leoben, 2015
MSc, Montanuniversität Leoben, 2016

Supervisory Committee

Dr. Peter Wild (Department of Mechanical Engineering)
Supervisor

Dr. Nedjib Djilali (Department of Mechanical Engineering)
Departmental Member

Dr. Jens Bornemann (Department of Electrical and Computer Engineering)
Outside Member

Abstract

Reducing energy consumption in pulp and paper refining requires a deep understanding of all the processes involved. This dissertation investigates fundamental mechanics of the low consistency mechanical refining process. Three studies investigate forces applied to wood fibers with the focus on how force profiles during bar passing events change with process variables such as fiber length and refiner load.

In the first study a high resolution rotary encoder and a piezo ceramic force sensor are implemented in a 16-inch laboratory-scale low consistency refiner to explore the effect of plate gaps on bar-force profiles. The rotary encoder data is used to locate the rotor bars relative to the stator bar in which the sensor is located. Force profiles for bar passing events are registered to the position of rotor bars relative to the stator bar in which the sensor is located and mean force profiles are produced. These mean force profiles have potential to shed light on the fundamental mechanisms of mechanical refining. For large gaps, there is a late peak in the force profiles that occurs toward the end of the bar passing event. For gaps that are less than the critical gap, below which fiber cutting occurs, there is an early peak in the force profiles that occurs at the start of the bar passing event. It is hypothesized that the early peak represents the corner force and, therefore, that corner force is causal in the onset of fiber cutting.

In the second study a set of piezo ceramic force sensors is implemented in a 52-inch mill-scale low consistency refiner to explore the effect of varying operating conditions on bar force profiles. Force profiles for individual bar passing events are identified based on key features in the time domain force data based on the knowledge acquired from the previous study in the pilot-scale refiner. The individual bar force profiles are classified as single peak events which feature one peak corresponding to the fiber compression force and as dual peak events corresponding to fiber compression force and the corner force. It is shown that dual peak events which are considered to represent the corner force, are present throughout the whole range of refining and increase with increased refining energy. After applying the dual peak analysis to the data from the previous study this behaviour was also found in the pilot-scale refiner data. Furthermore, it is found that different radial positions on the stator plate are subjected to different force profiles. This is thought to be due to the difference in tangential speed and a change in the fiber and floc material properties at different radial positions.

In the third study the effect of refiner plate wear on bar force sensor measurements is explored by applying the dual peak analysis to long term data acquired from the mill-scale refiner. Bar passing events are analysed based on the dual peak ratio and the timing of the early peak in the dual peak events. Force measurements are evaluated over the full run time of a set of refiner plates. When comparing force profiles with refiner plate wear measurements and discharge fiber analysis, it is found that the decrease in the prevalence of the corner force correlates with the wear of the leading edge of the refiner bars, or bar rounding, for the run time of the refiner plate. This is accompanied by a decrease in plate performance which is represented by a decrease in fiber length and freeness reduction for the same refiner load.

Table of Contents

List of Tables

List of Figures

Nomenclature

At	air dried ton (weight measurement for pulp)
BEL	bar edge length
BPE	bar passing event
Bt	bone dry ton (weight measurement for pulp)
C	consistency of the feedstock (%)
d_E	diameter of the encoder wheel
d_{ra}	diameter of the rotor axis
F	bar force
HC	high-consistency
LC	low-consistency
L_w	Length weighted fiber length
n	number of fibers
P	net power
p_g	gap between plates (mm)
Q	mass flow
RFS	refiner force sensor
s	bar width
SD	single disc refiner
SEL	specific edge load
SPF	spruce pine fir
SRE	specific refining energy
TMP	thermomechanical pulp
U	tangential speed
$\Delta\varphi_E$	angle of rotation of the encoder
$\Delta\varphi_{ra}$	angle of rotation of the rotor
ω	rotational speed

Definitions

Corner force	Force action on the corner of the refiner bar.
Critical gap	Plate gap below which fiber cutting occurs.
Defibration	Separation of wood chips into individual fibers.
Fibrillation	Brushing and collapsing of fiber walls during refining.
Fines	Fibers and fiber pieces smaller than 0.5 mm.
Floc	Fibers that have grouped together after having been separated from their original wood matrix.
Friction force	Force action on the surface of the refiner bar.
Grammage	A measure of the apparent density of a physical sheet of paper, also referred to as the basis weight.
Microfibrils	Bundles of celluloses strands with crystalline regions which make up the fiber walls.
Plate gap	Distance between refiner plates, usually between the stator and the respective rotor.
Residence Time	Amount of time that the fiber remains in between the plates during operation.
Shive	A fragment of a chip which is often the result of having passed through the refiner relatively unprocessed.

Acknowledgments

First I would like to thank my supervisor, Dr. Peter Wild. The combination of motivation, patience and enthusiasm that he provided as well as his leadership and guidance through out this project, made this work come together the way it did. Besides my supervisor I also want to express my sincere thank to Dr. James Olson (University of British Columbia), for supporting me with insightful comments and productive conversations and feedback on our research.

I also want to thank the staff of the Institute for Integrated Energy (IESVic), Pauline Shepherd, Susan Walton and Jeremy Riishede for their advice and support and for making the IESVic community a welcoming and nurturing environment.

I further want to thank the staff of the Pulp and Paper Centre at the University of British Columbia especially Meaghan Miller, Reanna Seifert and George Soong for their assistance during the refining trials at UBC, and for conducting the sample characterisations and hand sheet testing.

I also want to express my thanks to the staff at the Catalyst Paper Excellence Mill in Crofton, BC especially, Yu Sun and Chad Toth for their essential support and assistance in preparation for, during and after the mill trials.

Anyone who attempts a task like this one needs not only great support on an academic level but also a supportive and understanding network of family and friends. I therefore want to thank first my brilliant parents Alexandra and Christian. Their never ending and unconditional support is an important foundation in everything I do. Next I want to thank my brother Johannes for his wonderful encouragements and so much more. I also want to thank my friends and family both back in Austria and here in Canada for providing such a great environment for me to relax and recharge my batteries.

Finally, I want to thank my wonderful partner Michelle for her support through the ups and downs of this endeavour. Her patience and love really made this year long journey possible.

1 Introduction

The pulp and paper industry is among the most energy intensive sectors in Canada. In the Province of British Columbia, 11% of the total electrical energy production is consumed by this industry, 80% of which is used for mechanical refining [1]. With the ever increasing costs of energy, the long term survival of mechanical refining depends on the ability to decrease energy consumption per ton of pulp. To achieve this reduction, it is necessary to understand the relationships among process parameters, fiber and paper properties and energy consumption [2].

Due, in part, to the inaccessibility and harsh environment of the refining zone, most common approaches to quantify refining action use the specific refining energy (SRE). This energy-based quantifier is based on global process parameters such as power and flow rate and describe the refining process from macroscopic point of view.

To provide insight to more detailed aspects of the refining process, researchers have investigated the mechanics of the refining process at the scale of forces applied to fibers by refiner bars [3]. One of the approaches taken in this research is based on direct measurement of the forces applied to refiner bars by chips, flocs and fibers [4]. This research has provided insight into many aspects of refining both in the context of experimental, or pilot-scale LC refiners [5] as well as mill-scale HC [6] and LC refiners [7]. In the work presented here, a sensor is used to measure localized forces in both, pilot and mill-scale LC refiners with the goal of comparing and validating findings in both settings. Results and an in-depth analysis of the data are presented.

1.1 Background

Two types of processes are used to convert wood into pulp for use in paper making: mechanical refining and chemical refining [2]. In both, the feedstock is usually wood chips which are most commonly a byproduct of the lumber industry. Wood is a composite structure comprised from cells bonded together by a matrix material. Cells called fibers give wood its structural integrity [2]. The matrix bonding these together is a complex organic polymer called lignin which is located between the cells in a layer called the *middle lamella*. Figure 1 shows the schematic of a wood fiber. The fiber is comprised of several layers of fiber walls which consist of different

forms of *microfibrils*. These fibrils are bundles of celluloses strands with crystalline regions. In the primary wall the microfibrils are irregular and interwoven like a net [2]. The secondary wall, consists of three layers, S1, S2 and S3 which differ in thickness and microfibril orientation. The secondary wall comprises the bulk of the cell wall material and, therefore, largely defines the mechanical properties of the fiber [2].

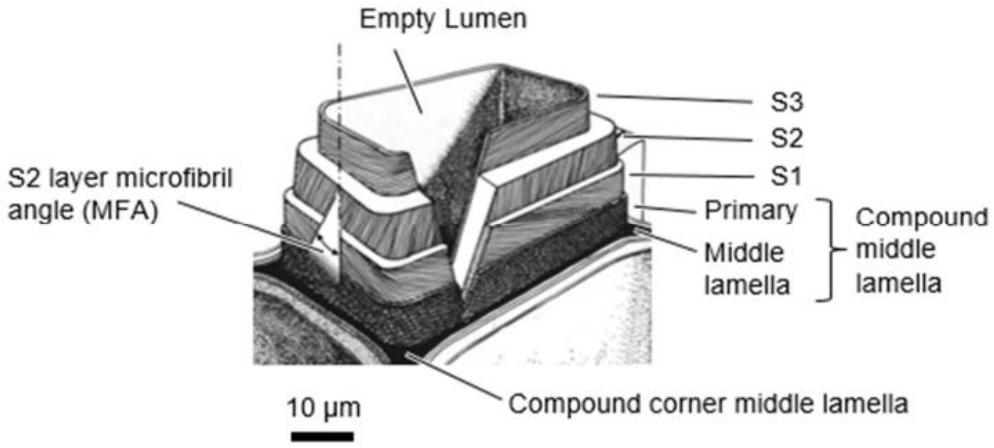

Figure 1: Schematic of a typical wood fiber and the laminar structure of a wood fiber [8].

In mechanical refining, fibers are mechanically separated from each other and from the lignin matrix. Prior to refining, the chips are washed and pretreated with steam to soften the lignin. During refining, the steam softened wood chips are subjected to repeated normal and shear forces which separate the wood fibers. The resulting pulp contains all of the lignin and fibers [2]. The lignin in the pulp reacts with atmospheric oxygen, giving the mechanical pulp a darker color over time, in a process is called *yellowing*. The brightness of unbleached mechanical pulp is 45 - 60% ISO brightness while fully bleached mechanical pulp can reach 55 - 85% ISO brightness [9].

In chemical refining, the lignin is dissolved by a chemical mixture called *white liquor* in which NaOH and Na_2S are the active components. This process is also called *Kraft process*. After the delignification, the remaining liquid or *black liquor,* is separated from the fiber. The organic components in the black liquor are commonly burned for energy production and production of steam for use in the pulp mill. Through a recovery process, NaOH and Na_2S can be reused in the Kraft process [9]. The resulting Kraft pulp contains a high fraction of intact fibers and no lignin. Longer fibers have better bonding capabilities as they have more surface to bond with each other

in the paper making process. As a result, paper made from Kraft pulp typically has high *tear index* [2] which describes the force necessary to prolong an existing tear through two layers of paper.

Mechanical refining reduces fiber length because the mechanical separation of the fibers from the wood matrix often leads to fiber breakage. Fiber fragments that are smaller than 0.5 mm, are referred to as *fines*. Mechanically refined pulp comprises more fibers of reduced length, compared to the intact fibers of the chemical pulp. The mechanically refined pulp also contains fiber fines and residual lignin [9]. A big advantage of the mechanical refining process is its high yield. While the yield in chemical refining lies close to 50% because the lignin gets washed out, the yield in mechanical refining lies above 95% as the lignin stays in the pulp [2].

Mechanical refiners typically comprise at least one rotating disc, *rotor*, and one stationary disc, *stator*, affixed with refiner plates or plate segments, as shown in Figure 2. Plates used in most commercial refiners are comprised of one or more refining zones on these plates which feature bars and groves whose geometry is defined by bar width, bar height, groove width and bar angle. In addition, *bar edge length* (BEL), is defined as the total length of bar edges swept by bar crossings during a single rotation of the disc. These parameters collectively define the *plate design* [2].

The makeup of the feedstock is usually described by its c*onsistency* which is defined as the percentage by mass of wood fibers in the total fiber-water mixture. The pulp and paper industry uses this term to distinguish between two major refining processes. In high-consistency (HC) refining, the stock enters the refiner in the form of wood chips or rough fibers at consistencies greater than 20%. High consistency refining is commonly used as the first or primary stage in multi-stage refining processes [2]. In low consistency (LC) refining, the feedstock comprises a slurry of fibers, often mixed with *shives* (groups of wood fibers that have not been separated) and fines, rather than chips, typically at less than 5% consistency. LC refining is commonly used as a post-treatment for chemical pulp but is also used as a later stage in refining for mechanical pulps [2].

The feedstock, composed of wood fibers and water, is fed through the eye of the stator. The circular motion of the rotor, as in a centrifugal pump, and the feed pressure result in a radially outward flow of pulp in the refining chamber. Pulp moves both in the grooves between the bars

on the rotor and stator plates and in the space between the bars of the stator and rotor [2]. Fiber flocs caught on the edges of the rotor bars are periodically dragged over the bars of the opposing plate. The passage of rotor bars over the stator bars, *bar passing events* (BPE), subjects the pulp fibers to cyclic shear, compression and bending and leads to delamination of the fibers. Geometric design parameters such as bar width, groove width and bar angle (i.e., relative to the radial direction) as well as process parameters such as *plate gap*, clearing between the refiner plates, *flow rate*, volume flow through the refiner, and consistency define the refining process and the resulting pulp properties [10].

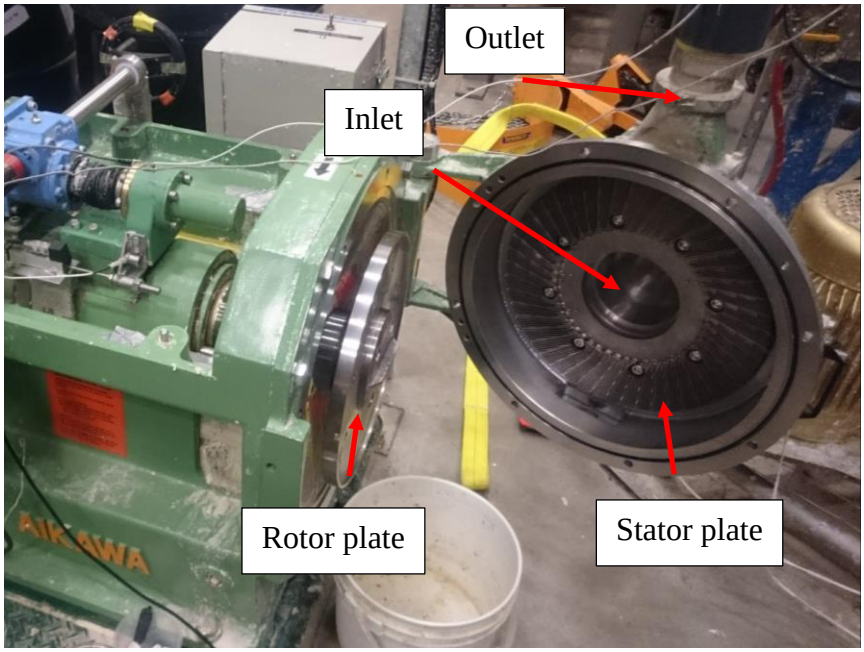

Figure 2: AIKAWA 16" single disc refiner with stator door open.

Refining action leads to significant heat generation which, in combination with the produced steam, softens the fibers and the lignin and aids the refining process. The refiner stock is collected at the periphery of the refining chamber and directed to further processing [2].

Shown in Figure 3 are schematic drawings of single, double and twin-disc refiners. The single-disc (SD) is the simplest design and is composed of one rotor, and one stationary disc or stator. The rotor can be moved in the axial direction to adjust the plate gap [11]. The double-disc design has two rotors, each driven by a separate motor and rotating in opposite directions [11]. In this design either both or one of the rotors moves in axial direction. This refiner is designed for

high intensity refining. It requires less energy to obtain the same *freeness*, which characterizes the drainage resistance of pulp [12].

The twin-disc refiner can be thought of as two single-disc refiners that share the same rotor. The rotor has refining plates/bars on both faces, creating *twin* refining zones. In the twin design, the rotor is supported only by radial bearings (i.e. no axial bearings) and is allowed to *float* axially between the stators. Equal distribution of stock on the two sides of the rotor is used to balance the gaps and refining forces in the two refining zones. This design provides increased refining area without a proportional increase in the disc diameter. The result is an increase in *production rate*, usually measured in tons of pulp produced per day (t/d), and is a major factor in the popularity of this design [11] [2]. Figure 4 shows the flow path of the pulp for a twin disc refiner. The pulp is feed from the center and passes on both sides of the stator through to the periphery where it exits the refiner [11].

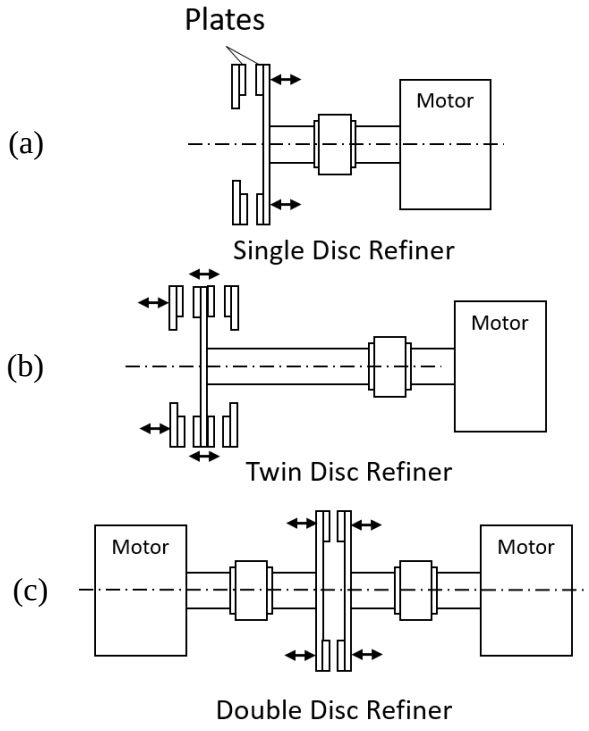

Figure 3: Schematic of three common mechanical refiner designs.
(a) single disc refiner, (b) twin-disc refiner, (c) double dis refiner.
The axial moving refiner plate is indicated through arrows. Based on [11]

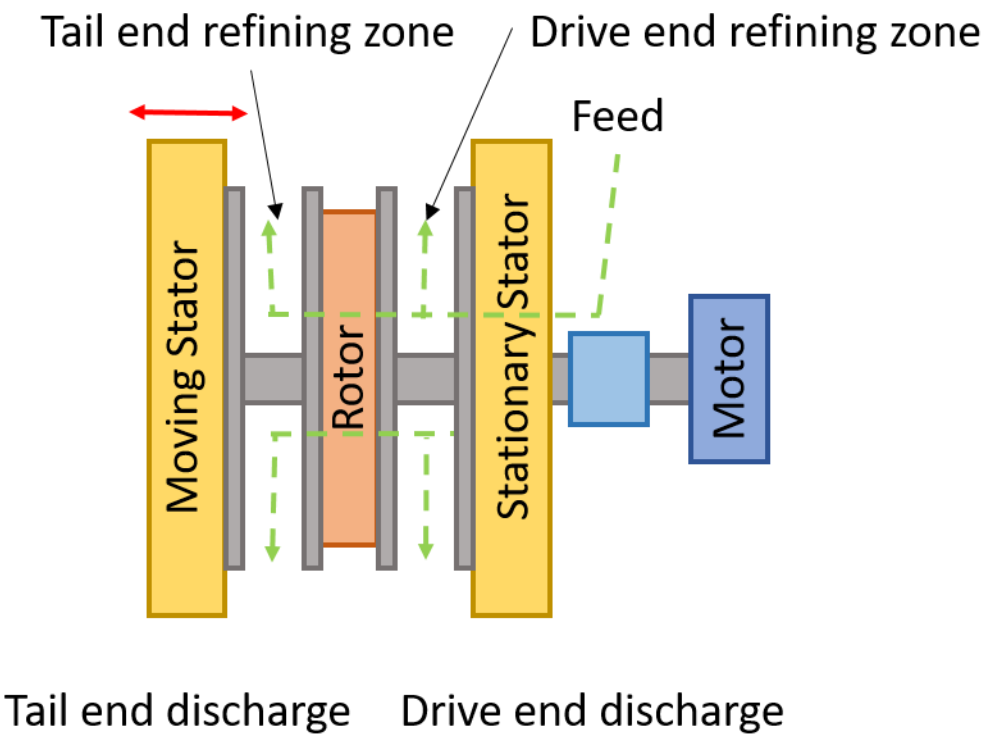

Figure 4: Schematic of a Twin-flo refiner.

Plate designs for HC refining and LC refining differ. *Breaker bars* are located in the radially innermost section of the refining zone of HC refiner plates, close to the feed zone. These bars are used to break woodchips into smaller pieces or *shives*, before moving to the outer parts of the refining zone where smaller bars then break the shives into fibers and *flocs* (i.e. bundles) of fibers. In LC refining, on the other hand, no breaker bars are needed as the feed material is already a pulp-water mixture. Plate patterns in LC refining typically feature bars that are more fine and grooves that are less deep than in HC refining. [13] [14].

Pretreatment of the fibers have significant impacts on the expended energy in refining and on the final fiber properties. Typical pretreatments include exposure of the wood fibers to sodium sulfite or sodium bisulfite which lowers the lignin softening temperature [9]. Softened lignin, for example, eases the fiber detachment in mechanical refining [2] which results in higher long fiber content and, therefore, higher paper strength while also reducing the energy expended to heat the stock by allowing the process to operate at lower temperature [9].

A good understanding of the relationships among the process variables and the final properties of the paper is essential to improving the LC refining process. In LC refining, refiner process variables include plate gap, rotational speed, pulp consistency, refining power and *specific energy* (i.e., the amount of energy transferred to the pulp per dry unit mass). These variables are key factors in determining pulp quality and energy consumption. Pulp properties, such as fiber length and freeness, are also affected by these process variables and are known to correlate with properties of the resulting paper, such as tear index and *tensile strength*, which indicate the strength of paper in tear and when pulled at opposite ends, respectively. For example, tear index was found to be lower when length weighted fiber length was lower [15].

As noted above, one of these process variables is the plate gap. Elahimehr and Luukkonen showed that plate gap is linearly and inversely related to *net refining power* [12] [16], which is the refining power in excess of no load power. Figure 5 shows an example of this relationship at three rotational speeds for a single disc LC refiner. In this figure, $^{1}/_{Gap}$ is the inverse of the plate gap which is variable. It is shown that, up to a certain *critical gap* (G_c), net power is linearly proportional to the inverse of gap size. This critical gap, correlates with the onset of fiber cutting as the gap is closed [17]. The critical gap is a function of rotational speed and increases as rotational speed increases. For gap sizes smaller than the critical gap, the relationship between the net power and inverse of gap deviates from linear. The figure also shows that the power-gap relationship is strongly affected by angular velocity and that, at a high angular velocity, significantly higher powers can be reached at the same gap [18].

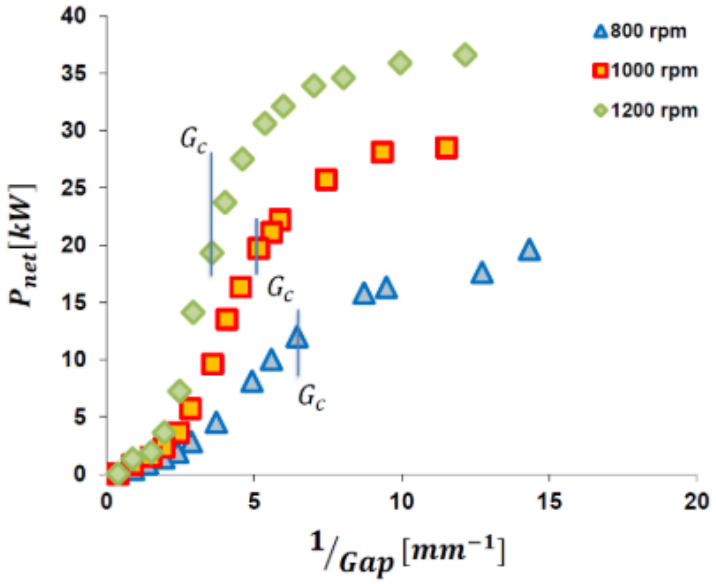

Figure 5: Net power vs inverse plate gap. [12]
Correlation between Net Power Number and inverse plate gap for a specific plate pattern (BEL=0.99 km/rev) for a single disc LC – refiner. Indicated is the critical gap Gc.

As discussed above small plate gaps correspond to a low fiber length, as shown in Figure 6. The figure shows further the constant fiber length for wide plate gaps and the change in fiber length after the critical plate gap. Decreasing plate gap has also been shown to cause decreasing tensile index [19].

Another key refiner process variable is the *Specific Energy*, which is the amount of energy transferred to the pulp per unit mass. It has been shown that, similar to the plate gap, the Specific Energy is closely related to the fiber length and the freeness of the resulting pulp mixture [19]. An increase in specific energy leads to a lower freeness. The relationship between freeness and Specific Energy is shown in Figure 7 for several different plate patterns at varying rotational speeds. Both, freeness and fiber length correlate with key paper properties such as tear index and tensile index [19].

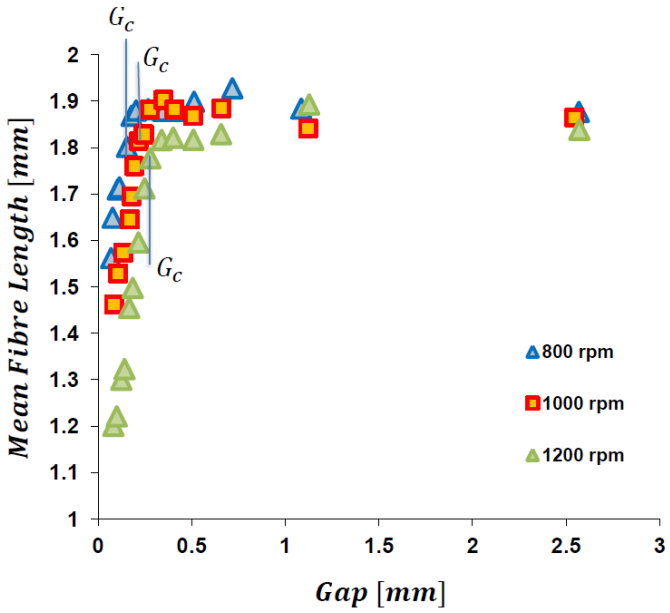

Figure 6: Influence of process variables on pulp properties.
Mean length weighted fiber length for various plate gaps for a specific plate (BEL=0.99 km/rev) [12]

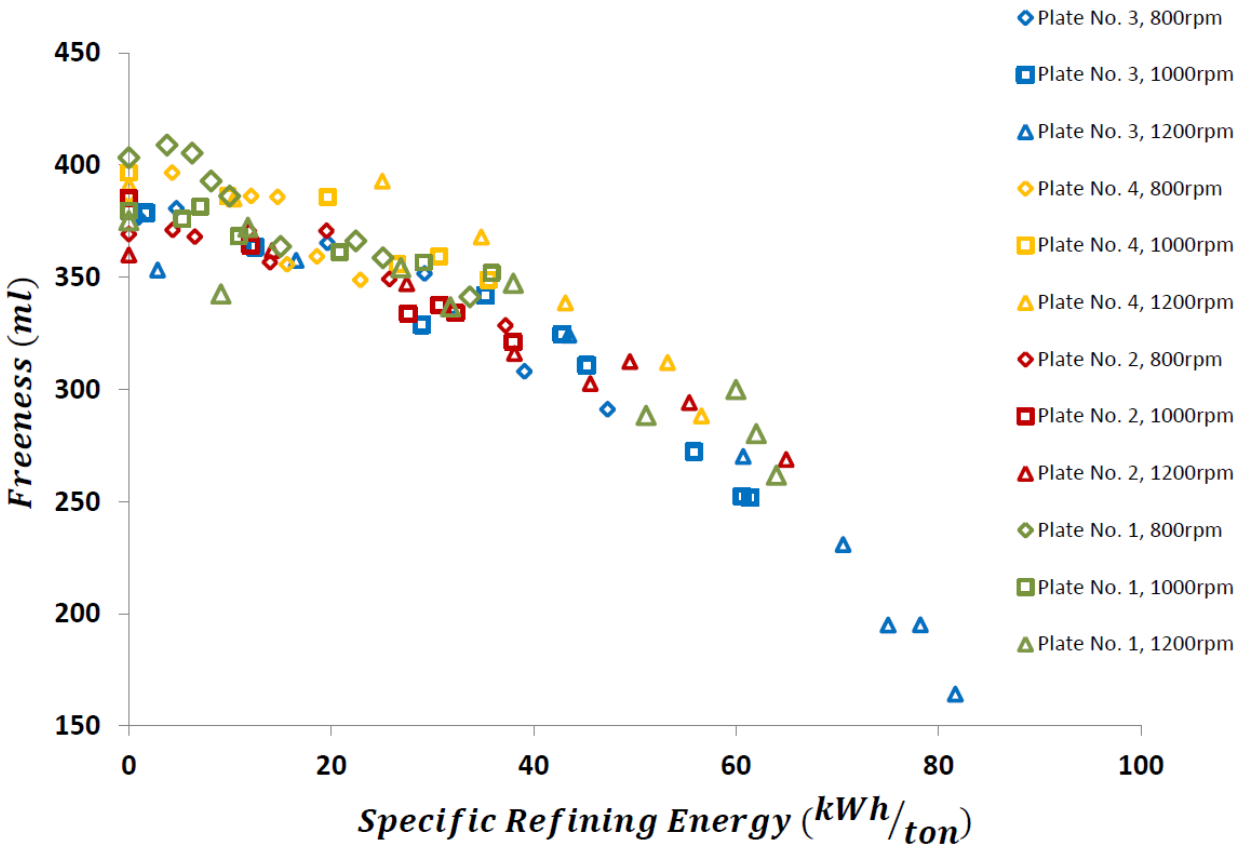

Figure 7: Freeness drop for increasing Net Specific Energy [12].
plate 1: BEL=5.59 km/rev, plate 2: BEL=2.74 km/rev, plate 3: BEL=0.99 km/rev, plate 4: BEL=2.01 km/rev

As suggested by Kerekes and Senger [21], it is ultimately the forces applied to the fibers that perform the work to develop fiber properties and these forces are directly related to the energy consumed in the refining process. Understanding these forces is, therefore, a necessary step in realizing further optimization of the refining process.

One of the first experimental studies of forces in LC refining was conducted by Goncharov [22] using strain gauges fixed to a L-shaped beam extending into the refining zone and replacing a short section of a refining bar. The sensor was only able to measure at a bar passing frequency of less than 2 kHz and had a range of 4N. The results show force peaks which appear when the rotor bars move on to the instrumented stator bar and the return of the force magnitude to zero before the rotor bar moves off the stator bar [22]. A drawback of this design was the low sampling frequency which was not sufficient for application in a production refiner with a bar passing frequency of upwards of 3 kHz.

Gradin et al. [23] developed force sensors to measure shear forces applied to individual bars inside a refiner and used this force data to calculate power distributions. Two sensor designs were developed (Figure 8). In the first design, the refiner bar was cut into segments and the strain gauge installed on each segment while in the second design, the strain gauges were positioned along the length of a continuous bar. The strain gauges measured the strain at the base of the refiner bar or bar segment resulting from the shear force applied to the bar tip (i.e., the force applied to the bar tip in the tangential direction). Drawbacks of this sensor design are that the strain gauges are exposed to the refining process (i.e. high temperature fluids) and are subject to abrasion from the pulp. Moreover, installing strain gauges inside the grooves is difficult and for smaller bars, may not be possible. The accuracy and survival of the sensors were not reported [23].

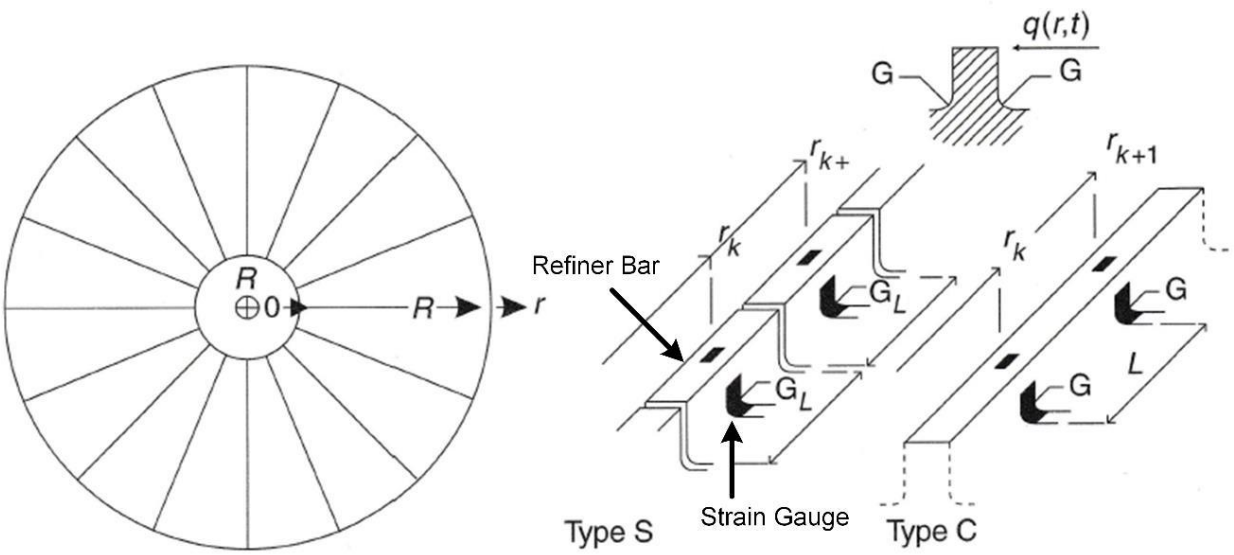

Figure 8: Strain gauge sensors developed by Gradin et al. [23].
Tangential force intensity and radial distance are shown by q(r,t) and r_k, respectively.

Forces during bar-passing events have also been studied using a single bar refiner [24]. This set up consists of two opposed, horizontally positioned discs with a vertical axis, as shown in Figure 9. A single bar is mounted to each disc (Figure 9 (b)). The bottom plate rotates at 3 rpm and the plate gap can be adjusted. Flocs, which were artificially placed on the floc holder shown in Figure 9 (b), are trapped between the bars as the bars cross, and the resulting normal and shear forces were measured [25].

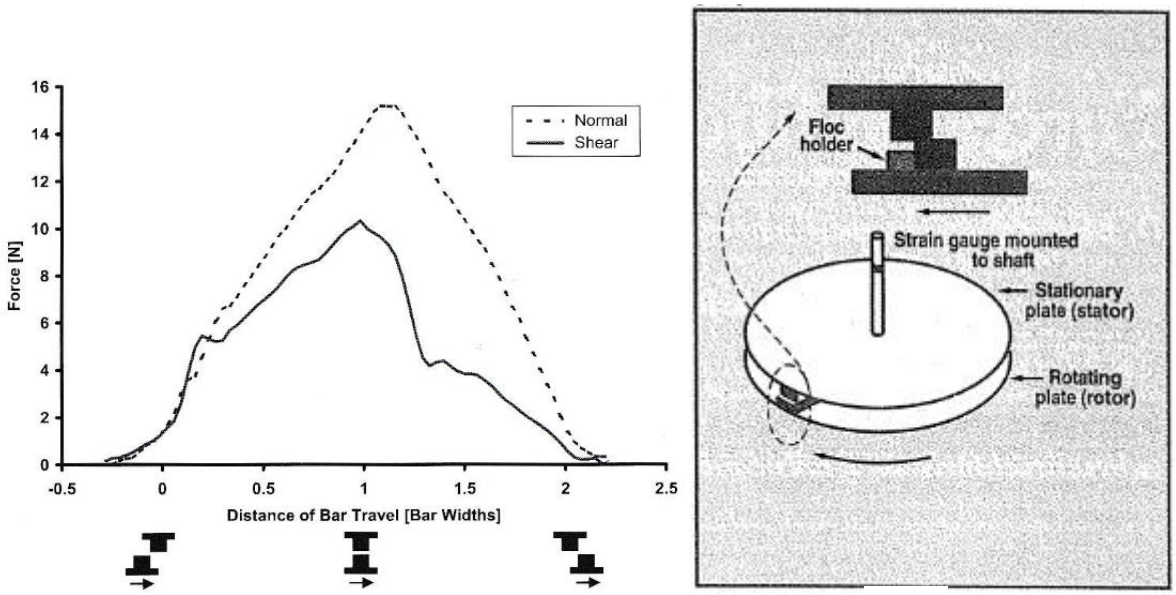

(a) (b)

Figure 9: Single bar refiner set up and force profile.
(a) normal and shear force profile over bar passing event as determined by Senger [24]
(b)Single bar refiner set up as described by Kerekes et. al. [25].

In this study, it was found that the normal force shows a symmetric force profile over the bar passing event with a peak at the center of the observed period, Figure 9 (a). In contrast to the normal force, the shear force shows an asymmetric profile over the bar passing event [24]. This behavior was also shown by Olender et al [26] and Prairie at al [27]. The shape of the shear force profile over a single bar passing event shows a slow increase in the first half of the bar passing. This correlates with the normal force profile. In the second part, after the bars overlap fully, the shear force shows a fast decline until it decreases at a similar rate as the normal force. This characteristic shape is assumed to be due to the fact that the total shear force at any point along the refiner bar is the sum of the friction force and a so called *ploughing* force or corner force [28]. The friction force is the part of the shear force that affects the fiber when it is dragged over the surface of the refiner bar. It is the part of the shear force that is proportional to the normal force and connected with it through the coefficient of friction. The corner force acts on the leading edge of the bar. As the leading edges of the bars only interact with each other in the first half of the bar passing, the literature suggests that the corner force is responsible for the asymmetric shape of the shear force profile [28]. The corner force shows a strong relationship with the form of the bar edge. A sharp edge results in a higher corner force [21].

To separate the corner force from the friction force it was suggested that the ratio between the average shear force and the average normal force represent an *equivalent coefficient of friction* [21]. Through this coefficient the friction force can be calculated for a known shear and normal force profile. The equivalent coefficient of friction was found to increase with increasing consistency and with increasing flow weight and it was seen to decrease with an increasing extent of bar wear for HC refining [21]. As the shear force at any point is the sum of the friction force and the corner force [28], the corner force can be determined through knowledge of the friction and shear force.

Olender developed a piezo ceramic refiner force sensor (RFS) based on the work of Siadat et al [10]. Olender's sensor was installed in a mill-scale refiner and in a pilot-scale refiner in the Andritz research center in Springfield, Ohio in the USA [26] and at the Catalyst Paper Corp. mill in Port Alberni, BC [29]. The sensor replaces a short length (5 mm) of the stator bar and houses two piezo ceramic elements that generate electric charge, which is converted to a measurable voltage with a charge amplifier, when submitted to a force. A photograph and section view of the sensor design are shown in Figure 10. The section view shows the probe tip, which replaces the refiner bar, sitting on two piezo elements which are seated on the plug. These components are contained in the sensor housing which has a sealed opening on its backside. The RFS has since then been used to measure forces in axial direction on the sensor tip, normal forces, and forces in the rotation plane, perpendicular on the refiner bar, shear forces. The sensor has been installed in mill and pilot-scale refiners as well as in HC and LC refining.

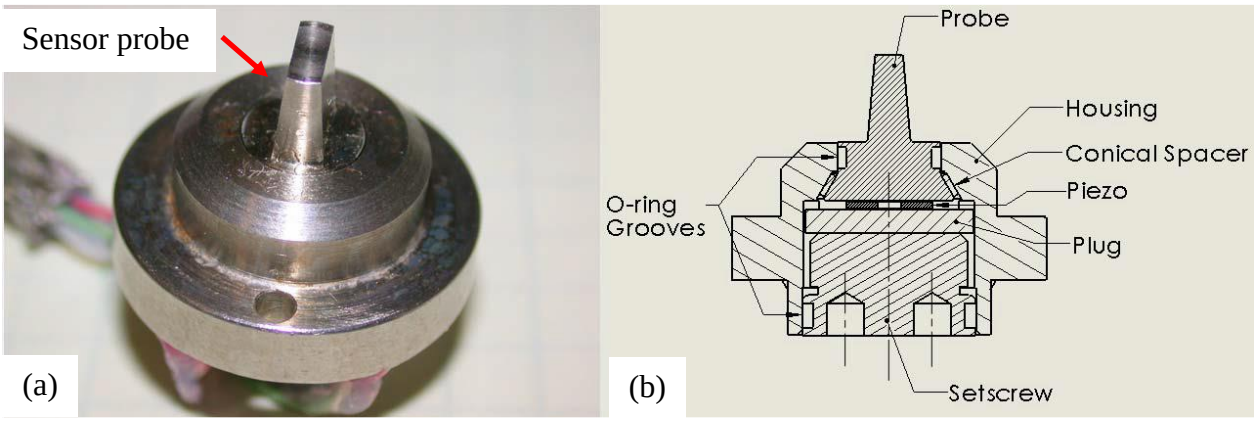

Figure 10: Refiner force sensor.
Photograph (a) and section view (b) of RFS designed by Olender [26].

The trials in Springfield where conducted in an HC primary stage chip refiner, whereas the trials in Port Alberni were conducted on a mill-scale HC reject refiner. Olender's findings show a difference in the force pattern for primary stage HC refining (Springfield) to reject HC refining (Port Alberni). Namely, the mean peak normal and shear forces were highest in the periphery of the refining zone for reject refining and highest overall close to the center of the refining zone in primary stage refining [26]. A possible explanation for the difference in these trends considers that shives, which are naturally more prevalent at the center of the primary stage chip refiner and not at the reject refiner, induce larger force impacts than refined pulp at the periphery of both refiners for a given plate gap [26].

Further, Olender investigated the prediction of plate clash based on force sensor data. They were able to detect plate clash events several seconds before a commercial accelerometer-based system in both refiners [29].

Prairie installed an RFS in one location in a Sunds Defibrator Conflo® JC-00 LC conical refiner at the FP Innovation Vancouver laboratory. Trials were conducted using Chemi-Thermo Mechanical Pulp (CTMP) at a consistency of 3.15%. It was shown that although the shear and normal force profiles are similar, the shear force magnitudes are typically 10-20% of the normal force magnitudes [4], [7].

Prairie analyzed the force data based on their distribution. They showed that normal and shear force distributions are essentially shaped normal with a small skew towards smaller force values. They also found that the median normal and shear forces increased with increasing SEL while the shape of these distributions is relatively independent of changes to SEL. Prairie suggested that the knowledge of the distribution of forces could provide greater insight to predict the probability of forces responsible for fiber cutting at different SEL [7].

In his research, Harirforoush installed a RFS in an AIKAWA/Advanced Fiber Technologies 16'' single-disc LC test refiner. He performed trials using mechanical softwood SPF pulp with 378 ml CSF at 2.5% and 3.5% consistency at a rotational speed of 800, 1000 and 1200 rpm. The distributions of the peak normal and shear forces show that the onset of fiber cutting consistently corresponds to a distinct transition in the length-weighted fiber length data. Based on this, he argues that this transition is caused by a fundamental transition in the fiber-bar interaction

and suggests that bar force sensors have potential to be used for in-process detection of fiber cutting [30].

Harirforoush also identifies a non-linear relationship between bar force magnitudes and length-weighted fiber length. He proposes that this behavior is similar to the relationship between length-weighted fiber length and the inverse of plate gap [31]. A reduction of the plate gap results in a relatively constant length-weighted fiber length, whereas the net refiner power and the mean peak normal and shear forces increase. These trends continue up to threshold values of mean peak normal and shear forces of approximately 8 N and 2.4 N, respectively. Above those thresholds, mean peak normal and shear forces were shown to continue to increase. The length-weighted fiber length, on the other hand, shows an inverses linear relationship with these forces [31] (Figure 11).

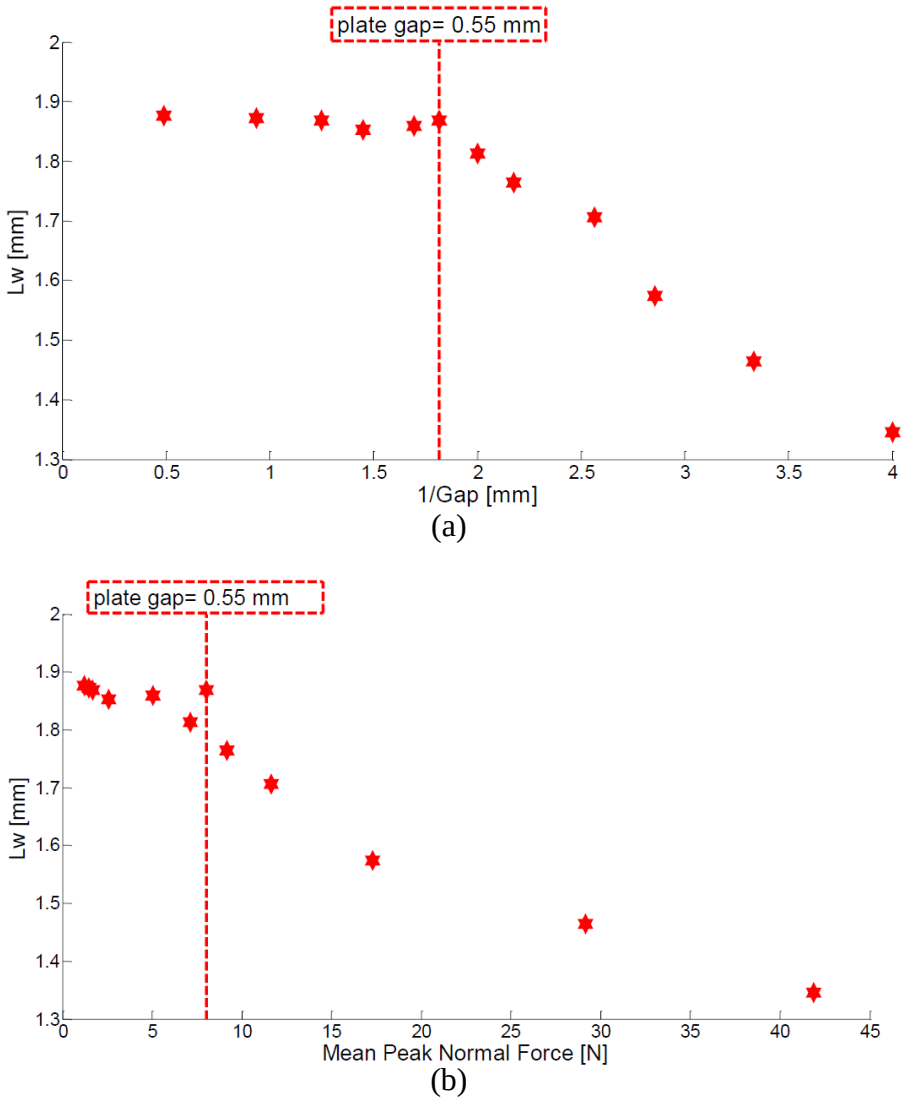

Figure 11: Power of the time domain of the normal force over the plate gap [31]. *Test conditions were rotational speed of 1200 rpm and pulp type was SPF.*

Furthermore, the effect of pulp furnishes on measured bar forces and, more specifically, on the detection of fiber cutting was investigated by Harirforoush. He conducted further trials using hemlock/balsam softwood thermomechanical pulp, spruce pine fir (SPF) softwood thermomechanical pulp, northern bleached softwood Kraft pulp, and aspen hardwood thermomechanical pulp at 3.0 to 3.5% consistency at rotational speeds of 1200 and 1400 rpm. He introduced the power of the time domain signal of the measured forces which is defined as the sum of absolute squares of the time domain divided by the signal length. Harirforoush uses this power value, which is different from the mechanical power, as an indicator of the onset of fiber cutting

which he showed to be a sensitive and reliable metric for determination of fiber cutting for a range of pulp furnishes [17].

In summary, the literature suggests that bar force measurements can provide insights into the refining process that energy-based observations cannot [23]. Analyses of measured bar force data have, to date, been conducted with a focus solely on peak force values. More specifically, these studies have focused on peak normal force [4], peak shear force [24] and the distributions of these parameters [7], [30]. The work presented here expands on previous work by assessing and interpreting qualitative and quantitative changes to measured bar force profiles during bar-passing events.

1.2 Objective

The overarching objective of this research is to investigate relationships between refiner process variables, including changes in fiber and pulp properties, and force profiles during bar passing events in mechanical LC refining. More specifically, this work explores insights gained from registration of bar force data to rotor bar position in an experimental refiner and the application of these insights to bar force data from a mill-scale refiner.

1.3 Outline

At the beginning of this work, with the goal to investigate the effects of plate gaps on bar-force profiles, a high resolution rotary encoder and a piezo ceramic force sensor are implemented in a 16-inch laboratory-scale low consistency refiner. The sensor replaces a short length of a stator bar and measures normal and shear forces applied during the passage of each rotor bar, while the rotary encoder is used to locate the rotor bars relative to the stator bar in which the sensor is located. With this set up, force profiles for bar passing events are registered to the position of rotor bars relative to the stator bar in which the sensor is located. The angular reference provided by the encoder makes it possible to generate mean force profiles which shed light on the fundamental mechanisms of mechanical refining. It was found that two types of force profiles exist. For large gaps, there is a single *late peak* in the force profiles that occurs toward the end of the bar passing

event. For gaps that are less than the *critical gap*, below which fiber cutting occurs, there is an *early peak* in the force profiles that occurs at the start of the bar passing event, additionally to the previously mentioned *late peak*. Through fiber length measurement data, it is shown that the occurrence of this early peak correlates with the decline in fiber length through fiber cutting. At this point it is hypothesized that the early peak represents the *corner force* and, therefore, that corner force is causal in the onset of fiber cutting.

To further investigate the force profile in LC refining, a set of piezo ceramic force sensors is implemented in a 52-inch mill-scale low consistency refiner. Here the objective is to explore the effect of varying operating conditions on bar force profiles. In this set up no rotary encoder is used, therefore force profiles for individual BPEs are identified based on key features in the time domain force data. The individual bar force profiles are classified as *single peak events* which feature one *late peak* corresponding to the fiber *compression force* and as *dual peak events* corresponding to fiber *compression force* and the *corner force* which is represented by *the early peak*. Bar passing events are then analysed in the same way as in the pilot-scale study based on their mean force profiles and their dual peak ratio in the bar passing event. It is shown that dual peak events which are considered to represent the corner force, are present throughout the whole range of refining and increase with increased refining energy. This increases the understanding of the way corner force contributes to the refining process. Furthermore, it is found that different radial positions on the stator plate are subjected to different force profiles. This is thought to be due to the difference in tangential speed and a change in the fiber and floc material properties at different radial positions.

To further the understating what conditions impact force profiles and especially the corner force, force measurements at the mill-scale refiner are evaluated over the full run time of a set of refiner plates. Findings are compared with refiner plate wear measurements and discharge fiber analysis. It is shown that the decrease in the prevalence of the corner force correlates with the wear of the leading edge of the refiner bars or bar rounding over the run time of the refiner plates. This is accompanied by a decrease in plate performance which is represented by a decrease in fiber length and freeness reduction for the same refiner loads.

The work described here is presented in three journal papers which are presented in Chapters 2 - 4 respectively with the corresponding results and discussion. In Chapter 2 the refiner bar force sensor and a rotary encoder are installed in a LC pilot-scale refiner to generate spatially registered bar force measurements. This work has been published in 2020 [32]. In Chapter 3 force sensors are installed in a mill-scale LC refiner and force profiles are analysed with regards to their dual peak ratio. This work has been published online in October 2021 [33]. In Chapter 4 long term trends of the force profiles are compared with wear characteristics on the refiner plates. This work has been published online in November 2021 [34]. The revisions to the published papers presented in Chapters 2 – 4, as suggested by the Examining Committee, are included as footnotes in these Chapters.

2 Measurement and interpretation of spatially registered bar-forces in LC refining

2.1 Abstract

A high resolution rotary encoder and a piezo electric force sensor are implemented in a 16-inch laboratory-scale low consistency refiner to explore the effect of plate gaps on bar-force profiles. The sensor replaces a short length of a stator bar and measures normal and shear forces applied during the passage of each rotor bar. The rotary encoder data is used to locate the rotor bars relative to the stator bar in which the sensor is located. Previous work with this type of force sensor focuses primarily on the distribution of the maximum force measured during the passage of each rotor bar over the sensor or *bar passing event, BPE*. In this work, force profiles for bar passing events are registered to the position of rotor bars relative to the stator bar in which the sensor is located. These registered force profiles are measured for a range of plate gaps and two different pulp furnishes. The angular reference provided by the encoder makes it possible to generate mean force profiles. As force data for individual BPEs is highly variable, these mean force profiles have potential to shed light on the fundamental mechanisms of mechanical refining. For large gaps, there is a *late peak* in the force profiles that occurs toward the end of the bar passing event. For gaps that are less than the *critical gap,* below which fiber cutting occurs, there is an *early peak* in the force profiles that occurs at the start of the bar passing event. It is hypothesized that the early peak represents the *corner force* and, therefore, that corner force is causal in the onset of fiber cutting. To explore this hypothesis, a model is presented connecting corner force and friction force to the progression geometric variables during the bar passing event such as the bar edge length engaged at any point in the bar passing event and the area covered by the rotor bar on the force sensor at any point in the bar passing event.

2.2 Introduction

In refining, it is ultimately the forces applied to fibers that perform the work to develop fiber properties and these forces are directly related to the energy consumed in the process. Understanding the forces on refiner bars or *bar forces* in refining is, therefore, a necessary step in realizing further optimization of the refining process, as suggested by Kerekes and Senger [21].

Traditional approaches to characterization of refining rely on readily available parameters such as net power, pulp flow rate, consistency, refiner plate geometry and rotational speed. Based on these parameters, measures of refining intensity (RI), including specific edge load (SEL), and specific refining energy (SRE), have been widely used to further characterize the refining process [35], [36].

SRE is the energy expended per unit mass of fiber and is calculated as,

$$SRE = \frac{P}{Q\ C} \tag{1}$$

where, P is net refiner power, Q is the mass flow rate of pulp and C is consistency. On its own, SRE does not uniquely describe refining action as it has been shown that the same SRE can lead to different pulp properties [37]. For example, high intensity LC refining can achieve a lower freeness than low intensity LC refining at the same SRE. It is also shown, however, that low intensity LC refining can achieve a higher tensile strength at the same SRE compared to high intensity LC refining [37]. Several studies have presented methodologies to predict pulp properties based on specific refining energy, including but not limited to Miller et al. [37], Elahimehr et al. [12].

Specific edge load (SEL) is a measure of refining intensity and the energy expended per bar-crossing with respect to the bar length [21], calculated as shown in Equation (2), where P is net refiner power, BEL is bar edge length, ω is rotational speed. BEL is determined empirically for each refiner plate [38].

$$SEL = \frac{P}{BEL\ \omega} \tag{2}$$

By inspection of Equation (2), it can be seen that an increase in rotational speed[1] can lead to a decrease in SEL while refiner power remains unchanged. SEL also offers insight into the influence of process variables on pulp quality. For example, a high SEL leads to a reduction in fiber wall thickness [11]. Further it has been shown that low SEL is a pre-condition for preserving

[1] At constant power

fiber length and strength development in LC refining of mechanical pulps. Knowledge of SEL allows a theoretical estimate of the final pulp qualities [39].

Based on SEL, Kerekes and Meltzer [38] propose a method to approximate the bar force, *F*, as shown in Equation (3).

$$F = \frac{SEL}{s} \tag{3}$$

In this expression, SEL is energy per bar length, *s* is the bar width and *F*, therefore, is the force per unit bar width[2] in the direction of bar movement [38]. By inspection, Equation (3) shows that, for the same SEL with different bar widths, the forces vary. This leads to the conclusion that bar forces per bar length, "*is a useful parameter to describe threshold force levels below which levels of fiber cutting can be avoided*" [38].

Prairie et at al. [27] measured forces on bars in a Sunds Defibrator Conflo® JC-00 LC refiner using a piezo electric force sensor, or Refiner Force Sensor (RFS), which is a predecessor of the sensor used in the current study. Prairie's study reveals important details of the normal and shear force profiles. In Figure 12, profiles of the shear and normal forces are shown over several bar passing events (BPE). The normal force profile has a distinct peak in the beginning followed by a sharp fall after the peak and low forces towards the end. Shear forces show a not so distinct peak followed by a decline similar to the normal force profile but less steep and several peaks at similar amplitudes.

[2]Note that Kerekes uses the term *length* for this parameter.

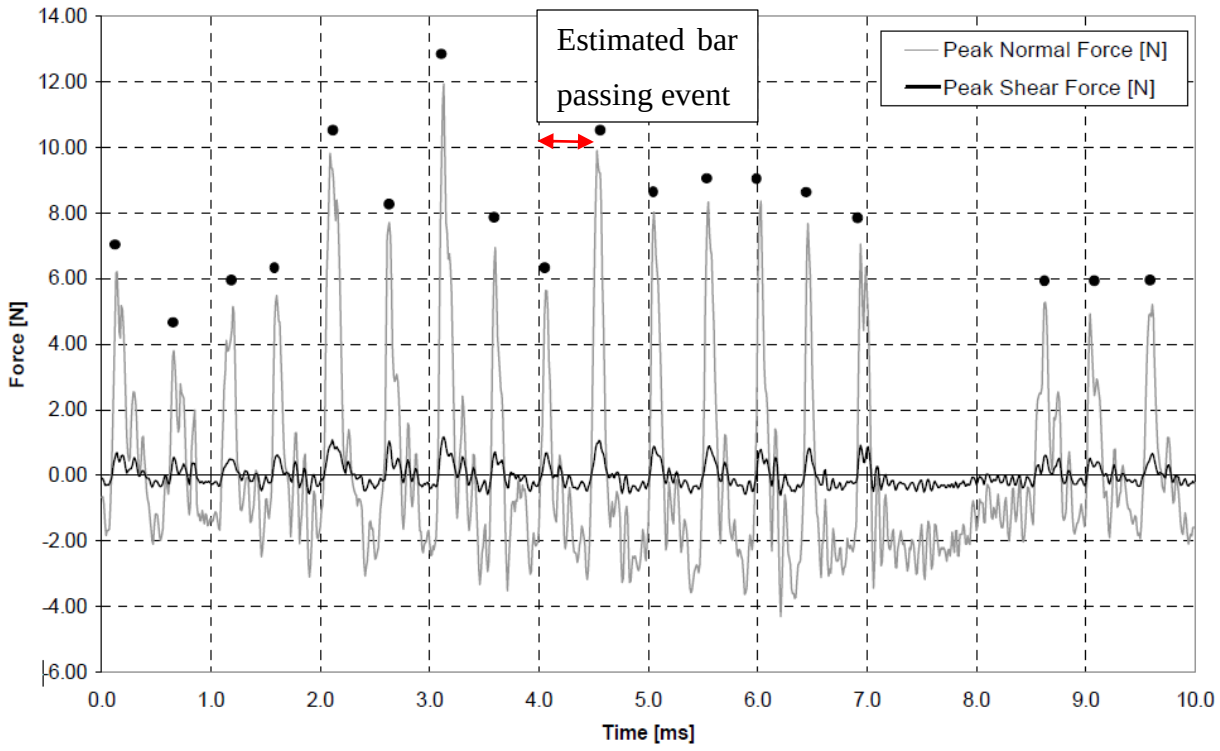

Figure 12: Typical unfiltered normal force and shear force profiles [27].

The shapes of the shear and normal force profiles can be explained by a model in which total shear force is the sum of the *friction force* and a so called *ploughing* or *corner* force. In this model, first introduced by Martinez et al. [25] and further developed by Kerekes et al. [35], the corner force arises as leading edge of the rotor bar approaches the forward edge of the stator bar, compressing pulp in the intervening gap [21]. The corner force has been shown to have a strong relationship to the shape of the bar edge. A sharper edge results in a higher corner force whereas a rounder edge results in a lower corner force [21]. Once the leading edge of the rotor bar passes beyond the forward edge of the stator bar, the corner force falls off and, over the second half of the BPE, the friction force, caused by the fibers being dragged over the surfaces of the refiner bars, dominates the signal.

In a study of normal and shear forces in LC refining, Harirforoush installed a RFS, based on the design used by Prairie [27], in an AIKAWA/Advanced Fiber Technologies Inc. 16'' single-disc low consistency (LC) refiner. Trials were conducted with chemi-thermomechanical softwood SPF pulp with 378 ml CSF at 2.5% and 3.5% consistency at a rotational speed of 800, 1000 and

1200 rpm. The analysis of the peak normal and shear forces shows that the onset of fiber cutting consistently corresponds to a distinct transition in the distribution of these peak forces as the plate gap is closed. The gap at which this occurs is referred to as the *critical gap* [18]. Based on this, Harirforoush argues that this transition is caused by a fundamental but unknown change in the fiber-bar interaction [17] [30].

In all previous studies using the RFS, analysis of the force data has been performed in the absence of data that defines the position of the rotor bars relative to the stator bar in which the RFS is located (Olender et al. [4], [26], Harirforoush et al. [31], Prairie et al. [7]). As a result, these studies have a limited ability to assess the mechanics of the interactions of the pulp with the refiner bars.

There is one study in which both bar force data and angular position data were collected. Fredrikson et al. [40] instrumented a RGP-44 TMP HC refiner with three RFS to measure bar forces and a rotary encoder to measure the angular position for the rotor. These measurements were used to associate features in the time domain force signals, such as peak force magnitude, with corresponding bars on the rotor [40]. However, the angular position measurements were not used to illuminate the details of the interaction between a rotor bar, a stator bar and the intervening pulp, at the scale of an individual bar.

In the current study, bar forces are measured with an RFS and the angular position of the rotor is measured, using methods similar to Fredrikson et al. [40]. In addition, a signal is collected once per revolution to enable spatial registration of the bar force data with the angular position of the rotor bars, relative to the bar in which the RFS is located. This spatially registered bar force data reveals a transition in the timing of the peak normal force, that is coincident with the onset of fiber cutting and which informs our understanding of the role of corner force in LC refining.

2.3 Methods

This section gives an overview of the experimental set up as well as how the data was collected and processed.

2.3.1 Refiner

The refiner used in this work is the AIKAWA 16” single-disc refiner located at the Pulp and Paper Center (PPC) at the University of British Columbia (UBC), Canada. The refiner is equipped with a power meter, variable speed drive and a variable plate actuation. The refiner plates are manufactured by AIKAWA FINEBAR and feature a BEL of 2.74 km/rev and bar angle of 15° from radial. The bar width, groove width, and groove depth of the plate are 1.6 mm, 3.2 mm, and 4.8 mm, respectively.

2.3.2 Force sensors

The RFS-type sensors were custom designed for the trails, based on the work of Olender et al. [41], Prairie et al. [27] and Harirforoush et al. [30]. In this design, the sensor probe replaces a 5 mm length of a bar on the stator plate, as shown in Figure 13. This probe is supported by two piezo elements which emit signals that are processed to independently determine the shear force and the normal force applied to the probe. A picture of the sensor is shown in Figure 14. Two sensors are positioned on opposite sides of the stator plate, as shown in Figure 15 (a) at a radius of 151mm. Data from sensor #1 is presented in this work.

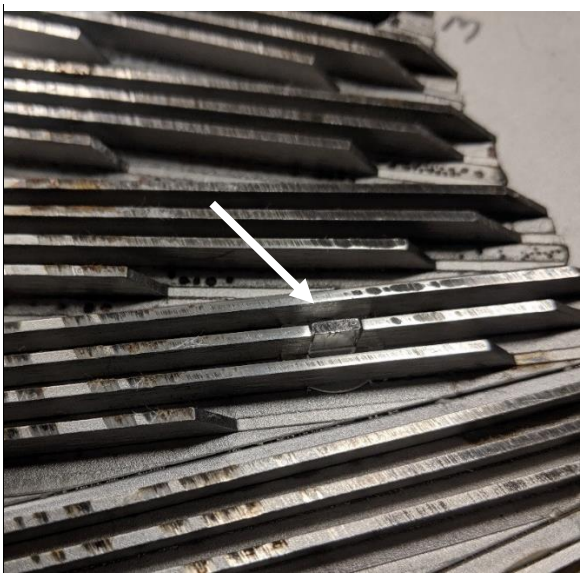

Figure 13: Refiner bar force sensor,
indicated by the arrow, replaces short section of a stator bar.

Figure 14: Picture of the RFS.

Both the stator and the rotor plates feature 48 clusters of three parallel bars each, at the radial position of the sensor (Figure 15 (a)). In Figure 15 (b), a top down view of a bar cluster is displayed. During a full revolution of the rotor, 144 rotor bars pass over each sensor. The sensors are located in the second bar of their respective bar clusters (see Figure 13).

(a) (b)

Figure 15: 16" refiner plates used in the test refiner at UBC. BEL 2.74 km/rev.
(a) stator plate with sensors indicated by the arrows (b) close up view of bar cluster

Each sensor is calibrated using a modal hammer (PCB Piezotronics/086D80-12911/ Depew, New York) as described in Prairie et al. [27]. This calibration is conducted before and

after the refiner trials and the calibration constants are compared to validate the functionality of the sensors and detect any damage they received during the refiner trials. Post–trial calibration of the sensors showed less than 10% variance with respect to initial pre-trial calibration.

2.3.3 Angular position measurement

A high resolution rotary encoder is adapted to the refiner (Figure 17) to measure the position of the rotor during the trials. The rotary encoder (SICK/ DFS60A-S4PC65536/ Richmond Hill, Ontario) has a resolution of 65,536 samples per revolution which gives a resolution of 182[3] increments per degree of rotation.

Figure 16 is an isometric view and Figure 17 a photograph of the encoder assembly installed in the refiner. The encoder is equipped with a measurement wheel which is in contact with the rotor shaft, and thereby, the rotation of the rotor shaft is translated to rotation of the encoder. The encoder is fixed to a spring loaded arm which holds the encoder wheel in contact with the rotor axis. The arm is clamped to the case of the refiner and is easily installed and removed.

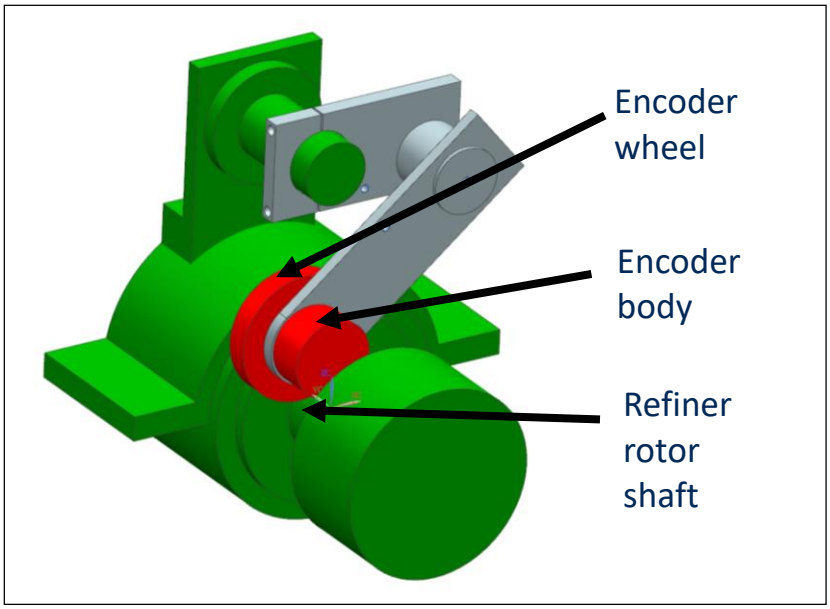

Figure 16: Isometric view of the Encoder arm.
Components in green are original to the refiner. Red indicates the encoder and the encoder wheel and grey indicates the encoder-mount to the refiner.

[3] 182.044

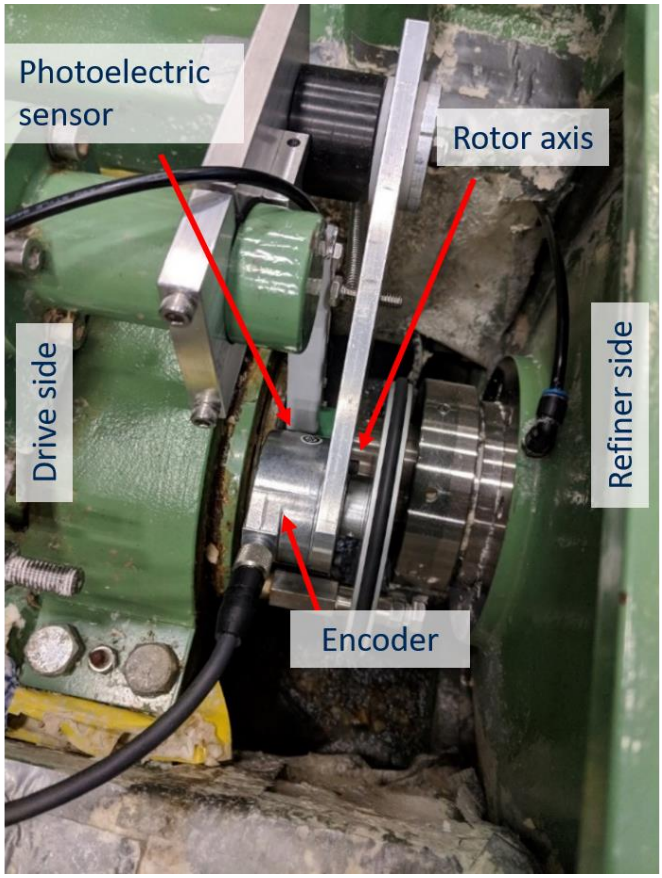

Figure 17: Picture of mounted Encoder on the test refiner at UBC.

In addition to the rotary encoder, a photoelectric sensor (position shown in Figure 17) is used to provide a reference for the angular position of the rotor axis, once per revolution. With this zero position known, the encoder data is converted to obtain the absolute angular position of the driveshaft.

Position data from the encoder is converted to determine rotor position using Equation (4), where the diameter of the encoder wheel, d_E, and the diameter of the rotor axis, d_{ra}, are used to calculate the relation between degrees of rotation of the rotor axis, $\Delta\varphi_{ra}$ and degrees of rotation of the encoder, $\Delta\varphi_E$.

$$\frac{\Delta\varphi_E}{d_E} = \frac{\Delta\varphi_{ra}}{d_{ra}} \tag{4}$$

For each data set collected, the deviation of the encoder data from the calculated value of 197.28° is calculated. The results of the frequency plot of these deviation values show that 90% of

the measurements lie within -0.15° and 0.1° of the calculated value for a full revolution of the rotor.

2.3.4 Test conditions

Two sets of trials are conducted, one using softwood pulp and the other using hardwood pulp[4]. The softwood pulp is Bleached Chemi-Thermal Mechanical Pulp from Quesnel River Pulp in Quesnel, BC. The pulp is made primarily from Lodgepole Pine and White Spruce and has an initial length weighted fiber length (L_W) of 1.9 mm. The hardwood pulp is bleached aspen CTMP from the Millar Western Mill in Whitecourt, Alberta and has an initial L_W of 0.9 mm. The consistency for both trials was held at 3.4% [5].

For both trials, the plate gap is incrementally decreased from a maximum of 3.5 mm (i.e. no load) to a minimum of 0.2 mm. Dilution water and seal water were added and considered in the consistency calculation. Pulp samples collected during the trials, are used to monitor consistency during the trials. The pulp flow rate is held constant at 250 liter/min.

Data samples are collected when stable refining conditions are reached (Appendix A). To ensure that the pulp sample represents the same refining conditions as the data samples the pulp samples are taken ten seconds after stable refining conditions are reached. This value is based on experience of the operator and the flow rate of the pulp from the refiner to the extraction point. Each data sample is one second long.

2.3.5 Data acquisition and processing

The force sensors, the rotary encoder and the photoelectric sensor are each sampled at 400kHz. As described above, the RFS emits two voltage signals when subjected to a force. The voltage signals are processed using custom charge amplifiers. The amplified signals are input to a DAQ system, comprised of a National Instruments data acquisition card (i.e. cDAQ-9188) connected to a Laptop running LabVIEW^{TM} software. The encoder and the photoelectric sensor are also connected to the cDAQ. LabVIEW is used to monitor the sensor signals, start and stop the recording and save the data sets to memory in the TDMS file format.

[4] Tables specifying refiner load and energy at each set point are included in Appendix III.
[5] These trials are not recirculation trials.

The pulp samples are used to determine pulp properties such as L_W[6], fine percentage, curl index, kink index and mean width of the fibers for each plate gap. These analyses are conducted at the UBC PPC on the Fiber Quality Analyzer (HiRes FQA, Optest Equipment Inc., Vancouver, British Columbia).

Processing of the RFS data follows the method used by Harirforoush and Olender [26] and uses MATLAB (Mathworks; Natick, MA, USA) to handle the data sets. The previously described calibration constants are used to calculate the normal and shear forces from the measured piezo signals.

2.4 Results

The relative positions of the rotor bars and the sensor during a BPE are illustrated in Figure 18. Five cases are shown, spanning from the point where the rotor bar first overlaps the sensor to the point where the rotor bar ceases to overlap the sensor. The *angular position of the rotor bar* is measured with reference to the midpoint of the overlapping range, at which point, the centerline of the rotor bar coincides with the center of the sensor. This midpoint is designated as the *center position* of the BPE and is used as the 0° reference point (see Center in Figure 18). During one BPE, the rotor rotates for 2.2°. The start of the BPE is at -1.1° and the end at 1.1°, indicated as "Start" and "End" in Figure 18. Negative and positive values indicate before and after the center position of the BPE, respectively. The overlapped area on the sensor is indicated through a yellow fill in Figure 18. It is worth noting that in the end of the BPE, the second bar starts to go into effect with the sensor. This interaction starts approximately between 0.8° and 0.9°. Note that the area of overlap between the rotor bar and the sensor is referred to simply as the *overlap area* from here forward.

[6] In this research, *length weighted fiber length* is used as the measure of fiber length.

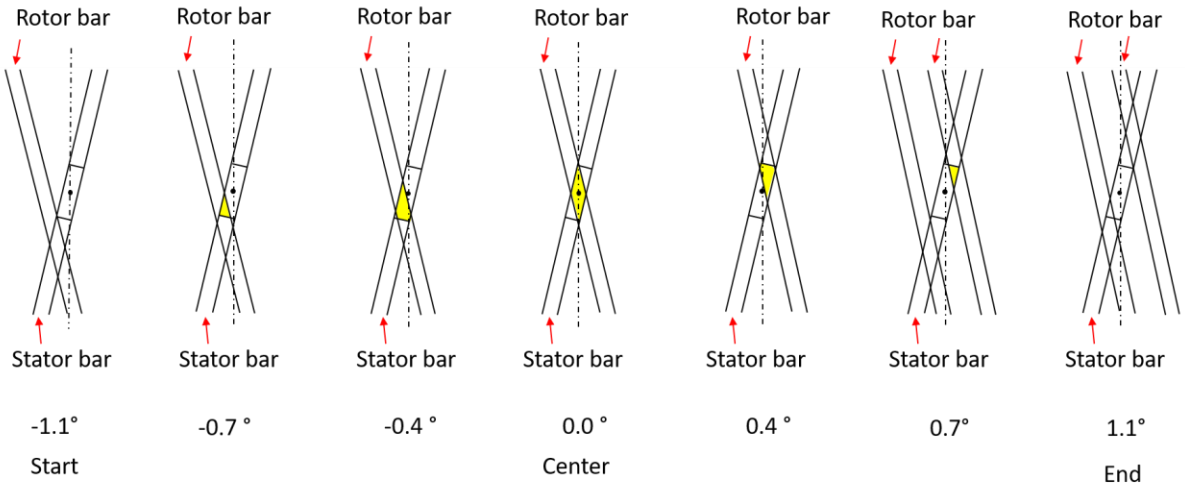

Figure 18: Incremental display of a BPE. View is in axial direction.

As previously noted, the rotor plate has 48 clusters of 3 bars each. The gap between adjacent bar clusters is three times greater than the gap between the bars within a bar cluster. As a result, the forces experienced by each of the three bars in a cluster are different, as shown by Harirforoush [31]. This analysis focuses primarily on data for the passage over the sensor of the first bar in each of the bar clusters on the rotor to avoid the complication of having multiple bars interacting with the sensor at the start of bar passage.

Based on the force and position data and the geometry of the refiner plate, the force measurements are registered spatially, with respect to the bars of the rotor plate. Normal and shear force profiles for a "typical BPE" with small plate gap (gap=0.20 mm) are shown in Figure 19. This figure shows a normal force peak between the start and the center of the BPE and a second peak between the center and the end of the event. The values of the forces shown in this figure are relative, rather than absolute, due to the lack of a DC or steady component in the piezo signals. Engagement of the rotor and stator bars and the pulp, indicated by the rise of the normal and shear force profiles, begins before the "start" of the BPE. The slope of this profile is, initially, low but transitions to a higher slope at approximately -0.9°.

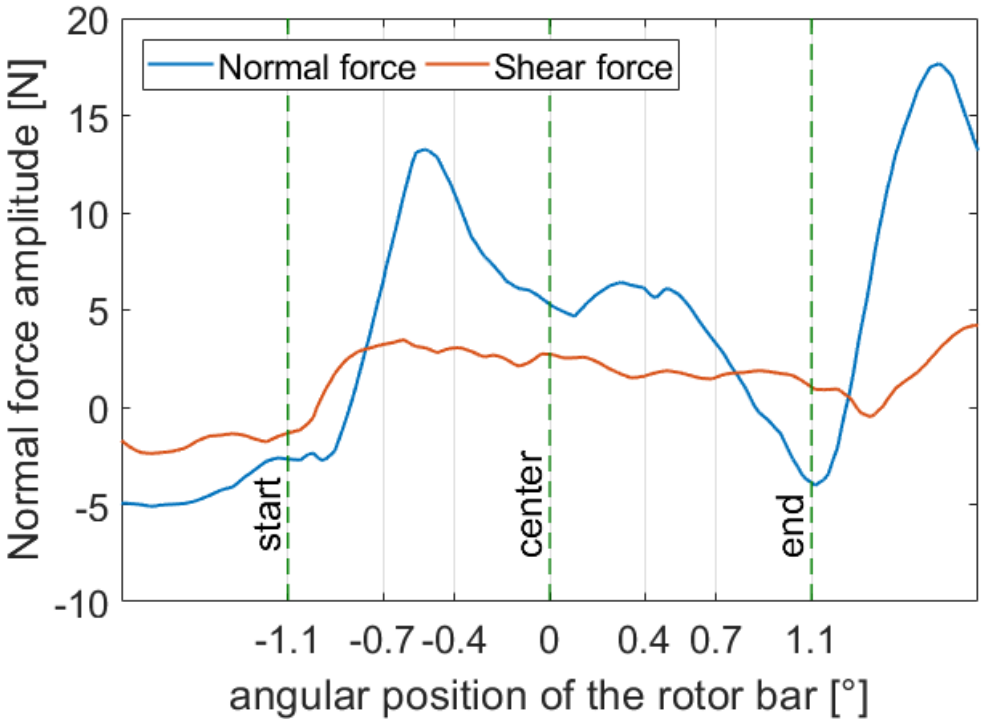

Figure 19: Normal and shear force plot for a single BPE at a closed plate gap (gap=0.20mm). Start, center and end of the BPE are indicated.

For a large plate gap, normal and shear force profiles for a "typical" BPE, as shown in Figure 20, are significantly different from the profiles for a small gap. For this large gap, force peaks occur between the center and the end position of the BPE. Engagement between the refiner bars and the pulp, indicated by the rise of the normal and shear force profiles, coincide approximately with start of the BPE. Engagement of the rotor and stator bars with the pulp, indicated by the initial rise in the force profiles, coincides approximately with the center position.

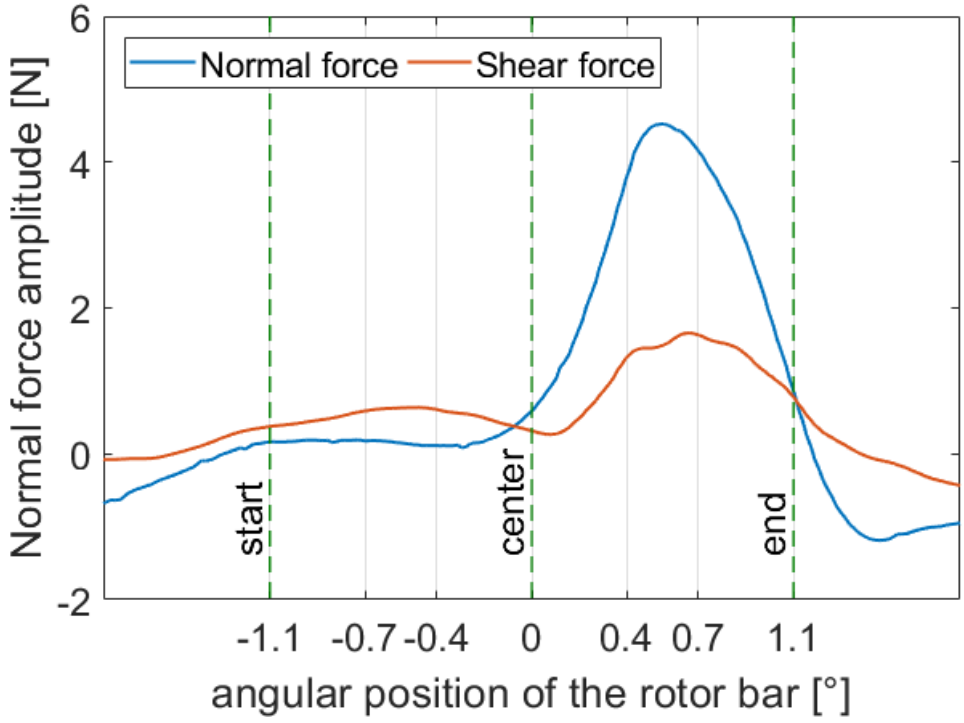

Figure 20: Normal and shear force plot for a single BPE at an open plate gap (gap=0.65mm). Start, center and end of the BPE are indicated.

Comparing the force plots for a single BPE shown in Figure 19 and Figure 20, two further differences are noted. First, as expected, force amplitudes are higher for a small pate gap. Second, at the small plate gap, there are two distinct peaks in the normal force profile; one in the first half of the BPE and one in the second half. At large plate gaps, only the second peak is present.

To investigate the generality of the characteristics of these "typical" force profiles, mean normal force profiles are calculated. For each of the 60 bar passing events acquired at a given gap, each force data set is interpolated to create a set of data points on a common angular interval of 0.05°. At each angular interval, the mean and standard deviation for the 60 data points is calculated. As noted earlier, this analysis includes only the forces.

Mean normal force profiles for the passage of the first bar of a selected rotor bar cluster over the stator bar in which the sensor is installed are shown in Figure 21 and Figure *22*, for plate gaps ranging from 0.62 to 0.2 mm. Figure 21 presents the data for softwood and Figure 22 presents the data for hardwood.

For softwood, the standard deviations of mean force have maximum values of 1.03 N and 2.3 N for the largest and smallest plate gaps, respectively. For hardwood, the standard deviations of mean force have maximum values of 0.41 N and 1.03 N for largest and smallest plate gap, respectively. The maximum values of standard deviation occur in the region of the peak mean force values. The standard deviations before -1.0° and after 1.2° are close to zero.

For large plate gaps, with both softwood and hardwood pulps, mean force increases gradually over the first half of the BPE, continues to increase up to a peak in the final quarter of the BPE and then falls to zero. As this peak appears late in the BPE, it is referred to as the *late peak*. This late peak is present for the full range of plate gaps and its amplitude increases as the plate gap closes and the peak mean force amplitudes are lower for hardwood than for softwood.

For small plate gaps, with both softwood and hardwood pulps, mean force begins to rise before the rotor bar overlaps the stator bar (i.e. the sensor probe). For softwood, the mean force rises to a distinct peak close to but before the midpoint of the BPE. For hardwood, the mean force rises to a plateau close to but after the midpoint of the BPE. In both cases, this peak appears early in the BPE and is, therefore, referred to as the *early peak*. Following this early peak or plateau, for both softwood and hardwood, the mean force then rises to the late peak. The plate gaps at which the early peak appears, for both hardwood and softwood, are shown in Table 1. In addition, for hardwood, there is a third smaller peak at the beginning of the BPE (Figure 22).

The mean force profiles for the second and third bars of the bar cluster on the rotor differ from the profile for the first bar. Figure 23 shows the mean force profile for softwood pulp at a small gap (i.e. 0.2 mm). At the beginning of the first BPE, the slope of the mean force profile is initially low and then transitions to a higher slope at approximately -0.9°. This behaviour is also present for larger gaps and for hardwood, as shown in Figure 21 and Figure *22*. For the second and third BPE no such low slope region exists. The force falls to a valley and then immediately rises again. For the third BPE, there is no *early peak* in the force profile.

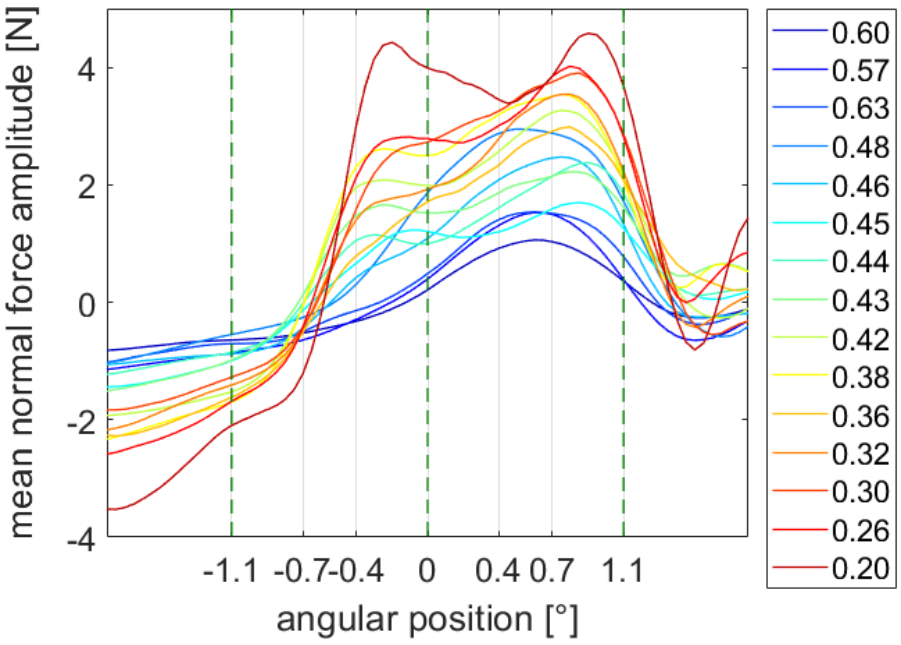

Figure 21: Average normal force profiles for a single BPE for softwood for several plate gaps. Start, center and end position of the BPE is indicated.

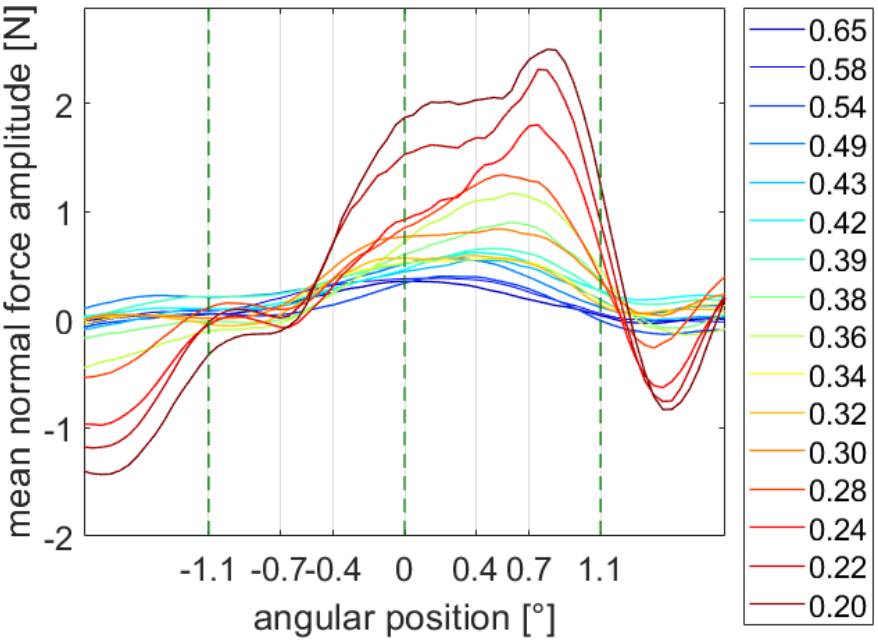

Figure 22: Average normal force profiles for a single BPE for hardwood for several plate gaps. Start, center and end position of the BPE is indicated.

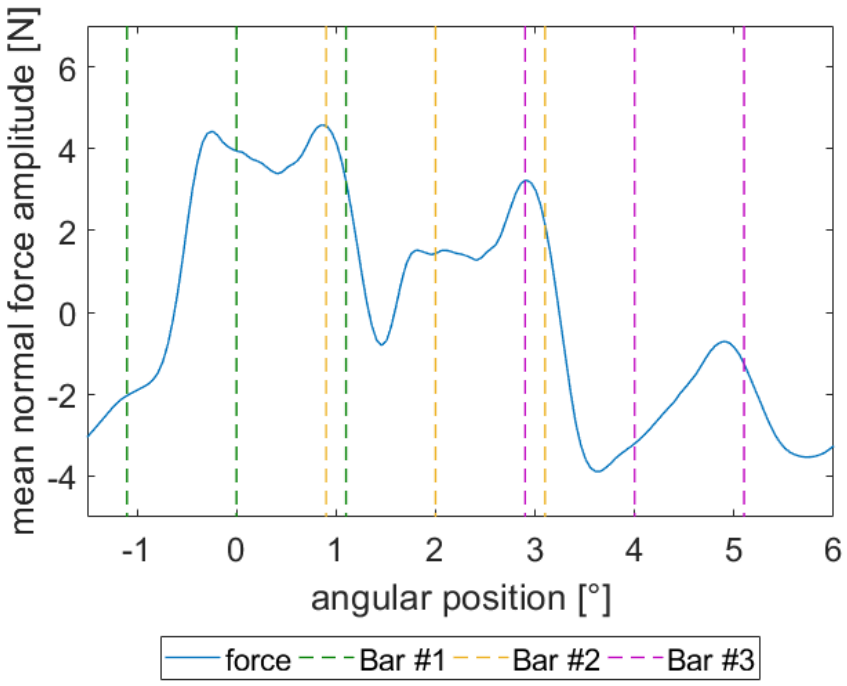

Figure 23: Average normal force profile.
Average normal force profile for a full bar cluster passing over the sensor for softwood pulp at plate gap=0.2mm. Start, center and end position of the individual BPE are indicated for the first, second and third bar in green, yellow and purple respectively.

Length weighted fiber length data for each plate gap is shown in Figure 24 and Figure 25 for the softwood and hardwood trials, respectively. The data in each of these plots follows two trend lines, one for large gaps and one for small gaps. It is notable that the plate gaps bounding the transitions in fiber length data trends are the same as the plate gaps bounding the transitions in mean force profiles, as shown in Table 1.[7]

[7] It is assumed that these bounding plate gaps include the critical gap. Below the critical gap, selection of preferred operating conditions would take into account the trade off between fibre length reduction and increased energy applied to the fibers.

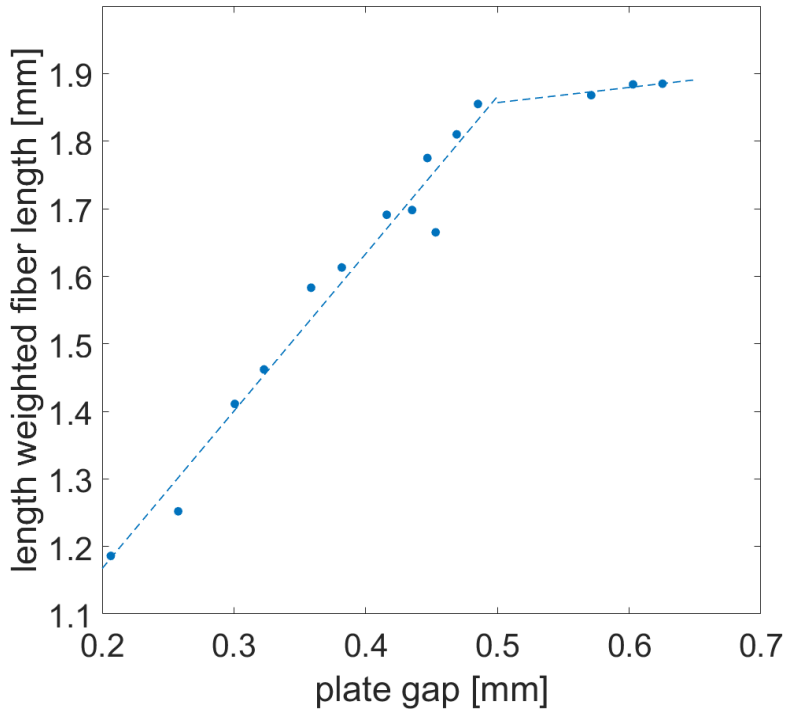

Figure 24: Length weighted fiber length data for softwood trials plotted over plate gaps.

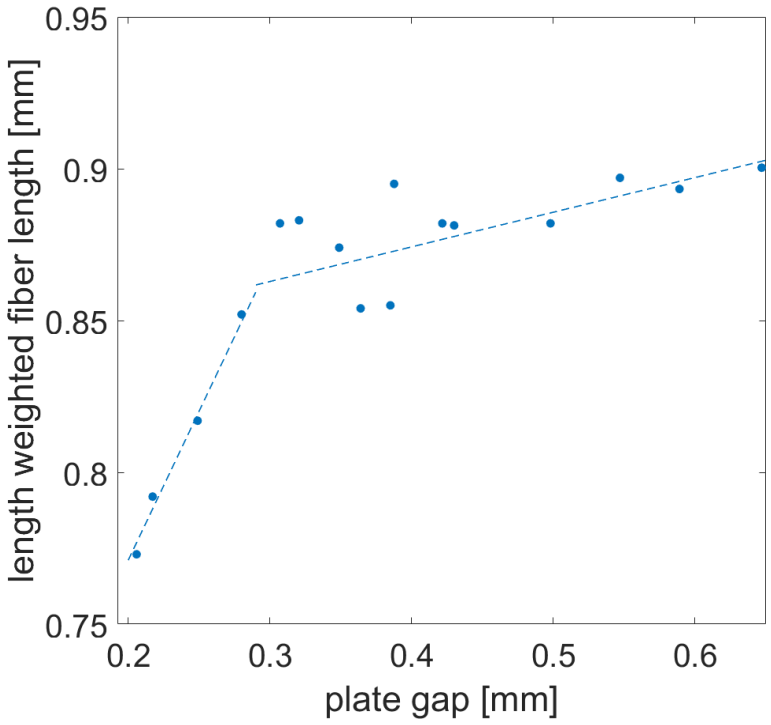

Figure 25: Length weighted fiber length data for hardwood trials plotted over plate gaps.

Table 1: Plate gaps bounding transition in fiber length and transition in force profile

	Plate gaps bounding fiber length transition (mm)	Plate gaps bounding mean force profile transition (mm)
Softwood	0.48 mm - 0.46 mm (Figure 24)	0.48 mm - 0.46 mm (Figure 21)
Hardwood	0.30 mm - 0.28 mm (Figure 25)	0.32 mm - 0.30 mm (Figure 22)

2.5 Discussion

The rotary encoder data are used to register measured bar forces to the relative position of the rotor bar as it passes over the stator bar in which the force sensor is installed. The registered force profiles are used to create mean force profiles based all BPEs for a selected rotor bar over the stator bar in which the sensor is installed. In all previous studies with the RFS alone [4] [6] [30], it was not possible to create mean force profiles because there was no way to align BPE data to a common angular reference point. As force data for individual BPEs is highly variable, the integration of position and force data to enable calculation of mean profiles represents a significant advance in the potential of the RFS technology to shed light on the fundamental mechanisms of mechanical refining.

The absence of the early peak from the mean force profiles at large gaps, where fiber cutting does not occur, and its presence at small gaps, where fiber cutting does occur, suggest that this early peak may be a direct manifestation of the mechanism of fiber cutting. This conclusion is reinforced by the observed correlation between the gaps corresponding to the transition to fiber cutting and the gaps corresponding to the emergence of the early peak in the mean force profile of the BPE. Furthermore, as the early peak occurs in the first half of the BPE, the early peak may be a manifestation of corner force, as discussed in the introduction, and that corner force, therefore, may be causal in fiber cutting.

To explore this hypothesis, models of corner force and friction force at small plate gaps are proposed. In the corner force model, it is assumed that, during a BPE at small plate gaps, the

leading edge of the rotor bar and the opposed edge of the sensor probe are both covered uniformly with fibers, as shown experimentally by Mohlin [42]. It is further assumed that this uniform coverage results in a corner force that is proportional to the length of the sensor probe edge that is engaged with or overlaps the oncoming rotor bar. This *engaged length* is defined as the length of the sensor probe edge that is covered by the rotor bar.

The engaged length, as shown in Figure 26 (a), begins to rise at the start of the BPE, reaches a maximum in the first half of the BPE, is constant until the center position and falls to zero during the second half of the BPE. This then leads to the corner force profile shown in Figure 26 (b).

In the friction force model, it is assumed that, as the rotor bar sweeps over the stator bar, pulp is compressed between the opposed surfaces of the rotor and stator bars and that the normal force increases as a power law function of the rotor angle, similar to the stress behaviour of pulp during wet pressing [43]. The friction force is assumed to be proportional to the normal force, as shown in Figure 26 (a).

The sum of the modelled corner force and friction force are fit to the mean force data for softwood pulp with a gap of 0.2 mm. The model and the experimental data are presented in Figure 26 a-c. The mathematical form of the models and the constants that result from fitting the models to the experimental data are presented in Appendix B.

The sum of the modeled corner force and friction force captures the two-peak form of the mean measured force profile, as shown in Figure 26 (c). The timing of the early peak and late peak is delayed relative to the experimental data and the model does not capture the low slope region at the beginning of the BPE. It is also recognized that this model has been fit to mean force data, which cannot capture all of the features of an individual BPE. Nonetheless, the approximate correlation between this simple model and the mean force data supports the hypothesis that dominant interactions in a BPE are corner force and friction force. Furthermore, the correlation between the plate gap at which the early peak appears and the transition in the fiber length data suggests that corner force is, indeed, causal in fiber cutting.

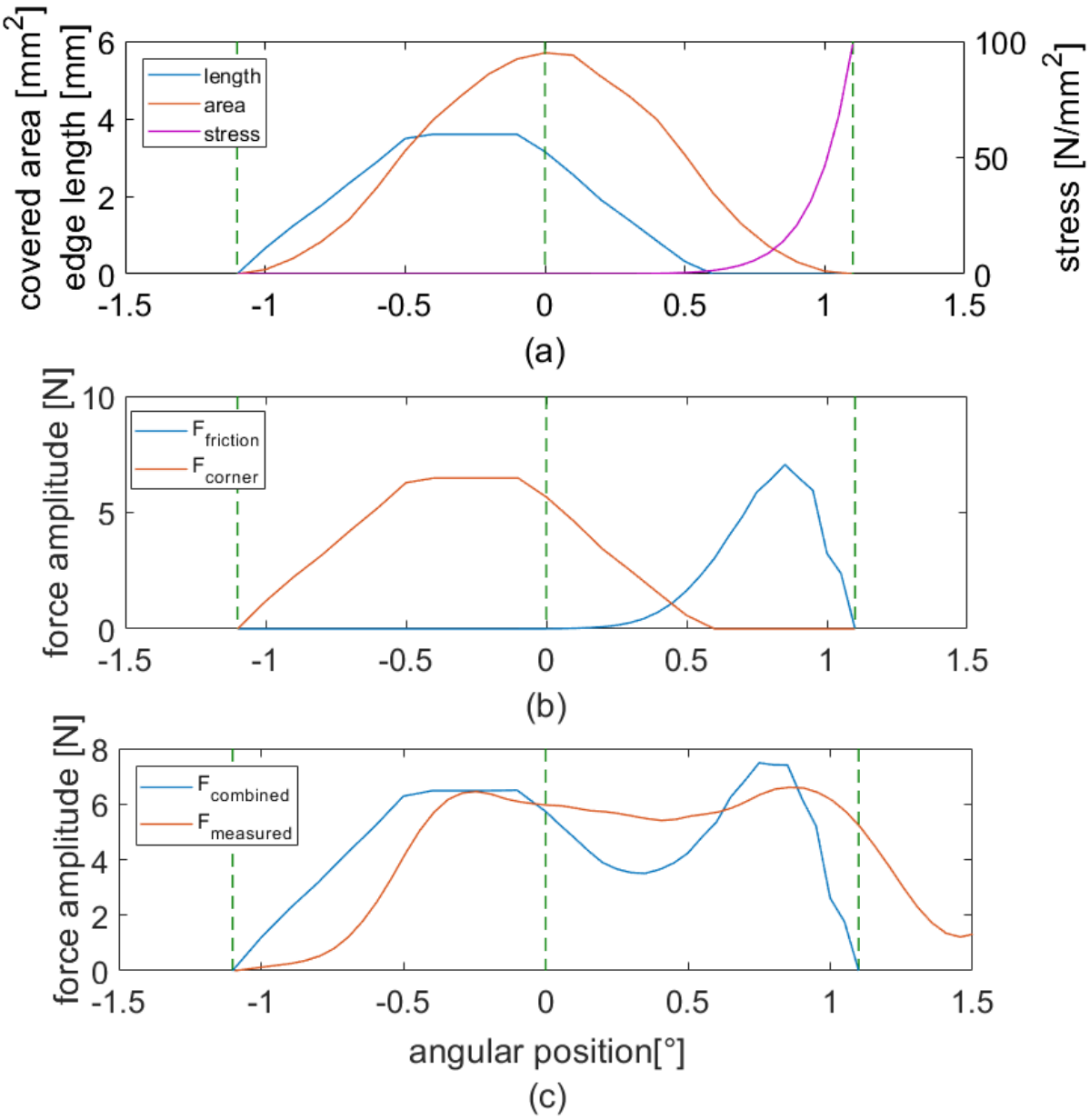

Figure 26: Covered area theory plots.
Progression of the overlap area on the sensor in orange and the engaged leading edge of the sensor in blue and the theorized stress curve in purple plotted over the angular position of the rotor bar (a), corner and friction force as calculated over the angular position (b), the combined force profile and the measurement force data for angular position (c).

Mean normal force data for the three BPEs of a bar cluster, as presented in Figure 23, shows three distinct features. First, there is a progressive decrease in maximum force amplitudes of these BPEs, as was also shown by Harirforoush [44]. Second, the early peak is prominent in the first

BPE, is diminished in the second event and absent from the final event. Third, the low slope region at the beginning of the first BPE, is absent from the second and third events.

On both the rotor and the stator plates, the bar clusters are separated by grooves which are three times the width of the grooves that separate the bars within the clusters. These large inter-cluster grooves have greater capacity to carry pulp than the smaller intra-cluster grooves. As this wide groove passes over the sensor, more pulp is trapped between the first bar in the rotor cluster and the sensor than is trapped by the second and third bars. The greater mass of trapped pulp leads to a high corner force and high friction force for the first BPE. Some of the pulp trapped by the first rotor bar remains in place on the sensor for the passage of the second bar and a lesser amount, for the passage of the third bar. This conceptual model of the interaction of the pulp with the rotor bars and the sensor is consistent with the first and second features of data shown in Figure 23.

The third feature of the BPE profiles in Figure 23, the low slope region at the beginning of the first BPE, is consistent with Vomhoff et al. [43], who shows that, in the early stage of wet pressing, water between fibers is displaced and the slope of the stress strain curve is low. Once fiber-fiber contact is established, water is expelled first from the fiber lumens and then from the fiber walls and the slope of the stress-strain curve increases accordingly. As noted above, the peak in the first BPE is preceded by the passage of the wide groove on the rotor, allowing time for pulp to recover to a state that is similar to the early and low-slope stage of wet pressing. The second and third BPEs are preceded by the passage of narrow grooves on the rotor allowing time only for the pulp to recover within the later and high-slope stage of wet pressing.

2.6 Conclusion

Bar-force sensors and a rotary encoder were installed in a 16” AIKAWA LC refiner and trials were conducted using softwood and hardwood pulps, both at a consistency of 3.5 %. The trials were conducted at 1200 rpm and the plate gap was incrementally decreased from 3.5 mm to 0.2 mm. The rotary encoder data are used to register measured bar forces to the relative position of the rotor bar as it passes over the stator bar in which the force sensor is installed. The registered force profiles are used to create mean force profiles based all BPEs for a selected rotor bar over the stator bar in which the sensor is installed. As force data for individual BPEs is highly variable,

these mean force profiles have potential to shed light on the fundamental mechanisms of mechanical refining.

The mean force profiles exhibit a distinct transition as the plate gap is closed that corresponds to the onset of fiber cutting. In addition, these profiles are consistent with a simple model of bar force comprised of the sum of corner force and friction force. Investigation of mean force profiles for the three BPEs within a cluster of rotor bars shows a behaviour that is consistent with previous work on wet pressing.

2.7 Appendix A

Table 2: Timing of data and pulp sample acquisition

Time	Action
00:00:00	Stable refining conditions reached, First data sample collection started
00:00:01	First data sample is collected Storing of first data sample is started
00:00:03	First data sample is written to memory, Second data sample is started
00:00:04	Second data sample is collected Storing of second data sample is started
00:00:06	Second data sample is written to memory, Third data sample is started
00:00:07	Third data sample is collected Storing of third data sample is started
00:00:09	Third data sample is written to memory
00:00:10	Pulp sample is collected from the collection position

2.8 Appendix B[8] – Corner force and shear force models

Total bar force, F_{total}, during a BPE is the sum of the friction force, F_F, and the corner force, F_C,

$$F_{total} = F_C + F_F \tag{5}$$

Mean peak normal force data for the softwood trials at plate gap 0.2mm is used to generate separate force profiles for the corner force and the friction force following the relation described in Equation (5). Based on these individual force plots and using the engaged area for friction force and engaged length for corner force, separate stress profiles for the BPE are generated. These stress plots are fitted with trend lines.

It was found that corner force is the product of the engaged length, l_E, and a constant, k_C.

$$F_C = l_E k_C \tag{6}$$

Friction force is found to be the product of the engaged area, A_E, and a power law term comprised of the angular position in the BPE, ϕ, the constant, k_F, and the exponent, e_F.

$$F_F = k_F A_E \phi^{e_F} \tag{7}$$

Equations (5) to (7) where used to generate the combined force plot in Figure 23 (c). The values of the used constants are displayed in Table 3.

Table 3: Values of constants used in friction force and corner force models.

Constant	Value
k_C	1.8
k_F	3.4
e_F	11.5

[8] A revised version of Appendix B can be found in Appendix II of this thesis.

3 Interpretation of force profiles in mill-scale LC refining

3.1 Abstract

A set of piezo ceramic force sensors is implemented in a 52-inch mill-scale low consistency refiner to explore the effect of varying operating conditions on bar force profiles. The sensor replaces a short length of a stator bar and measures normal and shear forces applied during the passage of each rotor bar. In previous work with this type of force sensor, a rotary encoder was used to investigate force profiles for individual *bar passing events* (BPE) on a 16-inch laboratory-scale refiner. In the work presented here, force profiles for individual BPEs are identified based on key features in the time domain force data. The individual bar force profiles are classified as *single peak* events which feature one peak corresponding to the *fiber compression force* and as *dual peak* events corresponding to fiber compression force and the *corner force.* The bar passing events are then analysed based on their *mean force profiles* and their *dual peak ratio* in the bar passing event. Findings are compared and validated by previous work on bar force profiles. It is shown that dual peak events which are considered to represent the corner force, are present through out the whole range of refining and increase with increased refining energy. This increases the understanding of the way corner force contributes to the refining process. Furthermore, it is found that different radial positions on the stator plate are subjected to different force profiles. This is thought to be due to the difference in tangential speed and a change in the fiber and floc material properties at different radial positions.

3.2 Introduction

Refining performance is controlled by the fundamental design and operating parameters such as refiner power, rotational speed, flow rate, consistency and plate geometry. To further characterize and compare the refining action, the specific refining energy (SRE) and specific edge load (SEL), are widely used [35], [36].

SRE is the energy expended per unit mass of fiber and is calculated as,

$$SRE = \frac{P}{Q\ C} \tag{8}$$

where, P is net refiner power, Q is the mass flow rate of pulp and C is consistency[9].

Several studies have presented methodologies to predict pulp properties based on SRE, including but not limited to Miller et al. [37], Elahimehr et al. [12]. However, on its own, SRE does not uniquely describe refining action as it has been shown that the same SRE can lead to different pulp properties [37]. For example, high intensity LC refining can achieve a lower freeness than low intensity LC refining at the same SRE and low intensity LC refining can achieve a higher tensile strength at the same SRE compared to high intensity LC refining [37].

Specific edge load (SEL) is a measure of refining intensity as the energy expended per bar-crossing per unit bar length [21], as shown in Equation (9)[10], where P is net refiner power, BEL is bar edge length, ω is rotational speed. BEL is a function of plate geometry including bar width, groove width and bar angle [38].

$$SEL = \frac{P}{BEL\ \omega} \tag{9}$$

By inspection of (9), it can be seen that, at constant refiner power, an increase in rotational speed leads to a decrease in SEL.

SEL offers insight into the influence of process variables on pulp quality at a macro-scale. For example, high SEL leads to a reduction in fiber wall thickness [2]. Further, it has been shown that low SEL is a pre-condition for preserving fiber length and strength development in LC refining of mechanical pulps. SEL enables theoretical estimates of the post-refining pulp properties [39] but is of limited use in revealing the mechanisms of refining at the scale of fibers and flocs and their interactions with the bars and grooves of a refiner plate.

Recently, however, Kerekes and Meltzer [38] proposed a method, based on SEL, to approximate the bar force, F, as shown in Equation (10)[11].

[9] Equation (8) is a repeat of Equation (1) in Chapter **2**.
[10] Equation (9) is a repeat of Equation (2) in Chapter **2.**
[11] Equation (10) is a repeat of Equation (3) in Chapter **2.**

$$F = \frac{SEL}{s} \tag{10}$$

In this expression, *SEL* is energy per unit bar length, *s* is the bar width and *F*, therefore, is the force per unit bar width[12] in the direction of bar movement [38]. Bar forces calculated in this manner can be used to quantify the refining process on a local-scale, as *F* is based on local bar width. Understanding bar forces is the key to understanding refining processes as these forces are the driving factor in fiber development [21].

Forces acting on bars have been described to include a *friction force* and a *ploughing* or *corner force* [25], [3], [35]. First introduced by Martinez et al. [25] and further developed by Kerekes et al. [35], the corner force arises as the leading edge of the rotor bar approaches the forward edge of the stator bar, compressing pulp in the intervening gap [21]. The corner force has been shown to have a strong relationship to the shape of the bar edge. A sharper edge results in a higher corner force whereas a rounder edge results in a lower corner force [21]. Once the leading edge of the rotor bar passes beyond the forward edge of the stator bar, the corner force falls off and, over the second half of the bar passing event (BPE), the friction force, caused by the fibers being dragged over the surfaces of the refiner bars, dominates the signal.

Recent models show that the friction force component normal to the refiner bar can be thought of as a fiber floc *compression force* [45], [46]. Eriksen et al. [45] used high-resolution pressure measurements in a stator bar to investigate pressures on the surfaces of refiner bars. This work shows that the magnitude of pressure peaks correlates with a model of hydrodynamic pressure resulting from water expulsion from the floc as its is compressed between the rotor and stator bars [46].

In a study of normal and shear forces in LC refining, Harirforoush installed a refiner force sensor (RFS), based on the design used by Prairie [27], in an AIKAWA/Advanced Fiber Technologies Inc. 16” single-disc low consistency (LC) refiner. Trials were conducted with chemi-thermomechanical softwood SPF pulp with 378 ml CSF at 2.5% and 3.5% consistency at rotational speeds of 800, 1000 and 1200 rpm. Analysis of peak normal and shear forces show that the onset of fiber cutting consistently corresponds to a distinct transition in the distribution of these peak

[12]Note that Kerekes uses the term *length* for this parameter.

forces as the plate gap is closed. The gap at which this occurs is referred to as the *critical gap* [18]. Based on this, Harirforoush argues that this transition is caused by a fundamental but unknown change in the fiber-bar interaction [17] [30].

In recent work, a bar-force sensor and a rotary encoder were installed in a 16" AIKAWA LC refiner and trials were conducted using softwood and hardwood pulps, both at a consistency of 3.5%. The trials were conducted at 1200 rpm and the plate gap was incrementally decreased from 3.5 mm to 0.2 mm. The rotary encoder data was used to register measured bar forces to the relative position of a rotor bar as it passes over the stator bar in which the force sensor is installed. The authors used the registered force profiles to create mean force profiles based on all BPEs for a selected rotor bar passing over the stator bar in which the sensor was installed. These mean force profiles exhibit a distinct transition as the plate gap is closed that corresponds to the onset of fiber cutting. For large gaps, the authors found a *late peak* in the force profiles that occurred toward the end of the bar passing event. For gaps that are less than the *critical gap,* below which fiber cutting occurs, the authors found an additional *early peak* in the force profiles that occurs close to the start of the bar passing event. This early peak correlates with the onset of fiber cutting leading to the hypothesis that the early peak represents the *corner force* and, therefore, that corner force is causal in the onset of fiber cutting [32].

In the presented work, bar force sensors are installed in a mill-scale twin-disc LC refiner at three radial locations. Force profiles for BPEs at each of these locations are found to have distinct characteristics and, based on a previous study in pilot-scale refiner [32], it is inferred that fiber cutting is prevalent in the mid and outer regions of the refining zone.

3.3 Methods

This section gives an overview of the experimental set up as well as how the data was collected and processed.

3.3.1 Refiner

The refiner used in this work is an Andritz TwinFlo 52" LC-tertiary refiner located at the Catalyst, Paper Excellence mill in Crofton BC. This is a twin disc refiner with two stator plates

and a double sided rotor which separates the two refining zones, as shown in Figure 27[13]. The refiner is fed from the motor or Drive End (DE). On the opposing side, the Tail End (TE) stator can be moved in the axial direction to adjust the gap between the two stator plates. The rotor "floats" on a splined shaft and, therefore, its axial position cannot be actively controlled. Separate discharge lines for each refiner side are located at the bottom of the refiner.

The rotor plates and stator plates for these trials, manufactured by Andritz Durametal, have different bar patterns, as shown in Table 4 and Figure 28. The standard operating speed for the refiner is 420 rpm and this was the operating speed throughout these trials.

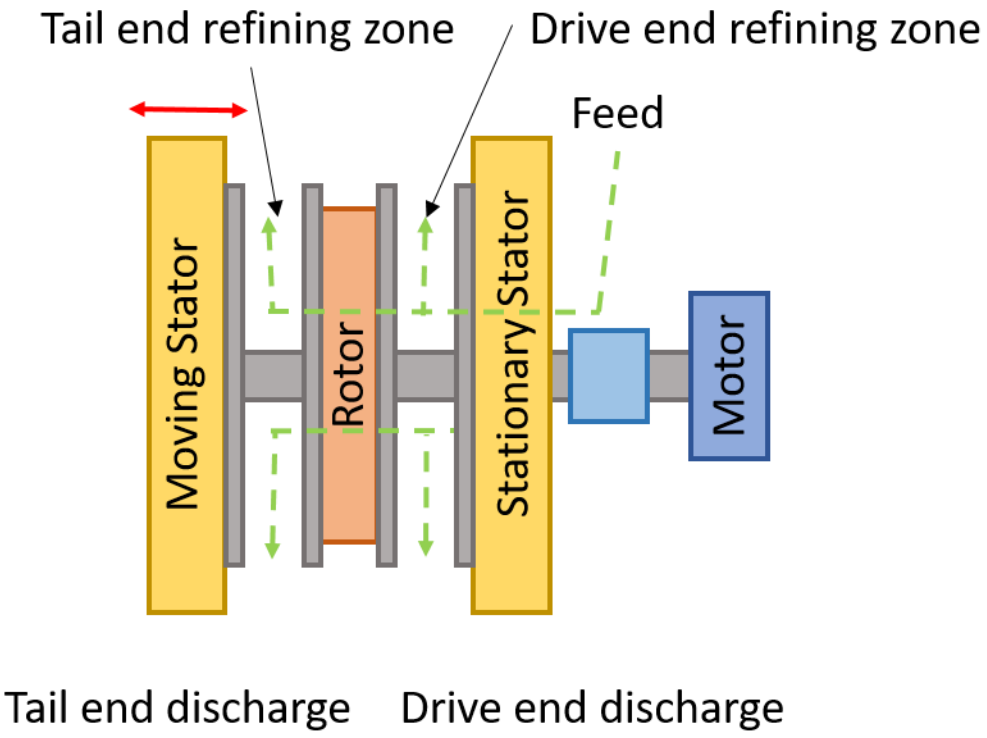

Figure 27: Layout of TwinFlo refiner at Catalyst, Paper Excellence mill in Crofton BC. The moving stator moves axially. The rotor is positioned floating in between the two stator plates.

[13] Figure 27 is a repeat of Figure 4 in Chapter 1.

Table 4: Bar geometries of the Andritz Durametal refiner plates used in the Twin Flo refiner.
The radial zones for the stator and rotor plate are indicated in Figure 28 (a) and (b), respectively.

	Stator			Rotor	
	Zone 1	Zone 2	Zone 3	Zone 1	Zone 2
Bar width [mm]	2.29	1.57	1.57	3.18	3.18
Groove width [mm]	3.81	2.69	2.36	3.81	3.18
Average bar angle [°]	22.5	22.5	22.5	35	35
BEL [km/rev]	325.39			105.42	

(a) (b)

Figure 28: Refiner plate segments with indicated zones for rotor(a) and stator (b).

3.3.2 Force sensors

The sensors used in these trials were custom designed, based on the work of Prairie et al. [4], Olender et al. [6], Harirforoush et al.[30] and Aigner et al. [32]. Each sensor probe replaces a section of a bar on the stator plate, 0.15 inches (3.8 mm) in length. The probe is supported by two piezo elements which emit signals that are processed to independently determine the forces applied to the probe tip. In the installed configuration the sensors measure two forces: the normal force, which is perpendicular to the refining plane or parallel to the refiner axis; and the shear force which lies in the refining plane and is perpendicular to the refiner bar [31].

Three sensors are installed in each one stator plate, each at a different radial position, as shown in Figure 29 (a). Figure 29 (b) presents a view of the back of the stator plate, showing the housings and tubing that protect the sensor bodies and wires from the refiner environment.

Signals from the force sensors are processed using custom charge amplifiers. The amplified signals are input to a data acquisition system, comprised of a National Instruments cDAQ-9188 data acquisition card connected to a desktop computer running LabVIEW™ software. LabVIEW is used to monitor the sensor signals, start and stop the recording and save the data sets to memory in TDMS file format. Processing of the RFS data follows the methods used by Harirforoush [31] and Olender [4], and MATLAB (Mathworks; Natick, MA, USA) is used to manage the data sets.

Each sensor is calibrated using a modal hammer (PCB Piezotronics/086D80-12911/ Depew, New York). This calibration is conducted before the sensors are installed in the refiner plate using a custom fixture. The resulting calibration constants are used to determine the normal and shear forces from the measured piezo signals. Calibration of sensors and subsequent conversion of voltage signals into force readings is based on previous work, as described by Prairie [27].

The installed sensors were recalibrated, *in situ*. Results of this recalibration indicate that the mid and outer sensors on the drive end of the refiner may not be functioning correctly. Therefore, discussion of radial variation in the measured forces is based on the measurements taken at the tail end of the refiner only.

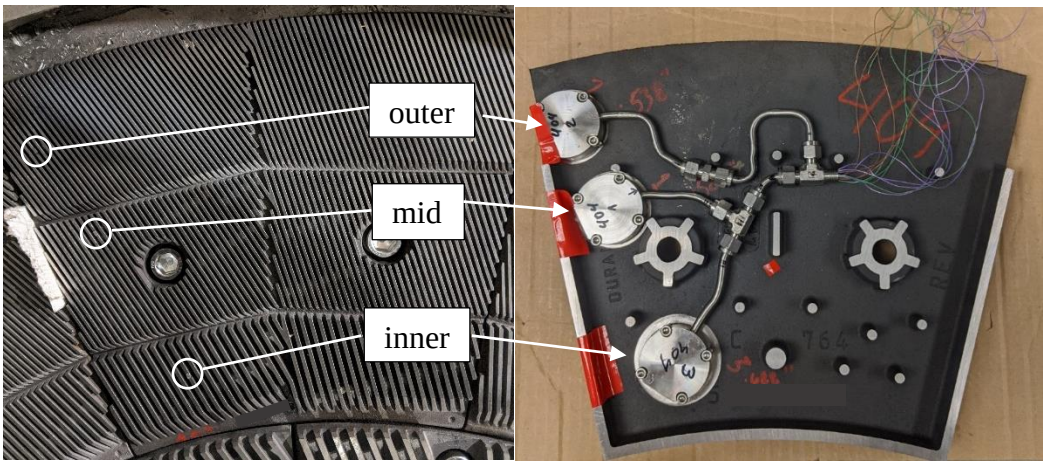

(a) (b)

(c)

Figure 29: Pictures of the stator pate with installed sensors. (a) front side of stator plate. (b) back side of stator plate. Housing of sensors and wiring visible. (c) close up of an installed sensor.

3.3.3 Pulp properties

Pulp samples taken during the trials are analysed at the mill using a KMAP fiber analyser (Valmet Technologies, Espoo, Finland). Pulp properties include average length weighted fiber length, fiber length fractions, consistency and freeness for each of the discharge lines and the feed line.

Some pulp samples from previous trials where analysed at the UBC Pulp and Paper Center (PPC). It has to be noted that the comparison between the fiber quality values from those two locations can only be done qualitatively because the measurement methods and fraction values of the KMAP is considered proprietary and can not be compared to the methods and values used at the PPC.

3.3.4 Power Curve Trials

Forces measured by the sensors were recorded during day-to-day operation of the refiner. In addition, trials were conducted to collect force data as the refiner load is increased (i.e. power curves). The complete list of trials is presented in the Appendix Table 6.

This work is based on data from all power curves, but in the interest of readability the main focus lies on power curve #5 which features the widest range of SRE values among all trials. The presented data ranges from 130 kWh/At (air dry ton) to 40 kWh/At in increments of 10 kWh/At. Also included in this trial is data from the No Load (NL) position of 0 kWh/At. The data from power curve #5 is consistent with results from other power curves.

For each power curve trial, the refiner is operated for 15 minutes at each of a number of SRE set points. While the refiner load is decreased (i.e. as the plate gap is increased) other operating conditions such as production rate are held constant. At each set point, the force sensors are sampled at 150 kHz for a 1 s period at intervals of 3 s for the full 15 minutes. During this time, the operational data of the refiner is also recorded (i.e. refiner power, feed and discharge flow rates, feed and discharge pressures). At the end of the 15-minute sample period at each SRE set point, pulp samples are taken from the feed stream and from each of the two discharge lines. After the pulp samples are drawn, the SRE is lowered to the next set point. In all power curve trials, the nominal operational speed of the refiner is 420 rpm and the feed consistency ranges between 3.4% and 4.2%. The pulp furnishes used in this trial is hemlock. The refiner is located in the third stage of the main Thermo-Mechanical Pulping (TMP) line.

3.3.5 Data processing

Peaks in the force signal are determined based on *local amplitude* and *prominence* of peaks, utilizing the peak analysis tool of MATLAB (version R2020a). The local amplitude describes the height difference between a valley and the subsequent adjacent peak. Prominence is a value widely used in topography and is a measure of the significance of a peak, relative to adjacent peaks [47]. This parameter is used to determine if a peak is *independent* or is part of another peak.

To identify which peaks correspond to which BPE, the previously determined peaks are further evaluated based on their temporal spacing. The temporal spacing of the peaks is compared

to the geometric spacing of the bars on the rotor on the circle whose radius corresponds to the position of a given sensor.

Referring to Figure 29 (a), each rotor and stator plate segment spans 30° and is separated into two or three radial zones, respectively. Each plate is also separated into two sides, each spanning 15°, within which all refiner bars are parallel to each other. Because of this the angle between a bar and the radial direction changes over the course of each side. At the center of each side, the angle between bars and the radial direction is equal to the average bar angle as noted in Table 4. At the beginning and the end of each side the angle between bars and the radial direction is the average bar angle plus 7.5° and minus 7.5°, respectively. As a result, the distance between adjacent rotor bars, along the circle corresponding to the sensor location, is not constant nor is the time interval between the passage of adjacent rotor bars over the sensor probe which, as noted earlier, is referred to here as the duration of the BPE.

The variations in the duration of the BPE, given that there are 12 plates with 2 sides each, repeats 24 times per revolution. The BPE durations for one side of the rotor plate, for a rotor speed of 420 rpm, are listed in Table 5.

Table 5: Bar passing event durations at each respective sensor position.
The inner, mid and outer sensor feature 16, 21 and 24 bars per bar segment side respectively

Sensor Position	# BPEs	BPE duration Range [ms]
Inner	16	0.358 – 0.426
Mid	21	0.264 – 0.315
Outer	24	0.239 – 0.286

It is assumed that the duration between force peaks, which represent individual BPE, correlates with the duration of bar passing events determined based on the plate pattern. Similarly, it is assumed that peaks which are closer together than the duration of a bar passing event can be considered as part of the same bar passing event[14]. Taking those considerations into account, a correlation algorithm is computed between the force peak data set and the data set representing the

[14] Two peaks that are closer together than the duration of a bar passing event are assumed to be part of a dual peak event.

bar pattern. Finding the closest correlation between the previously established bar pattern and the peak pattern from the peak analysis allows to associate each force peak with a bar in the plate segment side. After the force peaks are associated to a BPE, the valley preceding a force peak is defined as the start of the bar passing event. If two force peaks are associated to a BPE, the valley preceding the first is considered the start.

3.4 Results

Normal and shear force profiles for *typical* BPEs at 40 kWh/At and for 130 kWh/At are shown in Figure 30 for the inner, mid and outer sensor positions. As expected, the peak force magnitude is larger for high SRE than for low SRE. Furthermore, each of the three sensor positions shows a characteristic force profile. The BPE at the inner sensor position (Figure 30 (a), (b)) and the outer sensor position (Figure 30 (e), (f)) have a single force peak. For the inner sensor, these peaks are located in the third quarter of the BPE, whereas for the outer sensor these peaks are located in the first quarter of the BPE. This is true for the normal force and the shear force for both the inner and the outer sensor.

For the mid sensor, two peaks occur in the normal force plot during the BPE and are located in the second and third quarters of the BPE, respectively (Figure 30 (c), (d)). For the shear force plot only the second force peak is present.

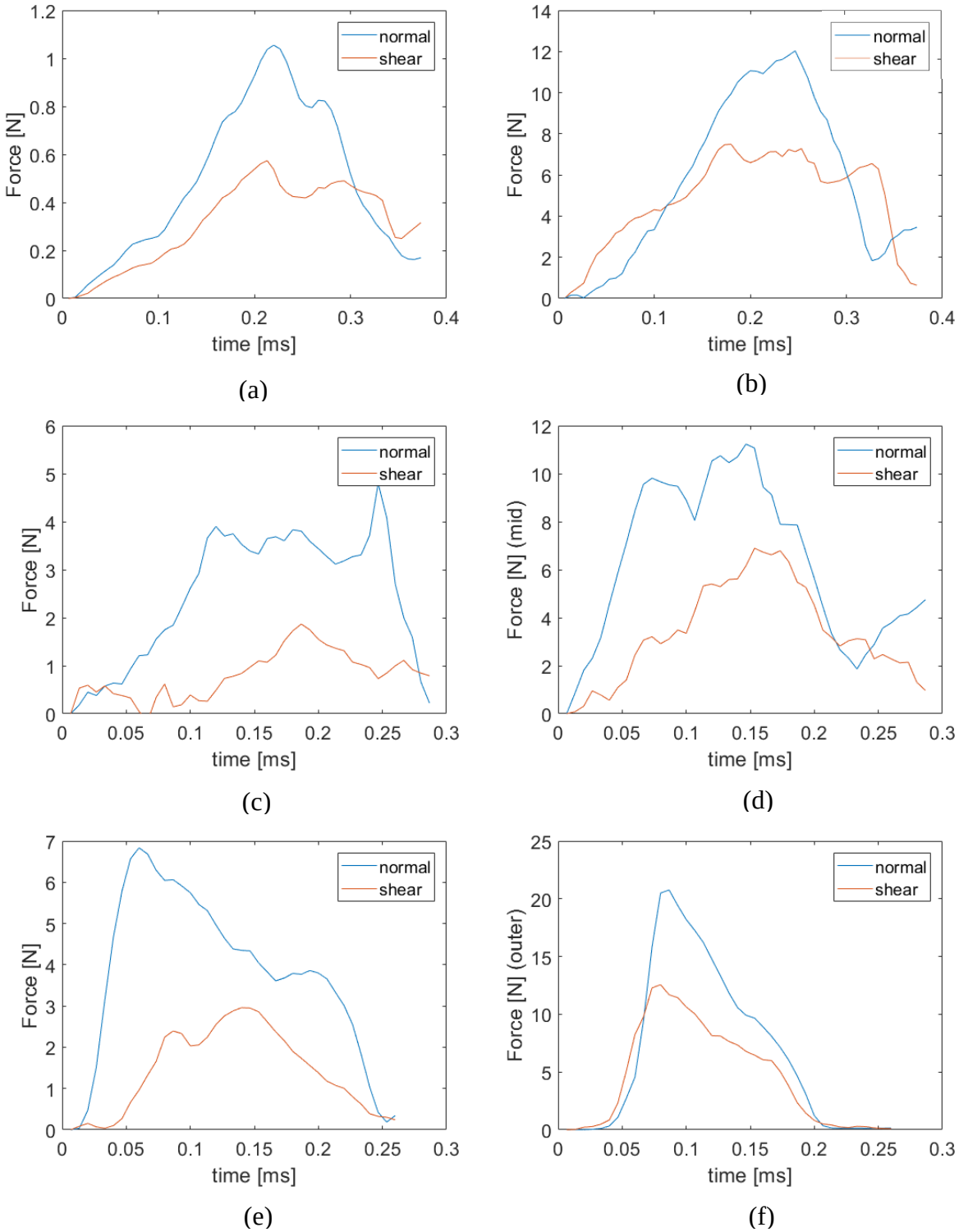

Figure 30: Typical normal and shear force profiles from the tail end side. 40 kWh/At in a), c), e) and 130 kWh/At in b), d), f) for the inner, mid, outer sensor respectively.

To determine the generality of these typical force profiles, mean normal force profiles are generated for each SRE level and for each sensor position, as in [32]. At the inner, mid and outer positions, respectively, 2688, 3528 and 3864 BPEs are recorded during the one second sample period. The force data for all BPEs are aligned using the valley preceding the force peak as the zero reference point. In the case of a bar passing event where two peaks are present, the valley preceding the first peak is used as the zero reference point. At each time step, the mean and standard deviation for all data sets at each SRE level is calculated. This force shape analysis includes only the normal forces.

The resulting mean force profiles (Figure 31 to Figure 33) confirm the trends of the typical bar passing events. Namely one peak appears for the inner and outer sensor and two peaks for the mid sensor. Additionally, when considering the full range of SRE, a transition occurs in the mean force profiles for the mid sensor. Specifically, at low SRE, there is only one force peak, whereas at high SRE there are two force peaks. This transition takes place between SRE values of 60 and 80 kWh/At. The mean shear force plots follow the trends of the mean normal force plots, therefore the focus of this work lies on the normal force.

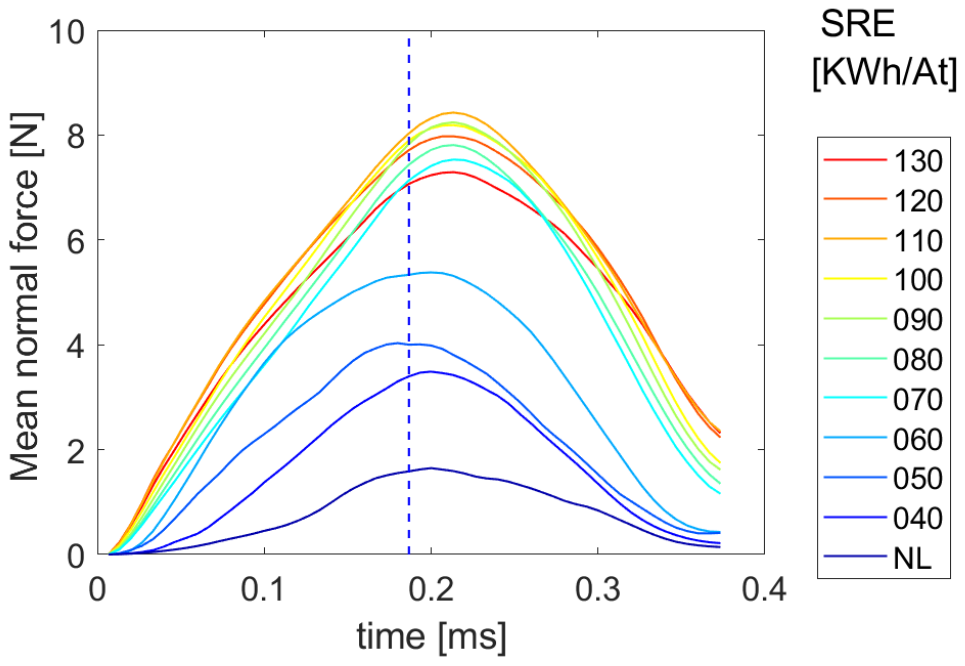

Figure 31: Average normal force profile for the inner sensor on the Tail end.
A dashed line indicates the mid point of the bar passing event. Each profile based on 332000 to 537000 BPE.

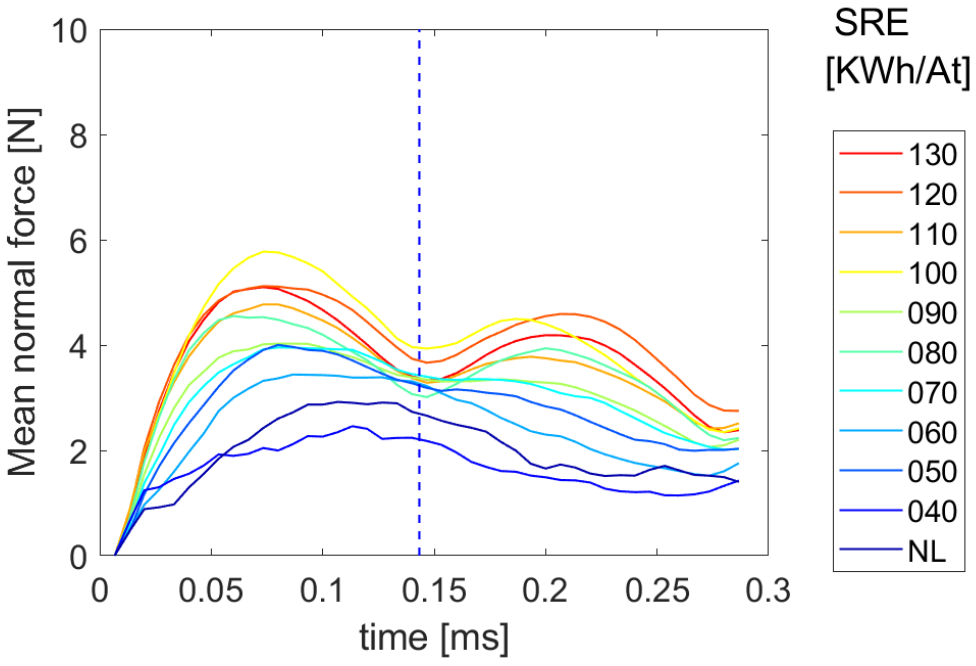

Figure 32: Average normal force profile for the mid sensor on the Tail end.
A dashed line indicates the mid point of the bar passing event. Each profile based on 423000 to 705000 BPE.

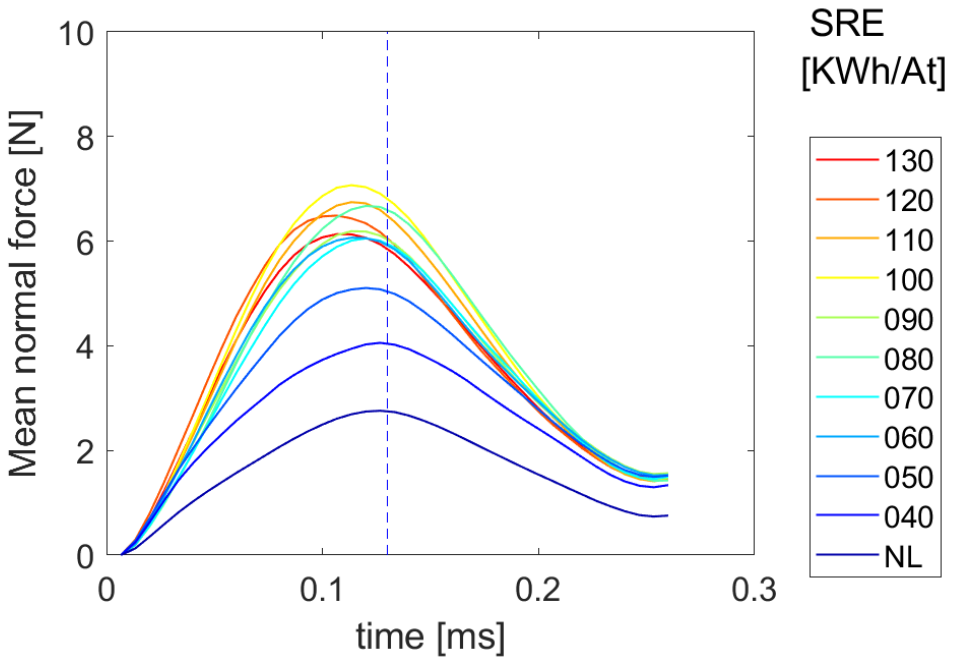

Figure 33: Average normal force profile for the outer sensor on the Tail end.
A dashed line indicates the mid point of the bar passing event. Each profile based on 461000 to 772000 BPE.

The mean force profiles for the mid sensor show that, at high SRE values (80-130 kWh/At), the dual peak behaviour is prevalent while, at low SRE values (NL-70 kWh/At), the single peak behaviour is prevalent. However, these plots do not show the relative contribution of these two behaviors. To explore the relative prevalence of single and dual peak events, the force profiles for each BPE, as previously identified, are categorized into those with one force peak (single peak) and those with two force peaks (double peak). The respective peak amplitude and peak position for each event at each sensor position are plotted in Figure 34, Figure 35 and Figure 36 for the inner, mid and outer sensor positions, respectively. The four plots in each of these figures shows data for single peak events and dual peak events at both 40 kWh/At and for 130 kWh/At.

Comparing the results for inner, mid and outer sensor position, shows that dual peak events are present at all three sensor locations and at both SRE levels and that dual peak events are more prevalent at high SRE. Furthermore, the mid sensor position shows the highest proportion of dual peaks at both low and high SRE.

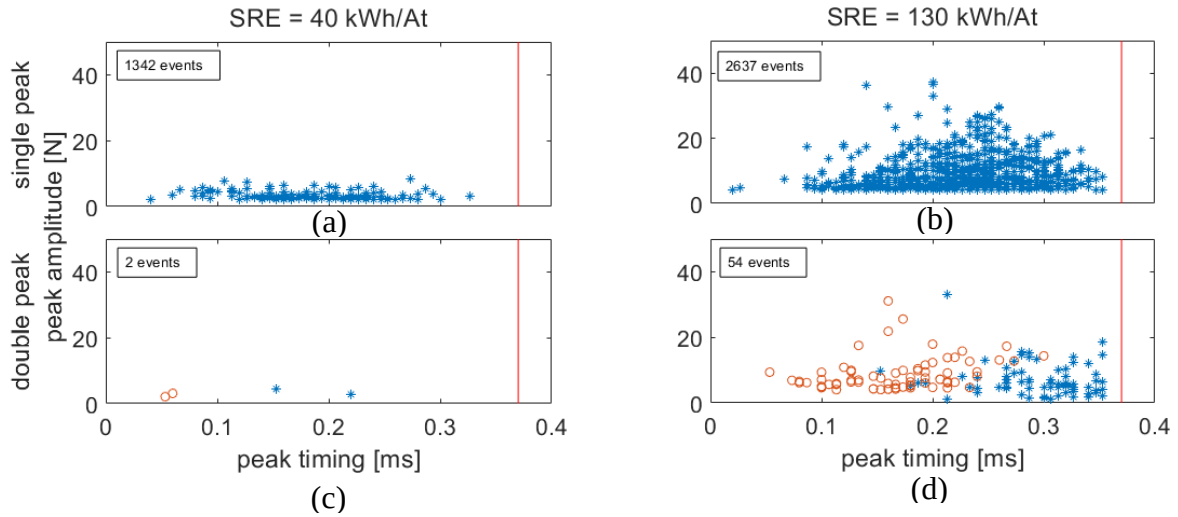

Figure 34:Single and dual peak events inner sensor.
Single and dual peak events at 40 kWh/At in a), c), and 130 kWh/At in b), d), for the inner sensor respectively. Early peaks in a dual peak event are indicated in orange, late peaks in dual peak events and peaks in single peak events in blue. The average duration of the respective bar passing events is indicated by the vertical line.

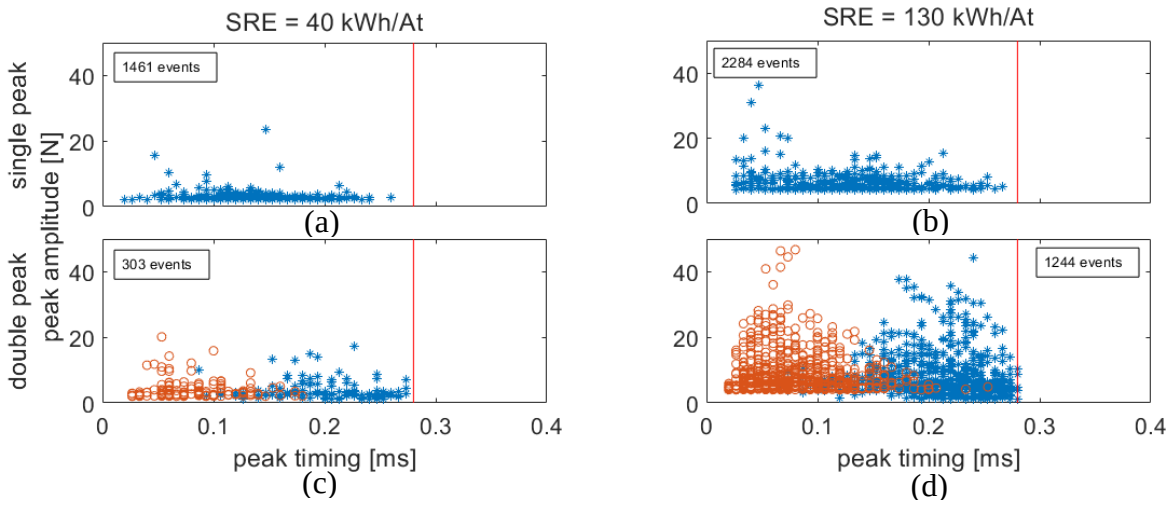

Figure 35: Single and dual peak events mid sensor.
Single and dual peak events at 40 kWh/At in a), c), and 130 kWh/At in b), d), for the mid sensor respectively. Early peaks in a dual peak event are indicated in orange, late peaks in dual peak events and peaks in single peak events in blue. The average duration of the respective bar passing events is indicated by the vertical line.

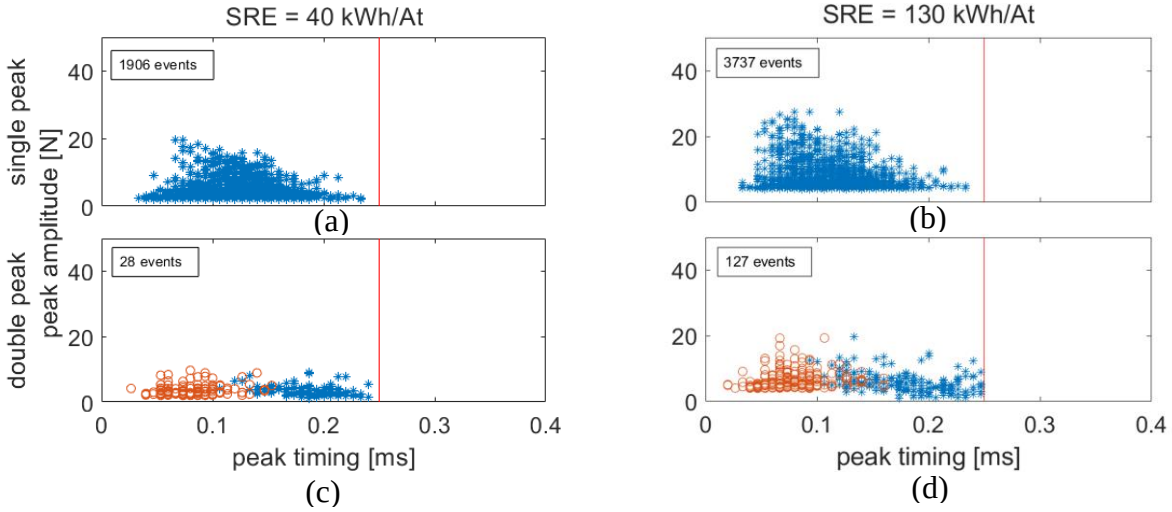

Figure 36: Single and dual peak events inner sensor.
Single and dual peak events at 40 kWh/At in a), c), and 130 kWh/At in b), d), for the outer sensor respectively. Early peaks in a dual peak event are indicated in orange, late peaks in dual peak events and peaks in single peak events in blue. The average duration of the respective bar passing events is indicated by the vertical line.

To explore the prevalence of dual peak events, the *dual peak ratio*, R_{DP}, is calculated for each SRE value. This ratio is the percentage of all BPEs that have two peaks, as shown in Equation (11).

$$R_{DP} = \frac{n_{DPE}}{n_{DPE} + n_{SPE}} * 100 \qquad (11)$$

Here, n_{DPE} is the number of dual peak events and n_{SPE} is the number of single peak events.

The dual peak ratio, confirms that dual peaks are present over the full range of refining energies and that this ratio increases with SRE increases, as shown in Figure 37. Of the three sensor positions, the mid sensor position shows the highest dual peak ratio. Both outer and inner sensors show lower dual peak ratios that increase as SRE increases.

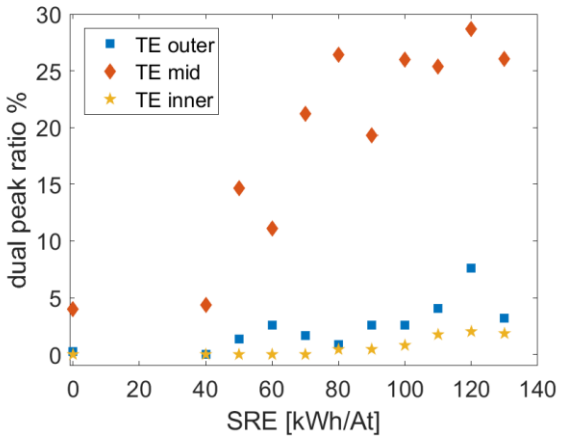

Figure 37: Dual peak ratio vs SRE.
Ratio of dual peak events to the total number of events in percent for each specific refining energy level during the power curve for each sensor on the tail end.

Normalized fiber length data and normalized freeness data for the discharge both decrease as SRE increases (Figure 38 a), b)). The fiber length data sees two stages in fiber length decrease. The first decrease is visible after 60 kWh/At and after 100kWh/At the decrease is continuous. For the freeness the decrease is visible after 60kWh/At.

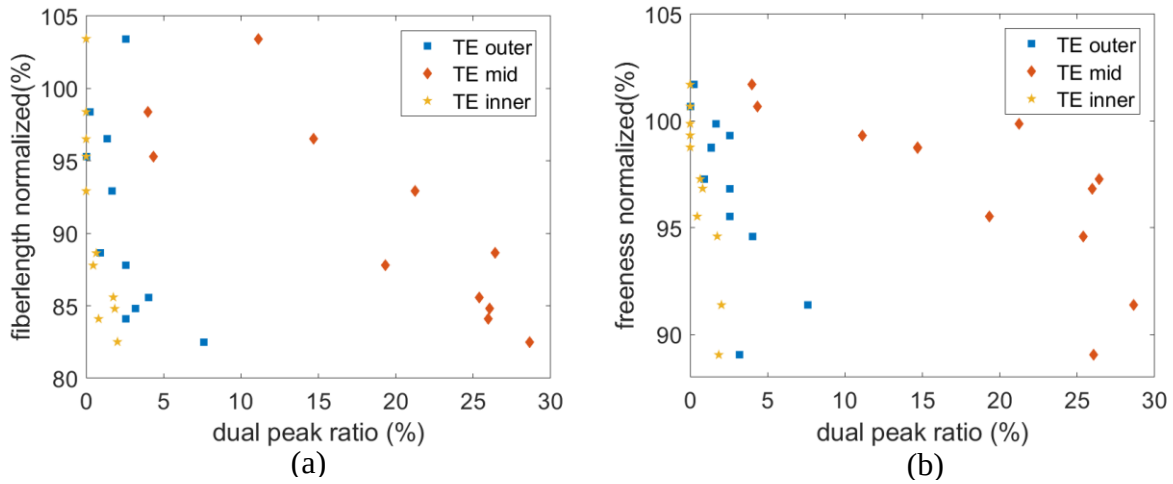

Figure 38: Fiber length and freeness vs dual peak ratio.
Normalized fiber length (a), freeness (b) for the tail end (TE) discharge line, plotted versus the dual peak ratio for outer, mid and inner sensor position. In order to normalize the data, all data values where divided by the feed fiber quality value of the respective SRE set point and multiplied with 100.

3.5 Discussion

The mean force plots show a characteristic profile at each sensor position. The inner sensor features profiles with a single peak that is skewed toward the third quarter of the BPE. At the mid sensor, the mean force profiles feature a single peak for low SRE and double peaks for high SRE. The transition between these two profiles occurs between 60 and 80 KWh/At, which coincides with the range of SRE in which fiber length and freeness both begin to decrease (Figure 38). For the outer sensor, the force profiles feature a single peak but, in contrast with the force profiles for the inner sensor, these peaks are skewed toward the beginning of the BPE.

In a previous study, based on mean force profiles measured with a single bar force sensor in a pilot-scale LC refiner, the authors showed that fiber cutting is associated with BPEs in which two force peaks occur [32], where the first peak is a “corner” force and the second peak is a friction force. This result suggests that, in the current study, the length reduction that occurs between 60 and 80 KWh/At, is occurring principally in the mid region of the refiner, *i.e.*, in the vicinity of the mid sensor and that minimal fiber cutting is occurring in the inner and outer regions of the refiner.

Analysis of the individual, rather than mean, BPE force profiles from the mill-scale refiner shows that dual peak events are present across a wider range of refining conditions than the mean force profiles alone suggest. In addition, as SRE increases, the dual peak ratio at all sensor locations increases while fiber length and freeness both decrease. The mid position shows the

highest dual peak ratio at all SRE levels. These results reinforce the finding that dual peak events are causal in fiber cutting and that fiber cutting occurs principally in the mid region of the mill-scale refiner with lesser amounts of fiber cutting occurring in the inner and outer regions.

To further explore the association of dual peak events with fiber cutting, bar force data collected from the pilot-scale LC refiner, as part of the earlier study [32], is re-analysed with a focus on individual, rather than mean, BPE force profiles. The resulting peak distribution plots (Figure 39) and dual peak ratio plot (Figure 40) show trends that are similar to mill-scale data (see Figure 34 to Figure 37). Namely, that dual peak events are present, although not prevalent, for a wider range of refining conditions than is indicated by the mean force profiles alone. Dual peak events are rare but present at low SRE, Figure 39 (a) and (c), and common at high SRE while significant numbers of single peak events are present for SRE values well within the fiber cutting range, Figure 39 (b) and (d).

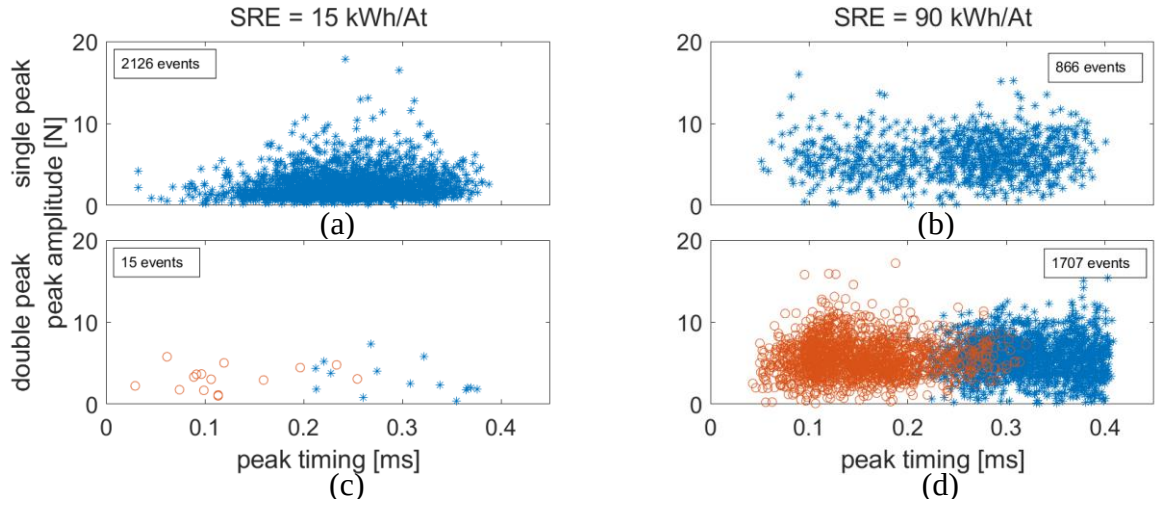

Figure 39: Single and dual peak events for pilot-scale refiner.
Single and dual peak events at 15 kWh/At in (a), (c) and 90 kWh/At in (b), (d) respectively for data acquired at 16" pilot-scale refiner. Early peaks in a dual peak event are indicated in orange, late peaks in dual peak events and peaks in single peak events in blue. The duration of a bar passing events is 0.4ms. The mean peak timings and peak amplitudes are indicated for single, early and late peak.

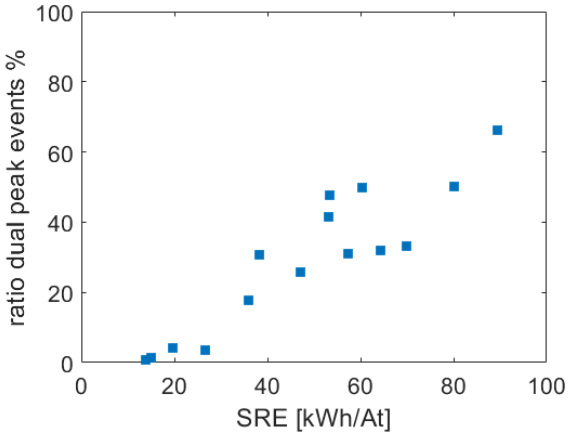

Figure 40: Dual peak ratio vs SRE.
Ratio of dual peak events to the total number of events in percent for each specific refining energy level during the test refiner trials.

Based on the mean force profiles from the mill-scale refiner, supported by the results from the pilot-scale refiner, the nature of refining action at each of the sensor locations can be hypothesized. At the mid position, the highest dual peak ratios are recorded. The early peak in these dual peak events is thought to represent corner force due to the interaction of flocs "stapled" to the leading edge of the rotor bar passes over the stator bar [25]. For smaller gaps and higher SRE values, this corner force leads to fiber cutting. The late peak in these dual peak events has been associated with a friction force [25], [32] or, as discussed earlier, pressure resulting from expulsion of water from the floc as it is compressed between the rotor and stator bars [46] but the mechanism underlying this late peak is less clear than for the early peak.

The inner sensor has the smallest dual peak ratios and the measured single peaks are late in the BPEs. These single peaks are, therefore, considered to be due to compression and not associated with fiber cutting.

At the outer position, single peak events are prevalent and the peaks in these events are skewed towards the beginning of the BPEs. If these single peak events are due solely to a friction or compression force, as proposed earlier, it would be concluded that significant fiber cutting does not occur in this region. On the other hand, if single peaks at this location are due to corner force, as suggested by their position early in the BPE, it would be concluded that fiber cutting does occur in the outer region of the refiner.

To explore the latter case, the authors consider work done by Eriksen et al. [46] in which an expression is developed for the pressure due to fiber compression , on the top of the bars in the refining zone (Equation (12)).

$$p \sim N \frac{a}{d} \rho U^2 \tag{12}$$

In this equation, a and d are the fiber diameter and the gap between opposed refiner bars, respectively, ρ is the density of water, *N* is the *crowding number* and *U* is the tangential velocity at the measurement position. The crowding number is defined as the number of fibers in a spherical volume of diameter equal to the length of a fiber and has been used to characterize flocculation of fibers in water suspensions [48]. Fiber diameter, plate gap and density of water are constant, for a given SRE, leaving only the crowding number and tangential velocity that vary with radial position.

For the inner, mid and outer sensor positions the tangential speeds are 22.2, 27.4 and 30.3 m/s, respectively. Pressures for 130 kWh/At are estimated based on the magnitudes of the mean peak normal force of the second or late peak at (see Figure 34 (d) to Figure 36 (d)) and the surface areas of the bar force sensor in each position. Based on Equation (12), the crowding number at the mid and outer sensors are 33% and 55% lower than at the inner sensor position, respectively.

This rudimentary analysis suggests that, due primarily to increasing tangential speed, local crowding number decreases with increasing radius which, in turn, leads to a reduction in the magnitude of the pressure due to fiber compression. The predicted decrease in this pressure with increasing radius suggests that fiber compression may be the mechanism that underlies the late peaks in the BPE data. This conclusion is consistent with the relative absence of late peaks from the data for the outer sensor, due to these peaks falling below the detection threshold for the force sensors, and the prevalence of BPEs with early peaks only.

3.6 Conclusion

Bar force sensors were installed in a 52-inch mill-scale double disc low consistency double disc refiner. Six sensors were installed, three on each side of the refiner at different radial positions.

Force measurements were taken continuously during normal operation and trials, i.e. power curves, were also conducted. In this work the trials data was analysed to explore the effect of varying operating conditions on bar force profiles. Previous work with this type of force sensor on a laboratory-scale refiner is used to compare findings.

Mean force profiles for the mill-scale refiner show different characteristics for different radial positions, one of these is that there is a transition from one to two peaks at the mid sensor. This transition correlates with the onset of fiber cutting.

Analysis of individual rather than mean force profiles shows that dual peaks are present at all three sensor locations through a wide range of refining conditions and that the prevalence of dual peaks increases as SRE increases and fiber length decreases.

Comparison with test refiner data that has been subjected to the individual force profile analysis described in the presented work, shows that key trends in the individual force profiles are present in both the pilot-scale and mill-scale data, namely: (a) a transition in the mean force profile from single to double peak profiles and (b) the presence of dual peak profiles when looking at individual force profiles for a wider range of refining than the mean force profiles suggest, validating the results of both studies.

To explain the different force profiles for the sensor positions in the mill-scale refiner, comparisons are drawn to work from the literature on the fiber compression pressure to show that the difference in tangential speed is a possible cause to produce the observed differences in the BPE force profiles.

3.7 Appendix A

Table 6: List of power curve trials conducted as of writing of this work.

Power curve number	Date	SRE range [kWh/At]	Target consistency
#1	January 9 2020	90, 100, 110, 120	3.8%
#2	January 23 2020	90, 100 110, 120, 130, 140	4.2%
#3	February 6 2020	120, 130, 140, 150	3.4%
#4	February 6 2020	75, 85, 95, 105, 115, 125	4.0%
#5	March 3 2021	No load, 40, 50, 60, 70, 80, 90, 100, 110, 120, 130,	3.8%

4 Effects of plate wear on bar forces and fiber properties in a mill-scale LC-refiner

4.1 Abstract

A set of piezo ceramic force sensors is implemented in a 52-inch mill-scale low consistency refiner to explore the effect of refiner plate wear on bar force sensor measurements. The sensor replaces a short length of a stator bar and measures normal and shear forces applied during the passage of each rotor bar. In previous work with this type of force sensor, force profiles for individual bar passing events (BPE) were investigated. In the work presented here, force profiles for individual BPEs are identified based on key features in the time domain force data. The individual bar force profiles are classified as single peak events which feature one peak corresponding to the fiber compression force and as dual peak events corresponding to fiber compression force and the corner force. The bar passing events are then analysed, based on dual peak ratio and time to peak of the early peak in the dual peak events. Force measurements are evaluated over the full run time of a set of refiner plates. Findings are compared with refiner plate wear measurements and discharge fiber analysis. It is shown that the decrease in the prevalence of the corner force correlates with the wear of the leading edge of the refiner bars or bar rounding of the run time of the refiner plate. This is accompanied by a decrease in plate performance which is represented by a decrease in fiber length and freeness reduction for the same refiner load.

4.2 Introduction

This work aims to combine refiner plate wear with bar force measurements. Therefore, the introduction is separated in two chapters discussing each individually.

4.2.1 Refiner plate wear

In low-consistency refining, wood fibers are developed for papermaking as they flow, in a water suspension, from the center to the periphery of the space between a rotating and a non-rotating disc separated by a small axial gap [49]. Grooved plate segments, or *plates*, are mounted to the opposed surfaces of these discs. These plates are in many cases made from ferrous alloys which are chosen for their wear resistance and corrosion resistance [50], [51]. The opposed

surfaces of the refiner plates are made up of bars and grooves with different geometries for refining zones and purposes. Grooves channel the fibers and allow the flow of the wood pulp radially outwards. The pulp fibers are periodically dragged out of the grooves and into the space between the bars of opposing discs. The passage of rotor bars over stator bars, or *bar passing events* (BPE), are thought to be the mechanism that develops fiber properties through the resulting application of shear and compression forces to the fibers [50], [52], [25].

The effectiveness of the refining process is measured through properties of the resulting fibers and paper and is a function of the net refining energy, among other things. The run time of a refiner plate is determined by its ability to maintain pulp quality at a given refiner load level. Deterioration of the refiner plate is a gradual process and calls for continued adjustment in the operation of the refiner to counter the resulting degradation in pulp quality [50].

A key aspect of bar geometry is the radius of the corner of the bar. In a new plate, this corner is typically sharp and, therefore, has a small radius. Over the run time of the plate, these corners can become rounded through a gradual process in which the material is removed through a combined abrasion and erosion mechanism [50], [53], [54].

The literature agrees that the radius of the leading edge of a bar affects how fiber flocs move into the gap between rotor and stator bars [55] and that rounded edges require more energy to attain a given pulp quality. However, there is no exact consensus over how this comes to happen. For example, Lundin et. al. [54] argue that the rounded bar edges reduce the amount of fiber moved into the gap between rotor and stator bars and that fewer fibers between the bars increase the severity of the refining process and promote crushing and cutting of these fibers. Following this train of thought, Batchelor et al. [3] have shown that force generation in bar crossings is a function of the radius of the leading bar edge. Other sources however suggest that rounding of the bar edges in the refining zone decreases the dwell time of fibers in the refiner and therefore reduces the amount of energy put into the fiber [50]. What the literature agrees on is that bar edge retention is critical to maintaining pulp quality in a refiner. When the bar edge deteriorates, i.e., rounds, the pulp quality is found to degrade and the energy needed to maintain the same quality goes up [56]–[58]. In their trials, Frazier et al. [59] found that bar rounding worsens progressively throughout the life of the plate and does not reach some equilibrium and stabilize.

In previous studies, several different parameters are use to describe changes in the bar edge profile. For instance, Batchelor et al. [3] and Konskenhely et al. [55] characterize bar edge rounding using the radius of curvature while Berger [56] uses a unspecified bar rounding factor. In a more complex approach, the shape of the bar edge, $h(x)$, has been described by Bordin et. al. [51], following Frazier's model [60], as shown in Equation (13).

$$h(x) = \Delta e^{(-\beta x)} \tag{13}$$

Here, Δ is the distance from the top of the bar to the point on the bar face where rounding begins. x is the dimensionless bar width ($0< x<1$) and β is a dimensionless coefficient [51]. A larger β indicates a sharper edge.

Bar height is another geometric parameter that is affected by plate wear. Reduction in bar height over time, leads to a decrease in groove depth which in turn affects the way in which pulp flows through the refiner. Frazier [60] showed that, as refiner plates wear, the thrust force needed to achieve the same refiner load, increases. In another study, Smith et al.[61] showed that increased wear on the refiner bars was destabilizing the refining process [61]. Frazier et al. argued that reduced bar height due to plate wear decreases the capacity of the refiner capacity [59], which they consider as the total volume of pulp-water mix contained in the refiner at any given time. Work on fiber trapping behaviour of worn refiner plates versus non worn plates suggests further that worn plates are less beneficial for transporting fibers into the gap between refiner bars [54]. Studies of plate wear in a twin disc LC refiner indicate that wear on the motor end is lower than that on the adjustable end and that rotor wear is slightly higher than stator wear [59].

4.2.2 Forces in refining

Understanding forces on refiner bars or bar forces in refining is, therefore, a necessary step toward optimizing the refining process, as suggested by Kerekes and Senger [21]. Forces acting on bars have been described as comprising a *friction force* and a *ploughing* or *corner force* [25], [3], [35]. First introduced by Martinez et al. [25] and further developed by Kerekes et al. [35], the corner force arises as the leading edge of the rotor bar approaches the forward edge of the stator bar, compressing pulp in the intervening gap [21]. The corner force has been shown to have a strong relationship to the shape of the bar edge. A sharper edge results in a higher corner force whereas a rounder edge results in a lower corner force [21]. Once the leading edge of the rotor bar

passes beyond the forward edge of the stator bar, the corner force falls off and, over the second half of the BPE, the friction force, caused by the fibers being dragged over the surfaces of the refiner bars, dominates the signal.

Recent models show that the friction force is accompanied by a force normal to the refiner bar which can be thought of as a fiber floc *compression force* [45], [46]. Eriksen et al. used high-resolution pressure measurements to investigate pressures on the surfaces of refiner bars [45]. This work shows that the magnitude of pressure peaks correlates with a model of hydrodynamic pressure resulting from water expulsion from the floc as it is compressed between the rotor and stator bars [46].

In a recent study by the authors, a bar-force sensor paired with a rotary encoder was installed in a 16" AIKAWA LC refiner and trials were conducted using softwood and hardwood pulps, both at a consistency of 3.5%. The trials were conducted at 1200 rpm, and the plate gap was incrementally decreased from 3.5 mm to 0.2 mm. The rotary encoder data was used to register measured bar forces to the relative position of a rotor bar as it passes over the stator bar in which the force sensor is installed. The authors used the registered force profiles to create mean force profiles based on all BPEs for a selected rotor bar passing over the stator bar in which the sensor was installed. These mean force profiles exhibit a distinct transition as the plate gap is closed which corresponds to the onset of fiber cutting. For large gaps, the authors found a *late peak* in the force profiles that occurred toward the end of the bar passing event. For gaps that are less than the *critical gap,* below which fiber cutting occurs, the authors found an additional *early peak* in the force profiles that occurs close to the start of the bar passing event. This early peak correlates with the onset of fiber cutting leading to the hypothesis that the early peak represents the *corner force* and, therefore, that corner force is causal in the onset of fiber cutting [32].

Furthering this ongoing study, a set of piezo ceramic force sensors was implemented in a 52-inch mill-scale low consistency refiner to explore the effect of varying operating conditions on bar force profiles. Force profiles for individual BPEs were identified based on key features in the time domain force data. The individual bar force profiles were classified as single peak events which feature one peak corresponding to the fiber compression force and as dual peak events corresponding to fiber compression force and the corner force. Bar passing events were first

analysed based on their mean force profiles. Evolving from this generalised view, the prevalence of dual peak events was investigated via the *dual peak ratio*, R_{DP}. This ratio is the percentage of all BPEs that have two peaks, as shown in Equation (14) [15].

$$R_{DP} = \frac{n_{DPE}}{n_{DPE} + n_{SPE}} * 100 \tag{14}$$

Here, n_{DPE} is the number of dual peak events and n_{SPE} is the number of single peak events.

The authors compared and validated their findings with bar force profiles from the test refiner trials from previous work. The authors showed that dual peak events which are considered to represent the corner force, are present through out the whole range of refining and increase with increased refining energy. This increases the understanding of the way corner force contributes to the refining process. Furthermore, it is found that different radial positions on the stator plate are subjected to different force profiles. This is thought to be due to the difference in tangential speed and a change in the fiber and floc material properties at different radial positions [33].

In the presented work, refiner bar force sensors are installed in a mill-scale LC refiner. The sensors measure forces on the refiner bars at different radial locations over the working life of the refiner plates. Plate wear is evaluated, based on the bar edge shape and the bar height, after the plates are decommissioned. The aim of this work is to identify changes in the force sensor measurements, namely the prevalence of the corner force and the position of the corner force in the bar passing event, over the run time of the refiner plates which can give an indication of the refiner plate performance.

4.3 Materials and Methods

This section gives an overview of the experimental setup of this work. The authors are describing the refiner used for this work as well as the used refiner plates. Also documented is the bar force sensor set up including the respective data acquisition and data processing used for the result section. In the last part of this section the methods used to analyse the plates after decommissioning are explained.

[15] Equation (14) is a repeat of Equation (11) in Chapter 3.

4.3.1 Refiner

The refiner used in this work is an Andritz TwinFlo 52" LC-tertiary refiner located at the Catalyst, Paper Excellence mill in Crofton BC. This is a twin disc refiner with two stator plates and a double sided rotor which separates the two refining zones, as shown in Figure 41[16]. The refiner is fed from the motor or Drive-End (DE). On the opposing side, the Tail-End (TE) stator can be moved in the axial direction to adjust the gap between the two stator plates. The rotor "floats" on a splined shaft and, therefore, its axial position cannot be actively controlled. Plate gap measurements only exist between the two stator plates. Separate discharge lines for each refiner side are located at the bottom of the refiner.

The rotor plates and stator plates for these trials, manufactured by Andritz Durametal, have different bar patterns, as shown in Table 7 and Figure 42[17]. The standard operating speed for the refiner is 420 rpm.

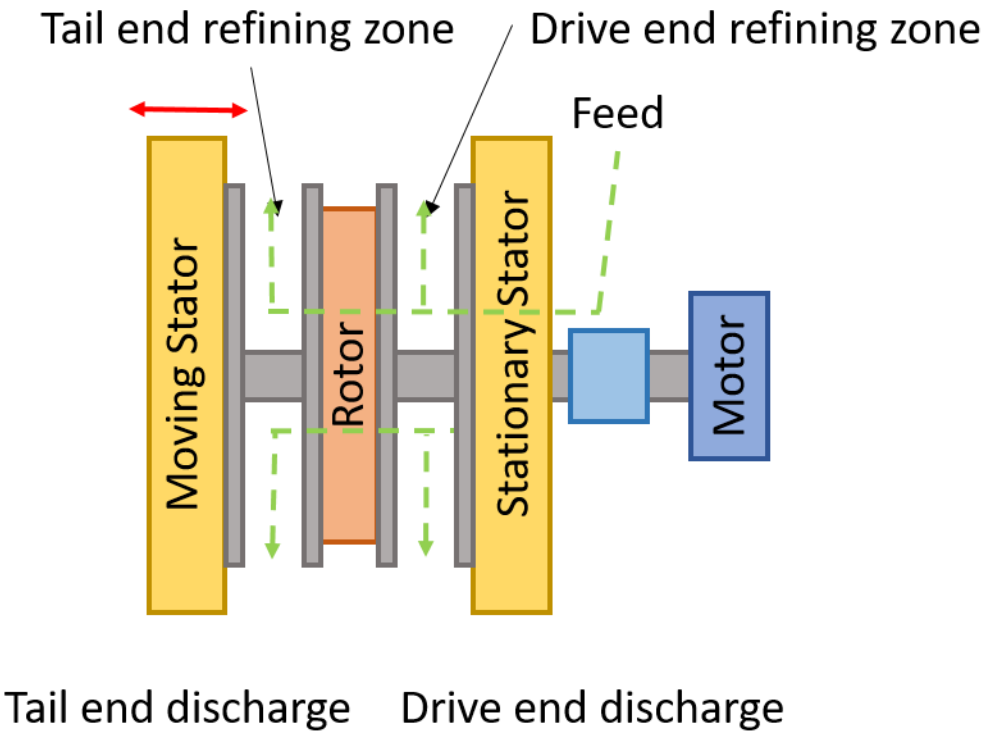

Figure 41: Layout of TwinFlo refiner at Catalyst, Paper Excellence mill in Crofton BC. The moving stator moves axially. The rotor is positioned floating in between the two stator plates.

[16] Figure 41 is a repeat of Figure 4 in Chapter 1.
[17] Figure 42 is a repeat of Figure 28 in Chapter 3.

(a) (b)

Figure 42: Refiner plate segments with indicated zones for rotor (a) and stator (b).

Table 7: Bar geometries of the Andritz Durametal refiner plates used in the Twin Flo refiner.
The radial zones for the stator and rotor plate are *indicated in Figure 42 (a) and* (b), respectively.

	Stator			Rotor	
	Zone 1	Zone 2	Zone 3	Zone 1	Zone 2
Bar width [mm]	2.29	1.57	1.57	3.18	3.18
Groove width [mm]	3.81	2.69	2.36	3.81	3.18
Average bar angle [°]	22.5	22.5	22.5	35	35
BEL [km/rev]	325.39			105.42	

4.3.2 Force sensors

The sensors used in these trials were custom designed, based on the work of Prairie et al. [4], Olender et al. [6], Harirforoush et al. [30] and Aigner et al. [32]. Each sensor probe replaces a section of a bar on the stator plate, 0.15 inches (3.8 mm) in length. The probe is supported by two piezo elements which emit signals that are processed to independently determine the forces applied to the probe tip. In the installed configuration the sensors measure two forces: the normal force, which is perpendicular to the refining plane or parallel to the refiner axis; and the shear force which lies in the refining plane and is perpendicular to the refiner bar [31].

Three sensors are installed in each one stator plate, each at a different radial position, as shown in Figure 43[18] (a). Figure 43 (b) presents a view of the back of the stator plate, showing the housings and tubing that protect the sensor bodies and wires from the refiner environment.

Signals from the force sensors are processed using custom charge amplifiers. The amplified signals are input to a data acquisition system, comprised of a National Instruments cDAQ-9188 data acquisition card connected to a desktop computer running LabVIEW™ software. LabVIEW is used to monitor the sensor signals, start and stop the recording and save the data sets to memory in TDMS file format. Processing of the RFS data follows the methods used by Harirforoush [31] and Olender [4], and MATLAB (Mathworks; Natick, MA, USA) is used to manage the data sets.

Each sensor is calibrated using a modal hammer (PCB Piezotronics/086D80-12911/ Depew, New York). This calibration is conducted before the sensors are installed in the refiner plate using a custom fixture. The resulting calibration constants are used to determine the normal and shear forces from the measured piezo signals. Calibration of sensors and subsequent conversion of voltage signals into force readings is based on previously described methods, as described by Prairie et al. [27]. The calibration is based on a linear regression of the peak signals from the piezo elements, measured at the output of the charge amplifier, and the corresponding peak signals from the modal hammer. To identify defects in the sensors, recalibration is conducted after the sensor are taken out of the plates and these recalibration values are compared with the initial calibration values.

[18] Figure 43 is a repeat of Figure 29 in Chapter 3.

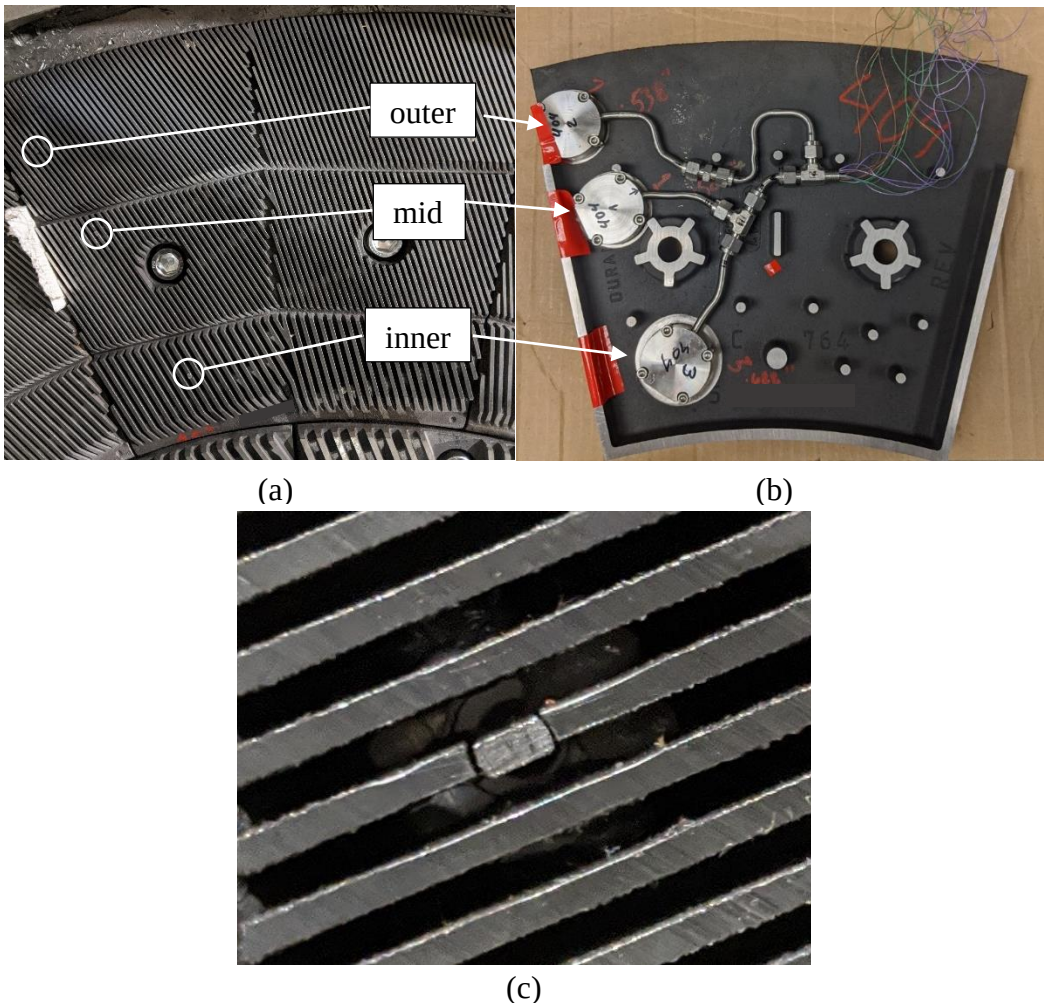

Figure 43: Pictures of the stator pate with installed sensors.
(a) front side of stator plate. (b) back side of stator plate. Housing of sensors and wiring visible. (c) close up of an installed sensor.

4.3.3 Pulp properties

Pulp samples acquired are analysed at the mill using a KMAP fiber analyser (Valmet Technologies, Espoo, Finland). Pulp properties include average fiber length, fiber length fractions, consistency and freeness for each of the discharge lines and the feed line.

4.3.4 Data acquisition

This work is based on data acquired during the whole work life of the refiner plates, approximately 10,000 hours. The sensors are sampled at 150 kHz for a 1 s period at intervals of 30 s for the whole duration of the sensor installation. During this time, the operational data of the refiner is also recorded (i.e. refiner power, feed and discharge flow rates, feed and discharge pressures). Pulp samples presented in this work are taken from the feed stream and from each of

the two discharge lines. The nominal operational speed of the refiner is 420 rpm, and the feed consistency ranges between 3.4% and 4.2%. The pulp furnishes used in this refiner is hemlock. The refiner is located in the third stage of the main Thermo-Mechanical Pulping (TMP) line.

4.3.5 Data processing

Peaks in the force signal are determined based on *local amplitude* and *prominence* of peaks, utilizing the peak analysis tool of MATLAB (version R2020a). The local amplitude describes the height difference between a valley and the subsequent adjacent peak. Prominence is a value widely used in topography and is a measure of the significance of a peak, relative to adjacent peaks [47]. This parameter is used to determine if a peak is *independent* or is part of another peak.

To identify which peaks correspond to which BPE, the previously determined peaks are further evaluated based on their temporal spacing. The temporal spacing of the peaks is compared to the geometric spacing of the bars on the rotor on the circle whose radius corresponds to the position of a given sensor.

Referring to Figure 43 (a), each rotor and stator plate segment spans 30° and is separated into two or three radial zones, respectively. Each plate is also separated into two sides, each spanning 15°, within which all refiner bars are parallel to each other. Because of this the angle between a bar and the radial direction changes over the course of each side. At the center of each side, the angle between bars and the radial direction is equal to the average bar angle as noted in Table 7. At the beginning and the end of each side the angle between bars and the radial direction is the average bar angle plus 7.5° and minus 7.5°, respectively. As a result, the distance between adjacent rotor bars, along the circle corresponding to the sensor location, is not constant nor is the time interval between the passage of adjacent rotor bars over the sensor probe which, as noted earlier, is referred to here as the duration of the BPE.

The variations in the duration of the BPE, given that there are 12 plates with 2 sides each, repeats 24 times per revolution. The BPE durations for one side of the rotor plate, for a rotor speed of 420 rpm, are listed in Table 8. Also noted in Table 8 are the number of data samples taken per BPE at each sensor location based on a sampling rate of 150 kHz (see section Data Acquisition).

Table 8: Bar passing event durations.
Bar passing event durations and number of samples per bar passing event at each respective sensor position. The inner, mid and outer sensor feature 16, 21 and 24 bars per bar segment side respectively.

Sensor Position	# BPEs	BPE duration Range [ms]	Samples per BPE
Inner	16	0.358 – 0.426	54 - 64
Mid	21	0.264 – 0.315	40 - 47
Outer	24	0.239 – 0.286	36 - 43

It is assumed that the duration between force peaks, which represent individual BPEs, correlates with the duration of bar passing events determined based on the plate pattern. Similarly, it is assumed that peaks which are closer together than the duration of a bar passing event, can be considered as part of the same bar passing event. Taking those considerations into account, a correlation algorithm is computed between the force peak data set and the data set representing the bar pattern. Finding the closest correlation between the previously established bar pattern and the peak pattern from the peak analysis allows to associate each force peak with a bar in the plate segment side. After the force peaks are associated to a BPE, the valley preceding a force peak is defined as the start of the bar passing event. If two force peaks are associated to a BPE, the valley preceding the first is considered the start.

In order to analyse the transition in force sensor measurements over the life time of the plates with respect to plate wear, two force sensor metrics are used in this work. The first, the dual peak ratio, is thought to show how the prevalence of the corner force behaves over the run time of the refiner plates. The dual peak ratio is calculated based on previous work [33] for each sensor position. The second metric used, is the time to peak (TTP) of the early force peak which is the time between the start of the BPE and the point at which the force profile reaches its first peak in a dual peak event.

4.3.6 Plate wear analysis

To analyse the plate wear, the radius of the bar edges is measured. To this end, molds of the bar profile where made similar to Frazier et al. [59]. The replica material used in this project was Blue Stuff by Greenstuffworld (Product number: 8436554365159ES, greenstuffworld.com). It is a thermo-plastic molding material, with a set time of approximately 15 min which can be reduced to mouldable conditions by immersion in hot water during 3 minutes. It was selected based on its precision, workability and reusability. After removal from the refiner the replicas were cut with a scalpel perpendicular to the bar orientation. Each cross-section was placed on a dissecting microscope equipped with a digital camera (Dino-eye edge, dinolite.com) with the cross-section of the bar in view. A digital image (see Figure 44) of the bar cross-section was taken and the radius of the edge was determined by defining 3 points (start, mid and end) on the curvature and fitting a circular segment through them.

Molds of the refiner bars were taken after the refiner plates reached the *end of plate life* after 9400 run time hours and were taken out of the refiner, at the radial position of the sensors on each of the stator plates as well as on the rotor plates at the 0° and 180° position.

Bar heights were measured with a dial calliper, both on the plates with 9400 run time hours and on the plates with zero run time hours. Calliper measurements were taken in the areas from which the molds were produced.

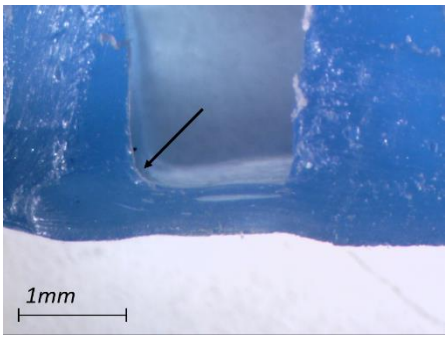

Figure 44: Microscopy image.
Microscopy image of a bar mold cross-section of the Tail end stator on the inner position.
Indicated is the rounded leading edge.

4.4 Results

The refiner plates were replaced after 9400 hours of operation, which is in line with the expected run time of these plates. All data presented in this work is presented with respect to the run time of the refiner while these plates were installed.

The installed sensors were recalibrated once, *in situ*, after 3000 run time hours when the refiner was opened to check on an unrelated component. This recalibration included only the normal component of the calibration constants as the calibration was done on installed plates and sensors for which calibration in shear direction is not possible. Results of this recalibration indicate that the mid and outer sensors on the drive-end of the refiner may not be functioning correctly as their sensitivity dropped off significantly. No data for these sensors is presented in this work. The remaining four sensors showed insignificant (<10%) changes in their calibration constants. Post-trial calibration, after the plates where removed at a run time of 9400 h, confirm the trends found in the in-situ recalibration at 3000 h. The sensors in the DE outer and DE mid positions, show significant changes in their calibration constants whereas the other four sensors show changes of less than 10% compared to the initial calibration prior to installation. The analysis presented here is, therefore, based solely on the data collected by the sensors at the DE inner position and the TE inner, mid and outer positions.

The results of these recalibrations suggest a loss of sensitivity, for the four remaining sensors, which may affect the trends in force magnitudes observed over the duration of the trial. Therefore, analysis and discussion of the data focuses on qualitative changes in the shape of force profiles during BPEs and TTP data as these results are relatively independent of force amplitude.

The dual peak ratio data is presented in Figure 45 (a) - Figure 48(a) and the TTP in Figure 45(b) - Figure 48(b) for the outer, mid, inner tail-end positions and the inner drive-end position, respectively. Each data point presents the average value for 24 hours of run time. Included in the graphs are linear trend lines over the whole plate run time to show the general trend of the data.

Analysis of the dual peak ratio shows a decrease over the run time of the plates for all sensors. For the outer sensor (tail-end) the ratio is high in the first 1000 hours and then falls off quickly (Figure 45 (a)). For the mid sensor the dual peak ratio is high until about 2000 hours and then falls continuously after that (Figure 46 (a)). The dual peak ratio for the inner sensor on the

tail-end is initially small compared to the other sensors but, like the other sensors, falls off after 2000 hours (Figure 47 (a)). The inner sensor on the drive-end shows similar behaviour to the inner sensor on the tail-end but its dual peak ratio is consistently twice as high (Figure 48 (a)).

The TTP of the early peak on the inner sensor on the drive-end is the only sensor with a declining trend over the plate run time (Figure 48 (b)). The outer mid and inner sensors show increasing trends for TTP (Figure 46 - Figure 47 (b)). The TTP data for all sensors shows no consistent trends in the first 2000 hours of runtime.

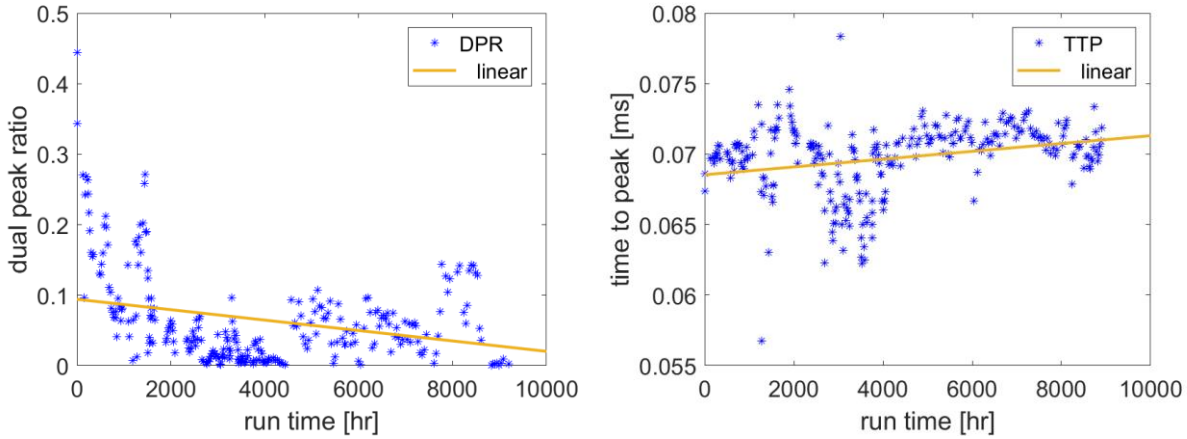

(a) (b)

Figure 45: Outer sensor position on the tail-end side.
Dual peak ratio (DPR) (a), time to peak (TTP) for the early force peak (b).
Values indicate the 50th percentile for each respective day.

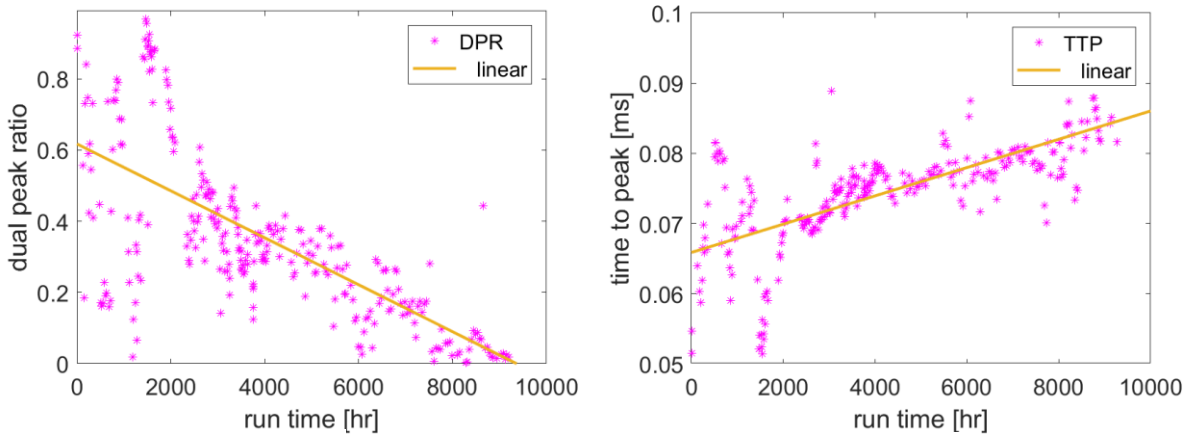

(a) (b)

Figure 46: Mid sensor position on the tail-end side.
Dual peak ratio (DPR) (a), time to peak (TTP) for the early force peak (b).
Values indicate the 50th percentile for each respective day.

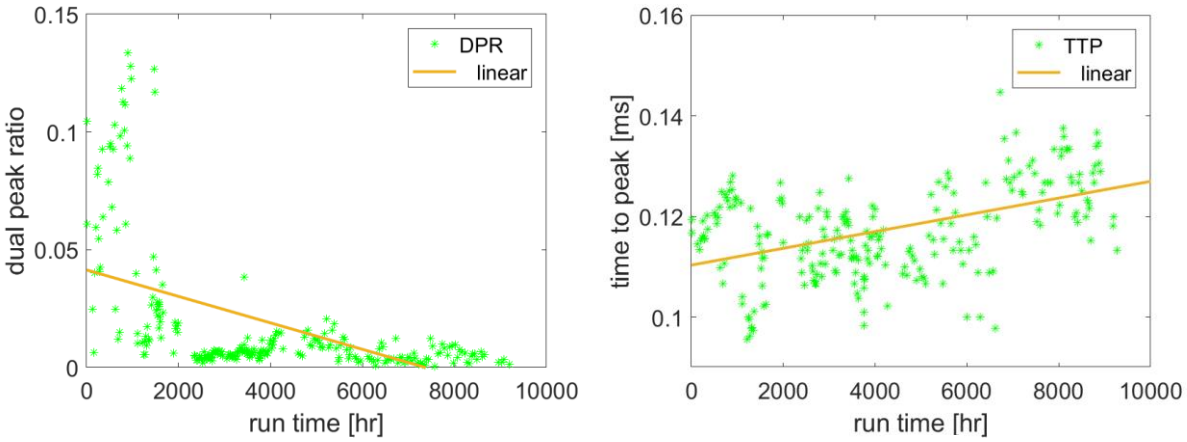

(a) (b)

Figure 47: Inner sensor position on the tail-end side.
Dual peak ratio (DPR) (a), time to peak (TTP) for the early force peak (b).
Values indicate the 50th percentile for each respective day.

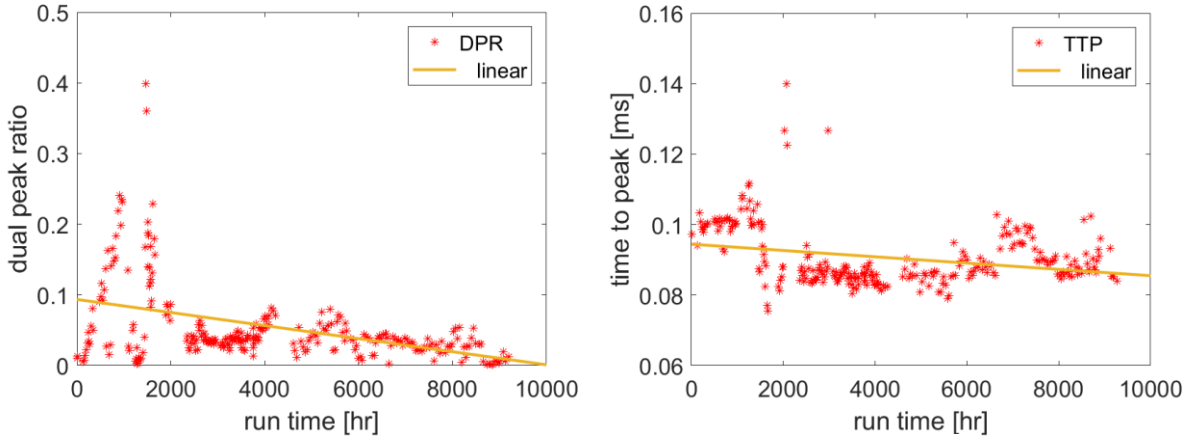

(a) (b)

Figure 48: Inner sensor position on the drive-end side.
Dual peak ratio (DPR) (a), time to peak (TTP) for the early force peak (b).
Values indicate the 50th percentile for each respective day.

Gap measurements between the two stator plates decrease over the run time of the refiner plates. Converting the LVDT readings into millimetres shows a decrease in plate gap of about 6mm (Figure 49) over the run time of the plates. The decrease in gap measurement is steady and not subjected to drastic changes in slope.

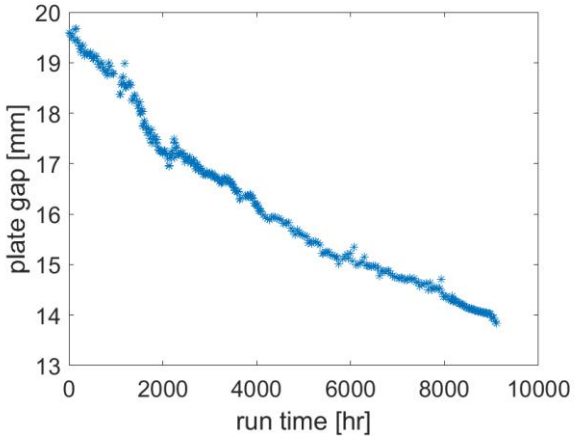

Figure 49: Plate gap measured by the LVDT.
Values indicate the 50th percentile for each respective observation period.

Bar edge radius increases are shown in Table 9 as a measure of the extent of bar edge rounding. These radii are based on the mean of 10 measurements at each position of the plates with 9400 run time hours subtracted by the average initial leading edge radius of a plate with 0 run time hours. Included are the respective standard deviations.

The extent of bar rounding on the tail-end stator was larger than on the drive-end stator and more rounding was measured on the rotor plates compared to the stator plates. Bar rounding on the rotor appears to be unaffected by radial position while the inner positions on the stators show larger radii than the other positions of each stator.

The measured bar height reductions are presented in Table 10 as a measure of the extent of bar wear. The presented values are based on the mean of 10 measurements at each position of the plates with 9400 run time hours which was subtracted from the mean of measurements on a plate with 0 runtime hours. Included are the respective standard deviations. Also included are the accumulated bar height reduction for the rotor and stator on the tail-end and the rotor and the stator on the drive-end.

The most significant bar height reduction was found at the outer position of the tail-end stator. At the mid position, the drive-end rotor experiences the most bar height reduction and at the inner position the tail-end rotor. The measurements of bar height reduction show that the reduction of the rotor bar height is higher than for the stator bars and that the reduction in bar height varies with radial position. Summing the bar height reductions of the stator and the rotor

shows that the total bar height reduction for the outer, mid and inner position are 4.72, 3.69 and 2.95mm, respectively, for the tail-end and 3.77, 4.59 and 2.77mm, respectively, for the drive-end while the total bar height reduction over both sides is 8.49, 8.28 and 5.72 mm, respectively.

Table 9: Radius increase on the leading bar edges.
Evaluated for tail-end and drive-end side on the used stator and rotor refiner plates at 9400 runtime hour. Presented values are based on averages out of 10 measurements each at the radial positions equal to the sensor positions and represent the difference between the initial radius[19] and the final, rounded, bar edge radius. On the rotors, measurements where taken on plate segments at 0° and 180° and averaged.

Leading edge radius increase [mm]						
	outer		mid		inner	
	mean	st dev	mean	st dev	mean	st dev
Stator TE	0.16	0.03	0.20	0.04	0.43	0.13
Rotor TE	0.32	0.06	0.42	0.10	0.37	0.09
Rotor DE	0.36	0.15	0.27	0.08	0.31	0.12
Stator DE	0.11	0.02	0.12	0.04	0.20	0.13

Table 10: Bar height reduction of the stator and rotor refiner bars.
Evaluated for tail-end and drive-end side on the used refiner plates at 9400 runtime hour subtracted from the initial bar height of a refiner plate at 0 runtime hours[20]. Presented values are based on averages out of 10 measurements at the radial positions equal to the sensor positions. On the rotors, measurements where taken on plate segments at 0° and 180° and the average is presented in this table. Also included in this table are the sum of the bar height reductions for each rotor and stator pair at each sensor position as well as the sum of the bar height reductions over all stators and rotors for each sensor position.

bar height reduction [mm]						
	outer		mid		inner	
	mean	st dev	mean	st dev	mean	st dev
Stator TE	2.62	0.15	2.02	0.13	0.94	0.22
Rotor TE	2.10	0.16	1.67	0.18	2.00	0.23
Rotor DE	2.57	0.15	2.57	0.17	1.46	0.27
Stator DE	1.20	0.17	2.02	0.24	1.31	0.10
TE (Stator + Rotor)	4.72		3.69		2.95	
DE (Stator + Rotor)	3.77		4.59		2.78	
sum (DE + TE)	8.49		8.28		5.72	

[19] Initial bar edge radii, on the plate with zero runtime hours, ranged from 0.01 to 0.04 mm.
[20] Nominal bar height values are presented in Table 4 in Chapter 3.

Fiber length and freeness analysis of the discharge pulp samples is presented in Figure 50 (a) and (b) over the run time of the refiner plates[21]. These data points are from individual trials (i.e. power curve trials) conducted over the run time of the refiner plates. Fiber length is presented as length reduction relative to the feed fiber length in percent and freeness is presented as freeness reduction relative to the feed freeness. Figure 50 (a)shows a decrease in the fiber length reduction over the duration of the plate installation, except over the first 1000 hours, where there is an initial increase of the fiber length reduction. Figure 50 (b) shows a similar trend for the freeness reduction, where for the same refiner load the reduction in freeness is lower later in the plate life. The exception is again the first 1000 hours where the freeness reduction increases.

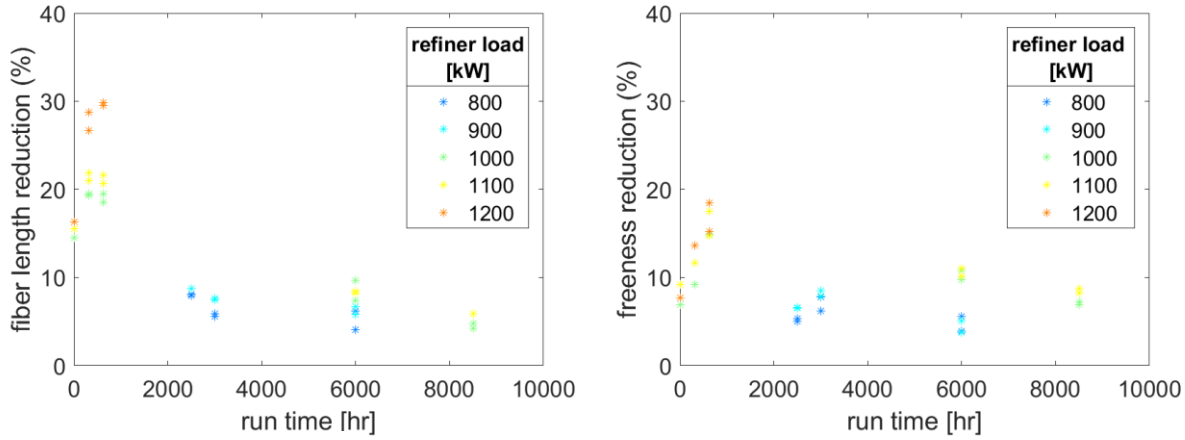

Figure 50: Fiber length and freeness reduction vs run time.
Discharge fiber length decrease (a) and Freeness reduction (b) in percent plotted over the run time of the refiner plates. Colors indicate refiner load with 800 kW in blue and 1200 kW in red.

[21] Colours indicate net refiner load levels.

4.5 Discussion

The measured plate gap falls continuously over the duration of the trial, as shown in Figure 49. At the end of the trial, the total reduction in the gap is 6.0 mm and this measurement can be used to estimate the reduction in bar height. The measured plate gap indicates the distance between the two stator plates and, therefore, the reduction in plate gap is the sum of the reductions in bar height for the plates on both stators and for the plates on both sides of the rotor. If total bar height reduction is assumed to be distributed equally among the plates on the two stators and two rotors, then the resulting bar height reduction for each stator and rotor is about 1.5 mm and the reduction on each side (tail and drive) is about 3.0 mm. The continuous decrease in the gap measurement indicates that bar height reduction is also continuous over the duration of the trial.

The direct measurements of bar height reduction, shown in Table 10, show that the reduction of the rotor bar height exceeds that of the stator bars and that the reduction in bar height varies with radial position. Summing the bar height reductions on each side and location shows that the total bar height reduction for the outer, mid and inner positions are 4.72, 3.69 and 2.95 mm, respectively, for the tail-end and 3.77, 4.59 and 2.77 mm, respectively, for the drive-end. The bar height reduction is highest for the mid and outer positions and lowest for the inner position. The bar height reductions for the inner position compare well with the bar height reduction estimate of 3.0 mm based on the gap measurements.

These results are consistent with previous studies. Frazier et al. [59] show that rotor bar wear is 2-5% higher than stator bar wear and Bordin et al. [51] report increased bar height reduction with increasing radial position. Although neither study provides a definitive cause for these behaviours, it is reasonable to assume that tangential speed, bar width and height, which are all different for different radial positions, may play a role in these trends. In fact, Bordin et. al. [51] found a similar conical-geometry wear of the gap clearance and postulated that this is due to the higher tangential velocity for higher radii.

Bar edge rounding data, shown in Table 9, indicates that leading edge wear on the rotor bars is larger than on the stator bars. The extent of bar edge rounding is also larger on the tail-end stator compared to the drive-end stator. This wear has also been reported in the literature, which shows that bar edge wear is higher on the rotor and highest on the tail-end of a LC twin disc refiner [59].

The literature provides a possible explanation for the difference in wear between the rotor and stator bars. In an *in situ* video study, it was shown that pulp fibers adhere to the stator bars for multiple BPEs but do not adhere to rotor bars [62]. A possible mechanism of increased wear on the rotor bars is that these fibers, which are stationary on the stator, *protect* the stator bars and prevent wear of the bar edge and the bar. On the rotor, on the other hand, no stationary fibers are present to protect the bars from wear and, hence, the increased wear on these bars.

For the same refiner load, fiber length reduction and freeness reduction are lower at the end of plate life, compared to earlier in the plate run time, as shown in Figure 50. This result is consistent with the literature which shows that rounded bar edges and decreased bar height results in longer fibers [55] and higher freeness [58] at the same refiner load level, relative to fibers refined with new plates.

All sensors show a decrease in the dual peak ratio as the run time of the plates increases. As discussed earlier, dual peak ratio has been shown to correlate with the prevalence of the corner force during bar passing events [33]. Therefore, the decrease in the dual peak ratio indicates a decrease in the prevalence of the corner force for all sensors. At the same time, the measured bar edge radius increases over the life of the plate. These results suggest that the rounding of the leading edge of the bar decreases the prevalence of the corner force in refining.

All sensors, with the exception of the drive-end inner sensor, show an increase in the time to peak (TTP), over the duration of the trial. Notably, the drive-end inner sensor does show an increasing trend beyond the 2000 h mark. As discussed below, the data for this first 2000 h for all sensors exhibits features suggesting that this is a *break-in-period* for the refiner plates in which the refining action is different than either new plates or partially worn plates.

TTP is believed to be a function of parameters including: tangential speed, number of fibers trapped between the stator bar and rotor bar or *crowding number* [46], local consistency, plate gap, bar edge shape, bar height and bar width. Throughout the trial, all of these parameters remain relatively constant with the exception of bar height and the bar edge shape. It is apparent, therefore, that the change in the bar edge shape and/or bar height are key factors driving the increase in the TTP for the corner force.

The results in this study suggest a correlation between the prevalence of the corner force and the bar height reduction. It is shown that, throughout the trial, the dual peak ratio is highest at the mid sensor position. In previous work, a high dual peak ratio was shown to indicate the prevalence of corner force [33]. As the bar height reduction at the mid position is also high, it is concluded that the higher prevalence of corner force at the mid position results in higher plate wear at the mid position.

In a previous work, based on these same trials in the twin-disc refiner, it was proposed that, although the dual peak ratio was low, the outer position also experiences a high prevalence of corner force [33]. The single peaks that are prevalent in the BPE data for this sensor are biased toward the beginning of the BPEs which suggests that these are corner force peaks. The prevalence of these single peak corner force events is consistent with the high levels of bar height reduction at the outer position.

Unlike the bar height reduction data, the bar edge rounding measurements do not clearly increase with radius. This result does not necessarily indicate that corner forces are not causal in bar edge rounding. As the bar height wear increases with radius, the wear on the edge of the bars may be masked by the previously discussed increasing wear on the top of the bar. This would prevent the radius of the bar edge from increasing with radius.

During the first 2000 h of the trial, there is a sharp increase followed by a rapid decline in fiber length reduction, freeness reduction and dual peak ratio for all sensors (see Figure 45 - Figure 48 (a) and Figure 50). During this period, the load to achieve a given freeness or fiber length reduction is higher than after 2000 h of operation. This suggests an extended break-in-period for the refiner bars in which the bar geometry moves through a transient state in which the refining action is different than either new plates or partially worn plates. This behaviour is thought to be due to primarily to changes in bar edge shape where small bar edge radii (0 h) and larger bar edge radii (2000+ h) produce a similar refining effect while medium bar edge radii (100-2000 h) produce a shorter fiber and a lower freeness. This result is somewhat consistent with the experience of the mill personnel who are aware of a break-in-period for new refiner plates. However, the break-in-period described by mill personnel is shorter in duration than the 2000 h indicated by the trial data.

4.6 Conclusion

Literature shows that plate wear reduces level of refining [56]–[58], [60]. Literature also shows that the prevalence of the corner force during the refining process is crucial in achieving the desired level of refining [25], [32], [35]. The presented work connects the change in refiner bar shape, namely the bar height reduction and bar edge rounding, with a change in the prevalence of corner force.

4.7 Acknowledgment

The authors gratefully acknowledge the assistance of Chad Toth, Pat Cooper and their colleagues at the Catalyst Paper Excellence mill at Crofton BC during the preparation for and execution of the refining trials.

This work is funded by a Collaborative Research and Development Grant provided by the Natural Sciences and Engineering Research Council of Canada (NSERC) and the following partners, who we thank for their ongoing support: AB Enzymes, Alberta Newsprint Company, Andritz, BC Hydro, Canfor, Catalyst Paper, FPInnovations, Holmen Paper, Meadow Lake Pulp (Paper Excellence), Millar Western, NORPAC, West Fraser, Westcan Engineering, and Winstone Pulp International.

5 Contributions and Recommendation

5.1 Contributions

Forces applied to refiner bars during bar passing events is the key mechanism by which fiber morphologies are developed for use in paper making. These forces have been measured in pilot-scale and mill-scale LC refiners using a force sensor technology, based on previous work, which has been further developed by the author to perform in these refiners. Short term trials in the pilot-scale LC refiner were carried out over a range of operating conditions and trials in a mill-scale LC refiner were carried out over a range of operating conditions and for the full lifetime of a set of refiner plates. The contributions of the presented work are as follows:

1. Force sensor measurements are combined with rotary encoder data to produce spatially-registered force readings: This set up enables detailed analysis of force profiles taking into account the position of the rotor bar relative to the stator bar. Based on this work, it is shown experimentally that friction force and corner force are present for bar passing events, as has been theorized in the literature.
2. Dual force-peak bar-passing events are associated with fiber cutting: It is shown that two distinct force profile types occur during bar passing events. One is a single peak profile which represents the friction force appearing late in the bar passing event. The other is a dual peak profile which includes both a corner force, early in the bar passing event, and a friction force, late in the bar passing event. It is shown that single peak profiles appear predominantly in the absence of significant fiber cutting while dual peak profiles are prevalent when there is significant fiber cutting.
3. Corner force is an indicator for fiber cutting: Through the analysis of the spatial registered bar-force data from the pilot-scale refiner, it is shown that the prevalence of corner force increases as refining energy increases. Further, it is shown that the increased prevalence of the corner force appears in the trial at the same plate gaps when fiber cutting is detected. This result suggests that corner force is a driving factor in fiber cutting.
4. Dual peak ratio is an indicator for fiber cutting: Based on analysis of the mill-scale trial data and comparison of these results with the pilot-scale data, *dual peak ratio*, is shown to be an indicator of the prevalence of corner force.

5. Refining action varies with radial position: Based on data gathered with sensors located at three different radial positions in the mill-scale refiner, it is shown that dual peak events are prevalent at the mid position and less prevalent at the outer and inner positions. This suggests that fiber cutting is prevalent at the mid position. Based on the position of the single peak events during BPEs, it is theorized that, at the outer position, single peak events occur that are caused by corner force rather than friction force. This further suggests that the outer position is also involved with fiber cutting.
6. Evidence of the validity of pilot-scale refiner trials: Data collected from both the mill-scale refiner and the pilot-scale refiner show that a high dual peak ratio is associated with fiber cutting. This result is also significant because it shows that research results based on trials in a pilot-scale refiner can be valid for mill-scale refiners.
7. Changes in bar shape due to wear can be observed in bar force data: It is shown that the physical changes in bar shape due to wear, both on the rotor and the stator, change the fiber-bar interaction. This change is seen in the "delay" of the corner force and in the declining prevalence of the corner force. This is a first step into the realm of wear monitoring of refiner plates based on bar force sensors.

As noted in Chapter 1, *the overarching objective of this research is to investigate relationships between refiner process variables, including changes in fiber and pulp properties, and force profiles during bar passing events in mechanical LC refining. More specifically, this work explores insights gained from registration of bar force data to rotor bar position in an experimental refiner and the application of these insights to bar force data from a mill-scale refiner*. The presented work shows that changes in key indicators of fiber development during refining, such as fiber length and freeness, correspond to qualitative changes to the force profiles measured during BPEs in both the pilot-scale and the mill-scale LC refiners.

5.2 Recommendations

The author recommends pilot and mill-scale trails in the future that focus on the following areas of research:

- Assess the balance between refining zones in a twin disc refiner to prevent production of non-homogenous pulp;
- Assess the impact of bar width on bar force profiles and fiber development
- Asses the impact of different edge shapes of force profiles and fiber development
- Use force measurements to identify the impact of fiber length and freeness on bar forces

6 References

[1] "BC Hydro - Mechanical Pulping Sessions," in *The Mechanical Pulping Process, Electrical Energy Requirements, Vancouver BC,* 2015, pp. 1–51.

[2] J. Kappel, "Mechanical Pulps: From Wood To Bleached Pulp." Tappi press, Atlanta, GA, 1999.

[3] W. J. Batchelor, D. M. Martinez, R. J. Kerekes, and D. Oullet, "Forces on fibres in low consistency refining: Shear Force," *Journal of Pulp and Paper Science,* vol. 23. pp. 11–18, 1997.

[4] B. Prairie, P. Wild, P. Byrnes, D. Olender, D. W. Francis, and D. Ouellet, "Forces during bar-passing events in low consistency refining: Effects of refiner tram," *Pulp Pap. Canada,* vol. 108, no. 9, pp. 34–37, 2007.

[5] R. Harirforoush, J. Olson, and P. Wild, "Bar force measurement in low consistency refining: The effect of plate pattern," *Nord. Pulp Pap. Res. J.*, vol. 33, no. 2, pp. 210–219, 2018.

[6] D. Olender, P. Wild, and P. Byrnes, "A piezoelectric forces sensor for mill-scale chip refiners," *Proc. Inst. Mech. Eng. Part E J. Process Mech. Eng.*, vol. 222, no. 2, pp. 115–122, 2008.

[7] B. Prairie, P. Wild, P. Byrnes, D. Olender, B. Francis, and D. Ouellet, "Forces During Bar-Passing Events in Low-Consistency Refining: Distributions and Relationships to Specific Edge Load," *J. Pulp Pap. Sci.*, vol. 34, no. 1, pp. 1–16, 2008.

[8] J. E. Jakes, C. G. Hunt, S. L. Zelinka, P. N. Ciesielski, and N. Z. Plaza, "Effects of moisture on diffusion in unmodified wood cell walls: A phenomenological polymer science approach," *Forests,* vol. 10, no. 12, 2019.

[9] B. Dalpke, "Topic-1-Introduction-and-overview," *Course pulp Pap. Univ. Br. Columbia,* 2018.

[10] A. Siadat, A. Bankes, P. M. Wild, J. Senger, and D. Ouellet, “Development of a piezoelectric force sensor for a chip refiner,” *Proc. Inst. Mech. Eng. Part E J. Process Mech. Eng.*, vol. 217, no. 2, pp. 133–141, 2003.

[11] B. Dalpke, “Topic-4-Mechanical pulping,” *Course pulp Pap. Univ. Br. Columbia*, 2018.

[12] A. Elahimehr, “Low Consistency Refining of Mechanical Pulp: The Relationship Between Plate Pattern, Operational Variables and Pulp Properties,” *Ph.D. Thesis*. University of British Columbia, 2014.

[13] A. Elahimehr, J. A. Olson, and D. M. Martinez, “Understanding LC refining:The effect of plate pattern and refiner operation,” *Nord. Pulp Pap. Res. J.*, vol. 28, no. 3, pp. 386–391, 2013.

[14] T. Lundin, *Tailoring pulp fibre properties in low consistency refining*. Åbo Akademi, 2008.

[15] D. Gorski, K. Mörseburg, J. Olson, and A. Luukkonen, “Fibre and fines quality development in pilot scale high and low consistency refining of ATMP,” *Nord. Pulp Pap. Res. J.*, vol. 27, no. 05, pp. 872–881, 2012.

[16] A. Luukkonen, J. A. Olson, and D. M. Martinez, “Low consistency refining of mechanical pulp, effect of gap, speed and power,” *J. Pulp Pap. Sci.*, vol. 36, no. 1–2, pp. 28–34, 2010.

[17] R. Harirforoush, J. Olson, and P. Wild, “Indications of the onset of fiber cutting in low consistency refining using a refiner force sensor: The effect of pulp furnish,” *Nord. Pulp Pap. Res. J.*, vol. 33, no. 1, pp. 58–68, 2018.

[18] A. Luukkonen, “Development of a methodology to optimize low consistency refining of mechanical pulp,” *Ph.D. Thesis*. University of British Columbia, 2007.

[19] A. Luukkonen, J. A. Olson, and D. M. Martinez, “Low consistency refining of mechanical pulp: A methodology to relate operating conditions to paper properties,” *J. Pulp Pap. Sci.*, vol. 36, no. 3–4, pp. 107–111, 2010.

[20] A. Luukkonen, J. Olson, and D. M. Martinez, “Low consistency refining of mechanical pulp: Relationships between refiner operating conditions and pulp properties,” *Nord. Pulp Pap. Res. J.*, vol. 27, no. 5, pp. 882–885, 2012.

[21] R. J. Kerekes and J. J. Senger, “Characterizing Refining Action in Low-Consistency Refiners by Forces on fibres,” *J. Pulp Pap. Sci.*, vol. 32, no. 1, pp. 1–8, 2006.

[22] E. V. Goncharov, V.N.; Smirnova, E.A.; Shemyakin, “Method for the determination of stresses between refiner blades,” *Bumazh. Prom.*, no. 27, pp. 134–138, 1970.

[23] P. A. Gradin, O. Johansson, J.-E. Berg, and S. Nyström, “Measurement of the power distribution in a single-disc refiner,” *J. Pulp Pap. Sci.*, vol. 25, no. 11, pp. 384–387, 1999.

[24] J. J. Senger and D. Ouellet, “Factors Affecting the Shear Forces in High-Consistency Refining,” *J. Pulp Pap. Sci.*, vol. 28, no. 11, pp. 364–368, 2002.

[25] D. M. Martinez and R. J. Kerekes, “Forces on bars in low consistency refining,” *Tappi Journal*, vol. 77, no. 12. pp. 119–123, 1994.

[26] D. Olender, “Forces on bars in high-consistency mill-scale refiners,” *Ph.D. Thesis*. University of Victoria, 2007.

[27] B. C. Prairie, “Measurement of Forces in a Low Consistency Refiner,” *Msc Thesis*. University of Victoria, 2005.

[28] A. Siadat, “The measurement of forces in chip refiners,” *Msc Thesis*. University of British Columbia, 2001.

[29] D. Olender, P. Francescutti, P. Wild, and P. Byrnes, “Refiner Plate Clash Detection Using an embedded Force Sensor,” *Nordic Pulp and Paper Research Journal*, vol. 22, no. 1. pp. 124–130, 2007.

[30] R. Harirforoush, J. Olson, and P. Wild, “In-process detection of fiber cutting in low consistency refining based on measurement of forces on refiner bars,” *Tappi J.*, vol. 16, no. 4, pp. 460–469, 2017.

[31] R. Harirforoush, P. Wild, and J. Olson, “The relation between net power, gap, and forces on bars in low consistency refining,” *Nord. Pulp Pap. Res. J.*, vol. 31, no. 1, pp. 71–78, 2016.

[32] M. Aigner, J. Olson, and P. Wild, “Measurement and interpretation of spatially registered bar-forces in LC refining,” *Nord. Pulp Pap. Res. J.*, vol. 35, no. 4, pp. 600–610, Nov. 2020.

[33] M. Aigner, J. Olson, Y. Sun, and P. Wild, “Interpretation of force profiles in mill-scale LC refining,” *Nord. Pulp Pap. Res. J.*, pp. 000010151520210058. https://doi.org/10.1515/npprj-, Oct. 2021.

[34] M. Aigner, J. Olson, Y. Sun, and P. Wild, “Effects of plate wear on bar forces and fibre properties in a mill scale LC-refiner, accepted, pending publication,” *Nord. Pulp Pap. Res. J.*, p. https://doi.org/10.1515/npprj-2021-0064, 2021.

[35] R. J. Kerekes, “Force-based characterization of refining intensity,” *Nord. Pulp Pap. Res. J.*, vol. 26, no. 01, pp. 014–020, 2011.

[36] J. A. Olson, J. Drozdiak, M. Martinez, R. Garner, A. G. Robertson, and R. Kerekes, “Characterizing fibre shortening in low-consistency refining using a comminution model,” *Powder Technol.*, vol. 129, no. 1–3, pp. 122–129, 2003.

[37] M. Miller, A. Luukkonen, and J. A. Olson, “Effect of LC refining intensity on fractionated and unfractionated mechanical pulp,” *Nord. Pulp Pap. Res. J.*, vol. 32, no. 3, pp. 386–394, 2017.

[38] R. J. Kerekes and F. P. Meltzer, “The Influence of Bar Width on Bar Forecs and Fibre Shortening in Low Consistency Pulp Refining,” *Nord. Pulp Pap. Res. J.*, vol. 33, no. May, pp. 1–13, 2018.

[39] T. Lundin, W. Batchelor, and P. Fardim, “Fiber trapping in low-consistency refining: New parameters to describe the refining process,” *Tappi J.*, vol. 8, no. 7, pp. 15–21, 2009.

[40] A. Fredrikson and L. Salminen, “Analysis method of high-consistency chip refiner forces,” *Nord. Pulp Pap. Res. J.*, vol. 27, no. 04, pp. 695–701, Oct. 2012.

[41] D. Olender, P. Francescutti, P. Wild, and P. Byrnes, “Refiner Plate Clash Detection Using an embedded Force Sensor,” *Nord. Pulp Pap. Res. J.*, vol. 22, no. 1, pp. 124–130, 2007.

[42] U.-B. Mohlin, “Inside an LC-refiner,” *11th Biennial Advances in refining and mechanical pulping: scientific technical advances*. Stockholm, Sweden, Feb 23 – 25, pp. 1–28, 2010.

[43] H. Vomhoff, “Dynamic compressibility of water- saturated fibre networks and influence of local stress variations in wet pressing,” *Ph.D. Thesis*. Institutionen för pappers-och massateknologi, Royal Institute of Technology, Stockholm, Sweden, 1998.

[44] R. Harirforoush, “The Potential Use of Bar Force Sensor Measurements for Control in Low Consistency Refining by,” *PhD. Thesis*. University of Victoria, 2018.

[45] O. Eriksen, Ø. Gregersen, and P.-Å. Krogstad, “Refining zone pressure in a mill-scale TMP refiner measured by fibre-optic sensors,” *Nord. Pulp Pap. Res. J.*, vol. 20, no. 4, pp. 468–476, 2007.

[46] O. Eriksen, C. Holmqvist, and U. Mohlin, “Fibre floc drainage – a possible cause for substantial pressure peaks in low-consistency refiners,” *Nord. Pulp Pap. Res. J.*, vol. 23, no. 3, pp. 321–326, Aug. 2008.

[47] M. Llobera, “Building past landscape perception with GIS: Understanding topographic prominence,” *J. Archaeol. Sci.*, vol. 28, no. 9, pp. 1005–1014, 2001.

[48] R. J. Kerekes and C. J. Schell, “Characterization of fibre flocculation regimes by a crowding factor,” *J. Pulp Pap. Sci.*, vol. 18, no. 1, pp. 32–38, 1992.

[49] S. Andersson, “Low Consistency Refining of Mechanical Pulp – Process Conditions and Energy Efficiency,” *PhD. Thesis*. Mid Sweden University, 2011.

[50] M. Scholl, P. Clayton, and Y. Jia, “Deterioration behavior of thermomechanical refiner plates,” *Wear*, vol. 203–204, pp. 65–76, 1997.

[51] R. Bordin, J. C. Roux, and J. F. Bloch, “Global description of refiner plate wear in low consistency beating,” *Nord. Pulp Pap. Res. J.*, vol. 22, no. 4, pp. 529–534, 2007.

[52] R. J. Kerekes, “Energy and Forces in Refining,” *Journal of Pulp and Paper Science*, vol. 36, no. 1–2. pp. 10–15, 2010.

[53] D. Christensen, Y. Jia, and P. Clayton, “Surface Deterioration of Refiner Plates for Thermomechanical Pulping,” *TAPPI pulping Conf.*, pp. 193-203. TAPPI PRESS, 1994.

[54] T. Lundin, W. Batchelor, and P. Fardim, “Effect of bar edge conditions on fibre trapping in low consistency refining,” *62nd Appita Annu. Conf. Exhib. Rotorua, New Zeal. 20-23 April 2008 Conf. Tech. Pap.*, pp. 199-206. Appita Inc, 2008.

[55] K. Koskenhely, K. Nieminen, E. Hiltunen, and H. Paulapuro, “Comparison of plate and conical fillings in refining of bleached softwood and hardwood pulps,” *Pap. ja Puu/Paper Timber*, vol. 87, no. 7, pp. 458–463, 2005.

[56] T. H. Berger, “The impact of plate material on pulp quality over time,” *Proc. 4 th Int. Refin. Conf. PIRA Int.*, vol. 18, pp. 307-315. Leatherhead, UK., paper, 1997.

[57] K. Ebeling, “A critical review of current Theories for the refinig of chmical pulps,” in *International Symposium on Fundamental Concepts of Refining*, 1980, pp. 1–29.

[58] J. Rihs, “Low consistency refining-theory vs practice,” in *3rd International Refining Conference, PIRA International, Leatherhead, U.K.*, 1995.

[59] W. Frazier, D. R. Danks, and B. Hodge, “Paper pulp refiner long-duration wear monitoring with polymer replicas,” *Wear*, vol. 267, pp. 1095–1099, 2009.

[60] W. C. Frazier, “Applying Hydrodynamic Lubrication Theory to Predict Refiner Behaviour,” *J. Pulp Pap. Sci.*, vol. 14, no. 1, pp. J1–J5, 1988.

[61] X. Hong-liang, L. Ji-rong, and X. Ze-hui, “Study on the new materials for fiberboard refiner plate of defibrator,” *J. For. Res.*, vol. 14, no. 1, pp. 89–92, 2003.

[62] L. P. Wittberg, M. Björkman, G. Khokhar, U. B. Mohlin, and A. Dahlkild, “Flow conditions in the grooves of a Low-Consistency refiner,” *Nord. Pulp Pap. Res. J.*, vol. 27, no. 2, pp. 173–183, 2012.

Appendix I - Pressure housing for sensors

The environment in the mill-scale refiner at Crofton, BC was deemed harsher than the bar force sensors and the wiring could withstand for an extended period of time without additional protection. The data that the mill provided was a temperature of about 100°C inside the refiner and a pressure of up to 50 psi above atmosphere. The temperature is similar to what the sensors have been shown to withstand in previous trials.

To protect the sensors from the pressure and the flow of the pulp or the long term, sensor housings in combination with a conduit for the sensor wires were installed. To protect the back of the sensors, custom housings were machined and installed on the back of the refiner plates (see Figure 51 (c)), covering the sensors. The housings are mounted with four 10-32 socket head screws and sealed with an O-ring (see Figure 51 (a)). To protect the front of the sensors, an O-ring groove was machined in the sensor housing itself (see Figure 51 (b)). Therefore, the only part of the sensors exposed to the refining environment is the probe tip. A schematic cross section of the sensor assembly with pressure housing installed in the refiner plate can be see in Figure 52.

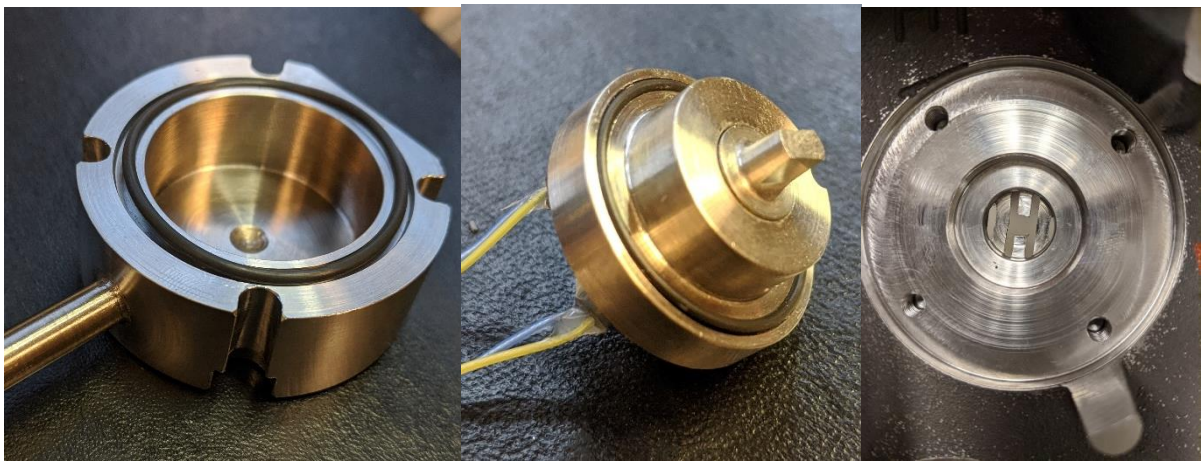

(a) (b) (c)

Figure 51: O-ring placement.
(a) Pressure housing and (b) Sensor. (c) Machined cavity in refiner plate for sensor and pressure housing.

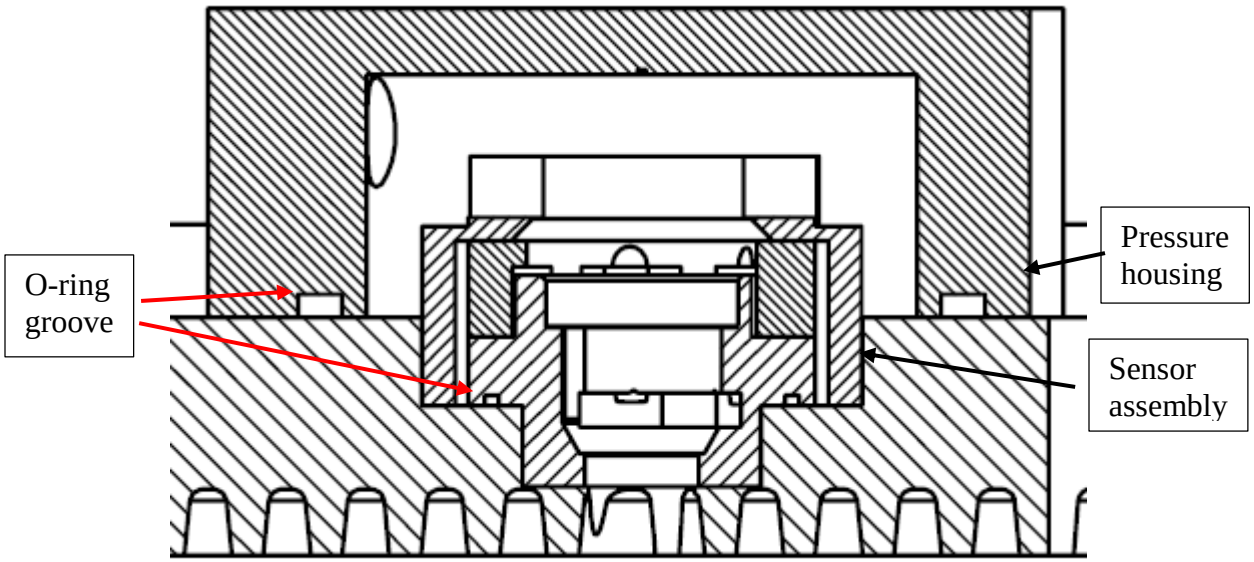

Figure 52: Cross-section through sensor assembly and pressure housing. O-ring grooves are indicated

To protect the sensor wiring from the environment, a 1/4" diameter stainless steel conduit was installed, with Yor-Lok fittings, connecting the previously described pressure housings to the feedthrough (see Figure 53).

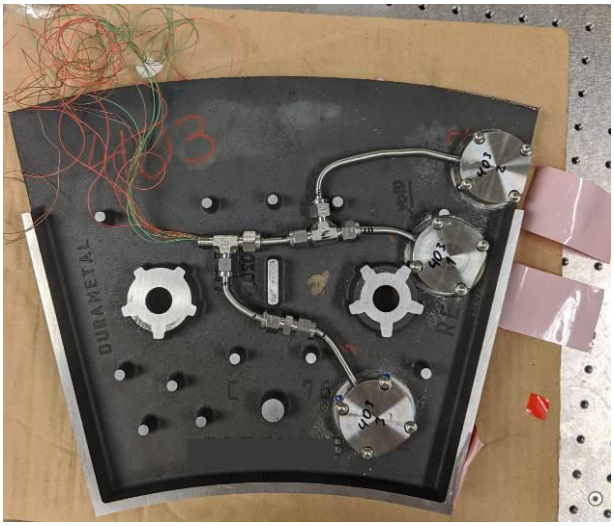

Figure 53: Installed sensors with pressure housings and wire conduit

The conduit and cables needed to be fed out of the refiner in a way which does not fail even when the conduit inside the refiner fails. To this end a pressure proof double feed through was set up using two multi-conductor feedthroughs (MFT-14-3-PTFE and MFT-040-12-PTFE, Omega Environmental, Canada) (see Figure 54 (a)). In this double feedthrough set up the conduit is first feed out of the refiner followed by a feedthrough which feeds the sensor wires out of the conduit (see Figure 54 (b)).

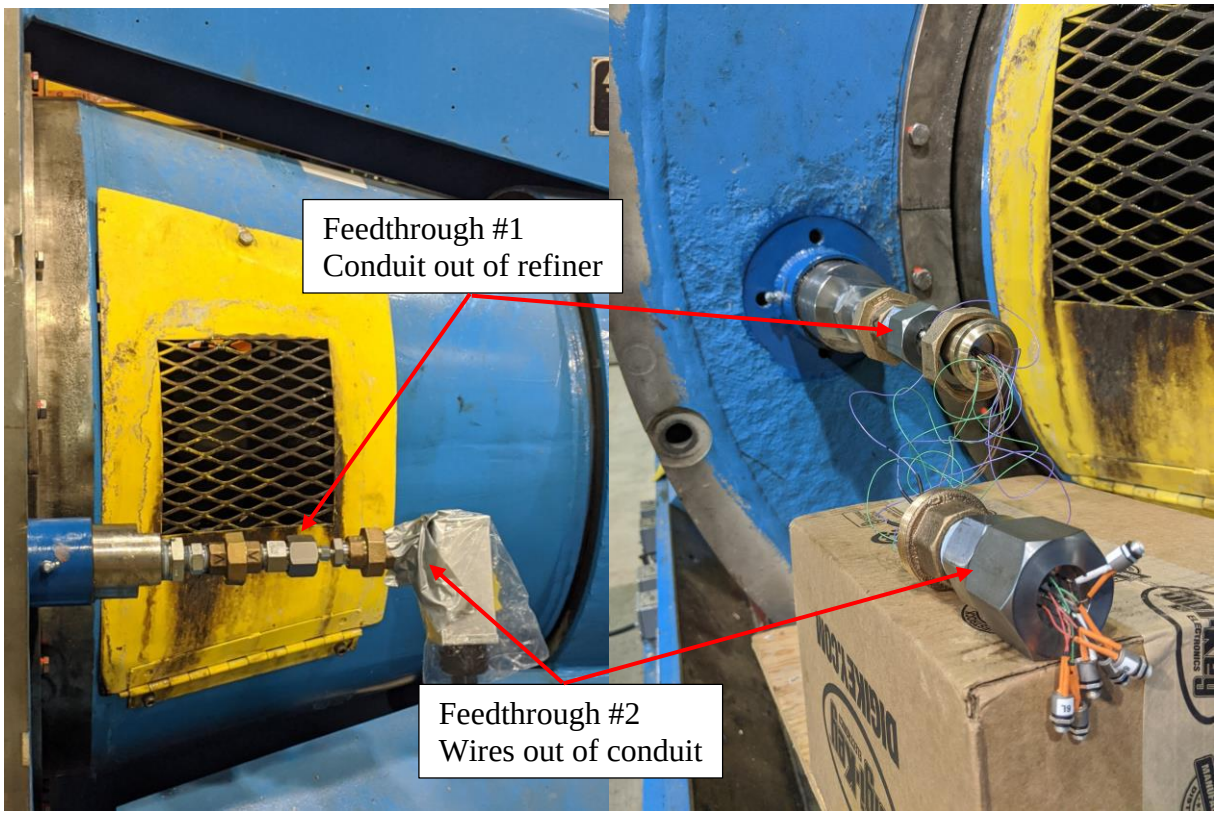

(a) (b)

Figure 54:Feedthrough pictures.
(a) Feedthrough set up assembled. (b) Feedthrough separated.

Appendix I – Corner force and shear force models

Total bar force, $\overrightarrow{F_{total}}$, during a BPE is the sum of the friction force, $\overrightarrow{F_F}$, and the corner force, $\overrightarrow{F_C}$,

$$\overrightarrow{F_{total}} = \overrightarrow{F_C} + \overrightarrow{F_F} \tag{15}$$

Each of these forces a component which is parallel to the axis of the refiner (normal component) and a component perpendicular to both the edge of refiner bar and to the axis of the refiner (shear component). As a result, Equation (15) can also be viewed as follows,

$$\begin{pmatrix} F_{total,N} \\ F_{total,S} \end{pmatrix} = \begin{pmatrix} F_{C,N} \\ F_{C,S} \end{pmatrix} + \begin{pmatrix} F_{F,N} \\ F_{F,S} \end{pmatrix} \tag{16}$$

Here, $F_{C,N}$ is the normal component of the corner force, $F_{C,S}$ is the shear direction component of the corner force, $F_{F,N}$ is the normal component in of the friction force and $F_{F,S}$ is the shear component of the friction force need to define these terms (see Figure 55).

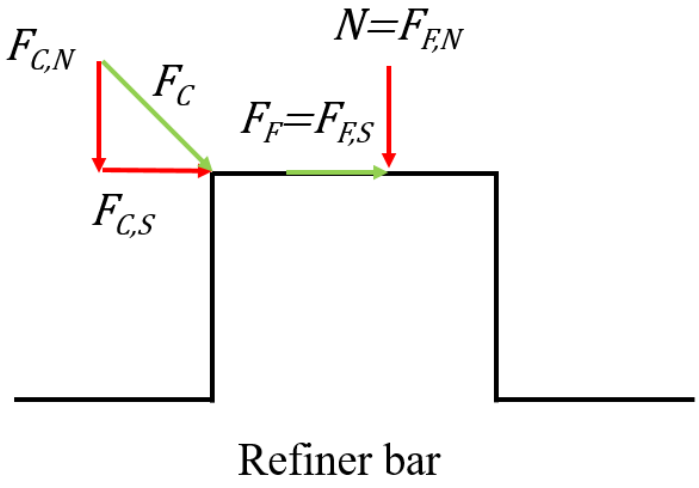

Figure 55: Force directions.
Force directions for corner force and friction force and force components acting on refiner bar.

Mean peak normal force data for the softwood trials at plate gap 0.2 mm is used to generate separate force profiles for the normal component of the corner force and the friction force following the relation described in Equation ((5)). Based on these individual force plots and using

the engaged area for friction force and engaged length for corner force, separate stress profiles for the BPE are generated (See Figure 26). These stress plots are fitted with trend lines.

It was found that the normal component of the corner force is the product of the engaged length, l_E, and a constant, k_C.

$$F_{C,N} = l_E k_C \tag{17}$$

The normal component of the friction force is found to be the product of the engaged area, A_E, and a power law term comprised of the angular position in the BPE, ϕ, the constant, k_F, and the exponent, e_F.

$$F_{F,N} = k_F A_E \phi^{e_F} \tag{18}$$

Equations (16) to (18) where used to generate the combined force plot in Figure 23 (c). The values of the used constants are displayed in Table 3.

Table 11: Values of constants used in friction force and corner force models.

Constant	Value
k_C	1.8
k_F	3.4
e_F	11.5

Appendix III – Refiner data UBC-trials

Table 12: Refiner data for softwood trial at PPC at UBC.
Plate gap, flowrate, net power, pulp sample consistency, SRE and SEL of each pulp sample point.

Plate Gap (mm)	Flow (L/min)	Net power (kW)	Consistency (%)	SRE (kWh/t)	SEL (J/m)
0.625	252	7.1	3.4	13.86	0.13
0.603	254	7.8	3.4	15.06	0.14
0.571	246	9.9	3.4	19.67	0.18
0.485	257	14.1	3.4	26.67	0.26
0.469	262	19.3	3.4	35.94	0.35
0.453	246	23.8	3.4	47.03	0.43
0.447	256	20.1	3.4	38.32	0.37
0.435	246	26.4	3.4	53.20	0.48
0.416	244	26.9	3.4	53.46	0.49
0.382	244	30.0	3.4	60.45	0.55
0.359	258	30.8	3.5	57.30	0.56
0.323	256	34.4	3.5	64.27	0.63
0.301	254	37.0	3.5	69.87	0.67
0.258	257	42.7	3.5	80.03	0.78
0.207	254	46.9	3.4	89.40	0.86

Table 13: Refiner data for hardwood trial at PPC at UBC.
Plate gap, flowrate, net power, pulp sample consistency, SRE and SEL of each pulp sample point.

Plate Gap (mm)	Flow (L/min)	Net power (kW)	Consistency (%)	SRE (kWh/t)	SEL (J/m)
0.647	256	0.5	3.3	0.91	0.01
0.589	244	0.7	3.3	1.41	0.01
0.547	247	1.1	3.3	2.15	0.02
0.498	258	1.7	3.3	3.39	0.03
0.430	247	3.5	3.3	7.12	0.06
0.422	243	2.3	3.3	4.76	0.04
0.388	246	3.2	3.3	6.50	0.06
0.385	250	6.8	3.3	13.74	0.12
0.365	245	10.0	3.3	20.29	0.18
0.364	250	9.5	3.3	19.08	0.17
0.349	242	3.6	3.3	7.40	0.07
0.333	247	16.9	3.3	34.04	0.31
0.321	259	5.1	3.3	9.98	0.09
0.307	258	6.3	3.3	12.25	0.11
0.280	261	12.8	3.3	24.56	0.23
0.249	252	17.3	3.3	34.31	0.32
0.217	243	20.5	3.4	41.73	0.37
0.206	248	22.3	3.4	44.64	0.41